EE

Internal Report
DESY M 96-04
February 1996

Studies of the Behaviour of Proton Spin Motion in HERA-p at High Energies

V. Balandin, N. Golubeva
Institute for Nuclear Research of the RAS, Moscow

D. P. Barber
Deutsches Elektronen-Synchrotron, Hamburg

CERN LIBRARIES, GENEVA
SCAN-9603283

SCAN9613

DESY behält sich alle Rechte für den Fall der Schutzrechtserteilung und für die wirtschaftliche Verwertung der in diesem Bericht enthaltenen Informationen vor.

DESY reserves all rights for commercial use of information included in this report, especially in case of filing application for or grant of patents.

"Die Verantwortung für den Inhalt dieses
Internen Berichtes liegt ausschließlich beim Verfasser"

Studies of the Behaviour of Proton Spin Motion in HERA-p at High Energies

V. Balandin, N. Golubeva
Institute for Nuclear Research of the RAS, Moscow
and
D.P. Barber,
Deutsches Elektronen-Synchrotron, DESY, Hamburg

Abstract

We present a summary in note form of preliminary investigations of spin motion at high energy in the HERA proton ring with the aim of exposing some key aspects and problems. In this paper our main aim will be not to try to explain "why?", but simply to show what happens using the numerical results obtained for the real structure of the real accelerator.

1 Proton Spin Motion on the Design Orbit i.e. in Zeroth Approximation with Respect to Orbital Oscillations

1.1 Notation

At a fixed point P on the ring, we can represent the one turn spin transformation (in zeroth approximation with respect to orbital motion) as the rotation:

$$R(\vec{n}_0(P,\gamma_0),\varphi(\gamma_0))$$

around the unit vector $\vec{n}_0$ ($|\vec{n}_0| = 1$) by an angle φ. The parameter γ_0 is the Lorentz factor. If for some value of γ_0 the angle $\varphi(\gamma_0) = 0\ (mod\ 2\pi)$, then

$$R(\vec{n}_0(P,\gamma_0),\varphi(\gamma_0)) = I$$

and hence the vector $\vec{n}_0(P,\gamma_0)$ can then be chosen arbitrarily. Obviously the vector $\vec{n}_0(P,\gamma_0)$ is a periodic function of the argument P (azimuth). The ratio $\nu_s^0 \equiv \varphi/2\pi$ is called the spin tune.

1.2 Structure of Nonflat HERA-p

Even when perfectly aligned, the HERA-p ring is nonflat – it has vertical bends. In particular it has three interaction sections with vertical magnets: the South, the North and the East and the vertical bends are interleaved with horizontal bends. The South and North interaction sections have the same optic. To increase the possible number of symmetries we have also studied the nonflat optic of HERA-p without vertical bends in the East. The structure of the nonflat HERA-p without vertical magnets in the East in zeroth approximation with respect to orbital motion is shown in Fig.1.

1.3 The Flat Test Model for HERA-p

In order to compare the results obtained with the results of other projects and also for the comparison of the behaviour of the spin vector in flat and nonflat rings we have also studied a flat test model obtained by removing

the vertical bends in the East, in the South and in the North interaction sections.

Note that the flat test model is very close to the original nonflat ring with respect to properties of the betatron oscillations. For this purpose see Figs.2-5, where the optical functions of both rings are shown.

1.4 Betatron and Synchrotron tunes for all models of HERA-p

In this subsection we bring together the tunes of all models of HERA-p discussed in this report.

	flat test model	nonflat ring	nonflat model (without vert.bends in the East)
Q_x	31.26478	31.26632	31.26606
Q_y	32.28875	32.28875	32.28875
Q_z	0.00063	0.00063	0.00063

Q_y and Q_z are model independent (except Fig.40) and Q_x has a slight model dependence.

	IP - East	
a	HBEND	1.5128515970
b	VBEND	-0.0057438700
c	HBEND	0.0604149598
d	VBEND	0.0057433499
e	HBEND	0.0029594000
	IP - South	
e	HBEND	0.0029594000
d	VBEND	0.0057433499
c	HBEND	0.0604149598
b	VBEND	-0.0057438700
a	HBEND	1.5103747370
f	VBEND	0.0000014000
	IP - West	
a	HBEND	1.5103739970
b	VBEND	-0.0057438700
c	HBEND	0.0604149598
d	VBEND	0.0057433499
e	HBEND	0.0029594000
	IP - North	
e	HBEND	0.0029594000
d	VBEND	0.0057433499
c	HBEND	0.0604149598
b	VBEND	-0.0057438700
a	HBEND	1.5128515970

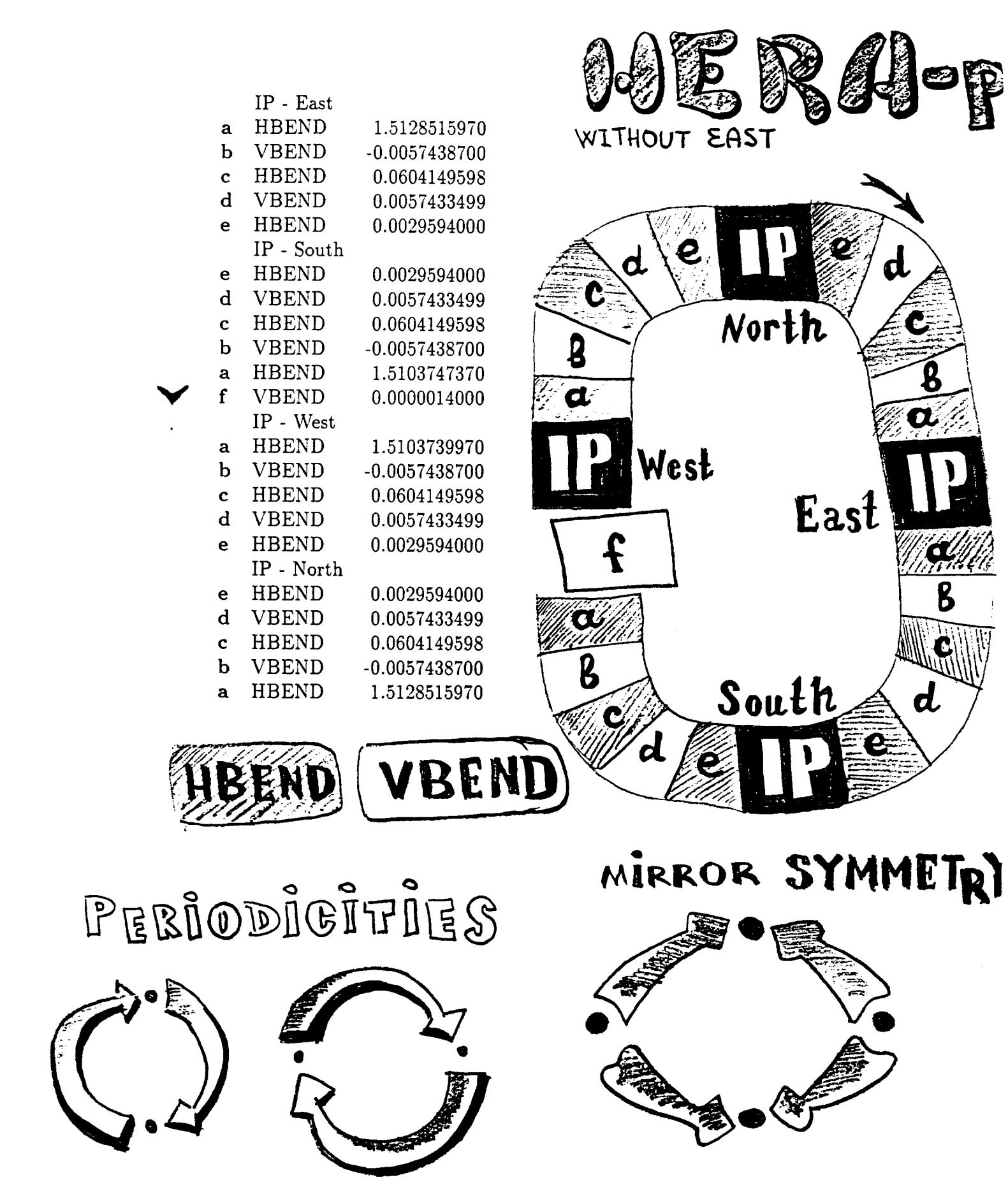

Figure 1: The magnet structure of the nonflat HERA-p along the design orbit (i.e. in zeroth approximation with respect to orbital motion). Groups of successive horizontal (vertical) bending magnets are represented as one element (i.e. lumped together).

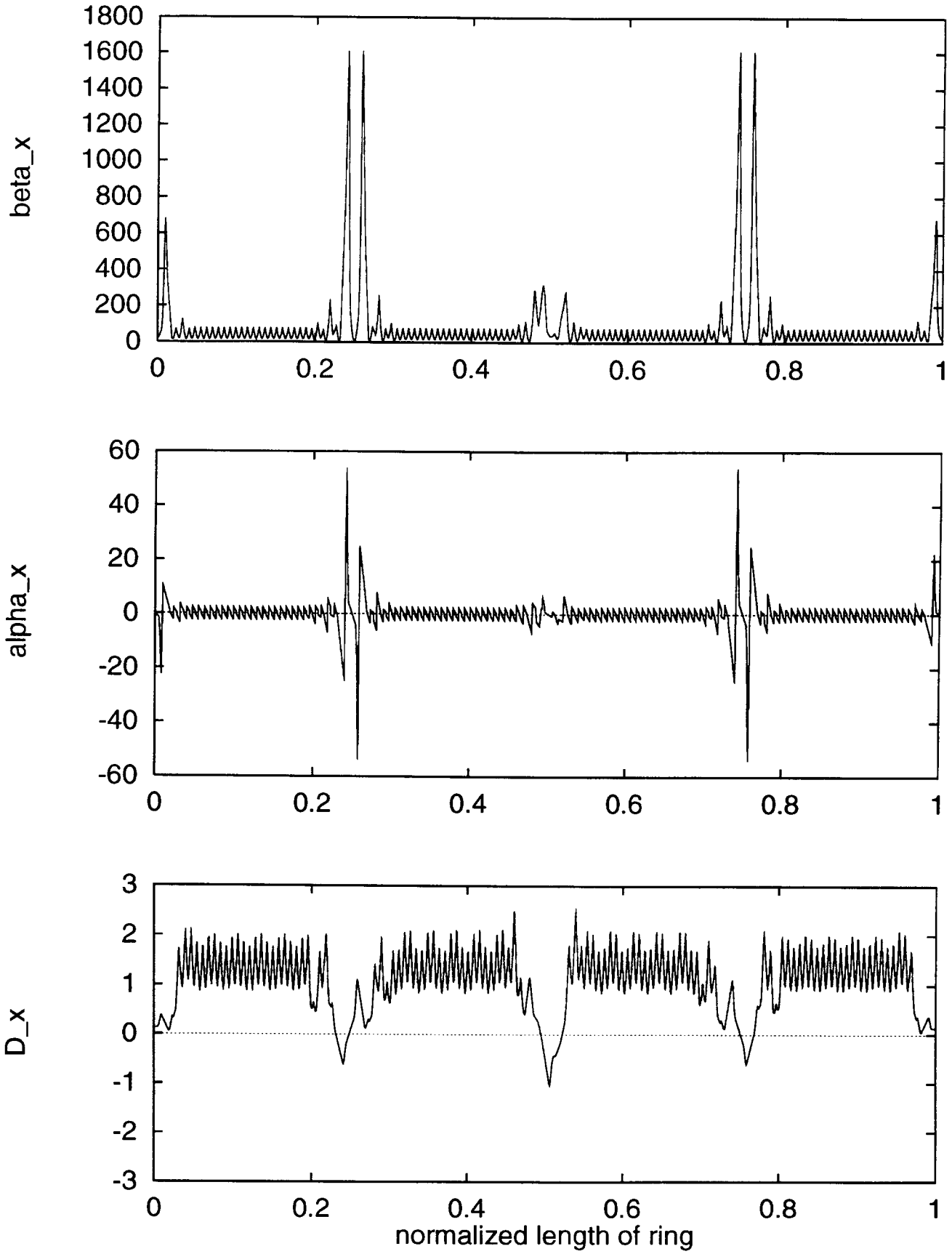

Figure 2: Behaviour of the horizontal optical functions along the ring. The length of the ring has been scaled to unity. Flat HERA-p at E = 820 GeV. The start point is the East IP.

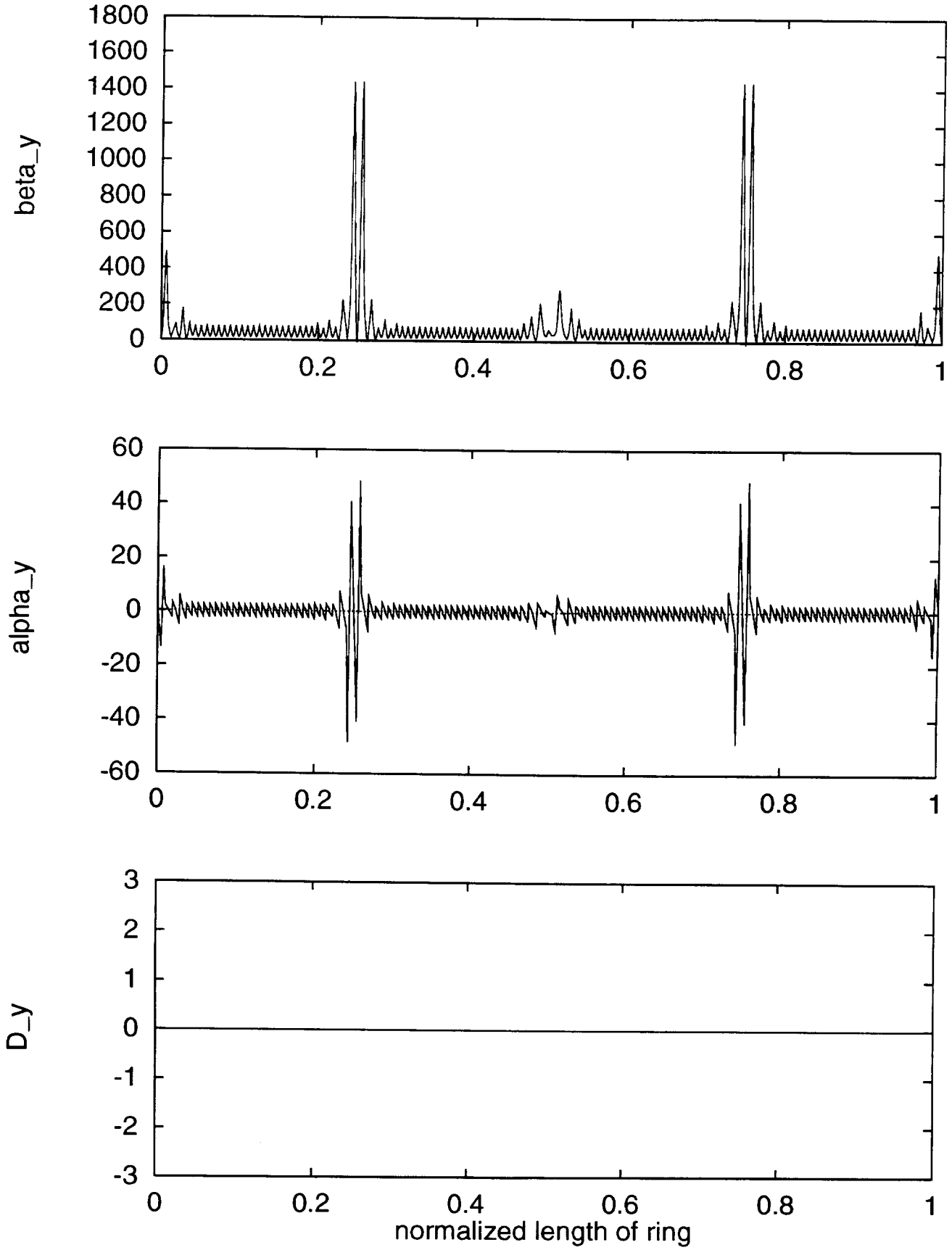

Figure 3: Behaviour of the vertical optical functions along the ring. The length of the ring has been scaled to unity. Flat HERA-p at E = 820 GeV. The start point is the East IP.

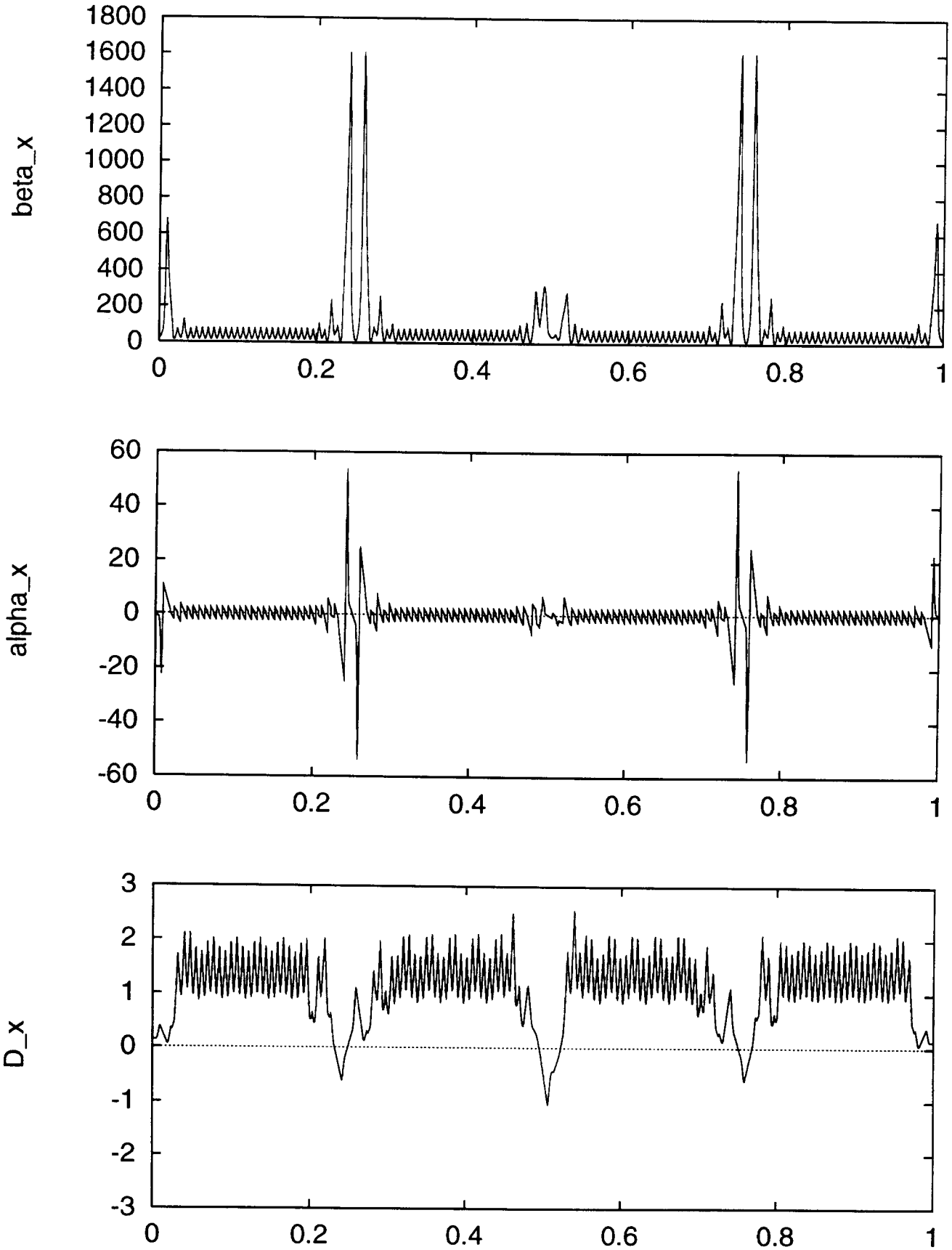

Figure 4: Behaviour of the horizontal optical functions along the ring. The length of the ring has been scaled to unity. Nonflat HERA-p at E = 820 GeV. The start point is the East IP.

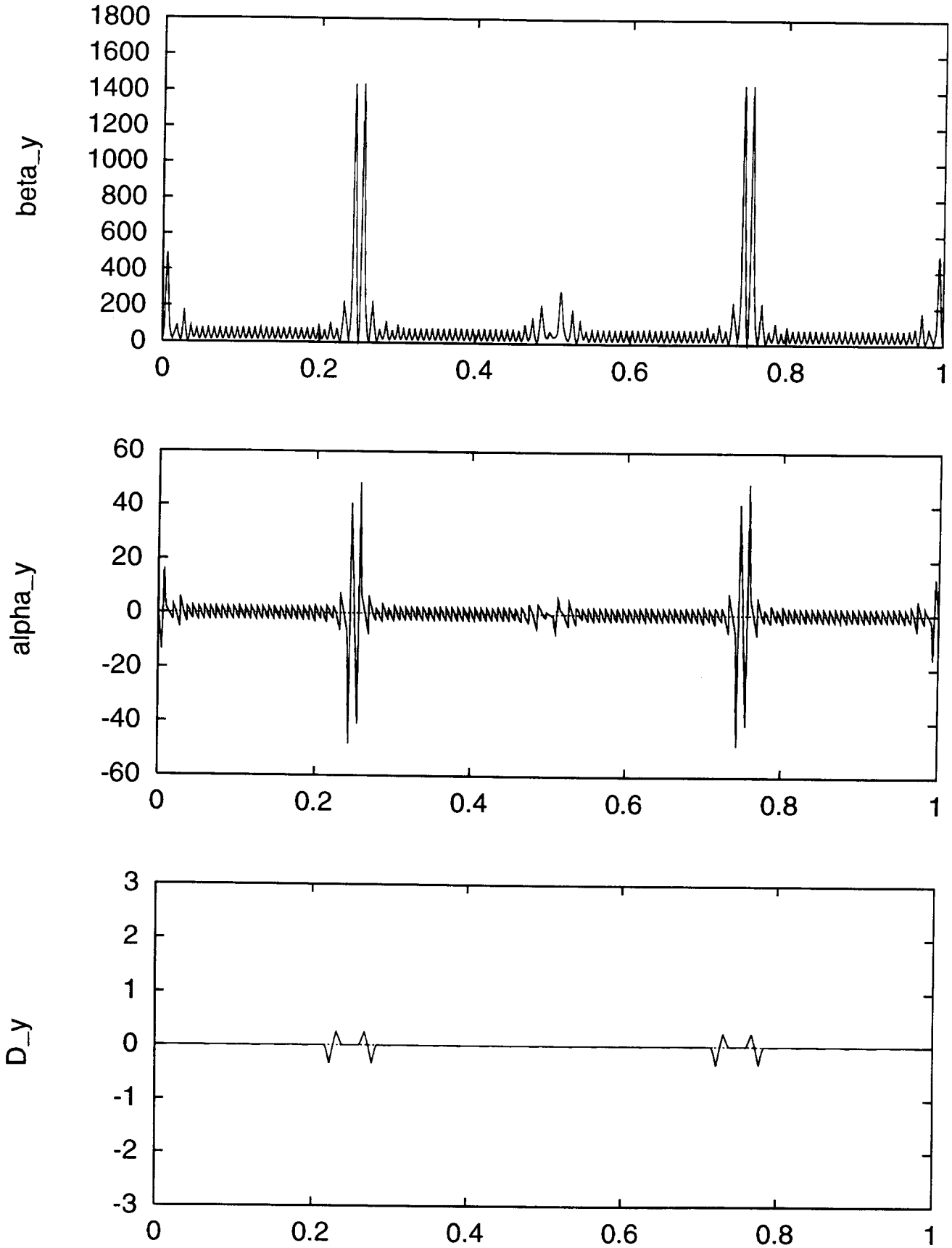

Figure 5: Behaviour of the vertical optical functions along the ring. The length of the ring has been scaled to unity. Nonflat HERA-p at E = 820 GeV. The start point is the East IP.

1.5 Comparison of the Behaviour of $\vec{n}_0$ and ν_s^0 for Flat and Nonflat Models of HERA-p

Figs.6-8 show the behaviour of the spin tune ν_s^0 and the vector $\vec{n}_0$ as a function of the energy for a narrow energy region at high energy for all variants of the optic of HERA-p considered in this paper. In all figures only the fractional part of the spin tune is shown (it may be naturally defined in the region from 0 up to 0.5 - not in the region from 0 up to 1). For better visualization we have chosen the continuous (as a function of the energy) branches of the spin tune and the vector $\vec{n}_0$. They are not in the correspondence one to another in the sense that the revolution matrix of spin motion could be either the matrix $R(\vec{n}_0, \nu_s^0)$ or $R(-\vec{n}_0, \nu_s^0)$.

For the nonflat variants of HERA-p (Figs.7-8) the fractional part of the spin tune is never equal to zero. This means that the resonance condition for imperfection resonances [1] is never satisfied in the energy region considered. In fact for nonflat HERA-p the resonance condition is not satisfied all the way from 40 GeV up to 820 GeV. But this does not mean that we can completely avoid the problem of imperfection resonances, because for some energies the fractional part of the spin tune is still uncomfortably close to zero. In this paper we do not study the problem of imperfection resonances. Instead we are mainly interested in the effect of betatron and synchrotron oscillations on the spin motion.

[1] 'Imperfection resonances' are depolarizing resonances driven by misalignments when the l's are zero in equation 2 below. They are particularly troublesome during acceleration.

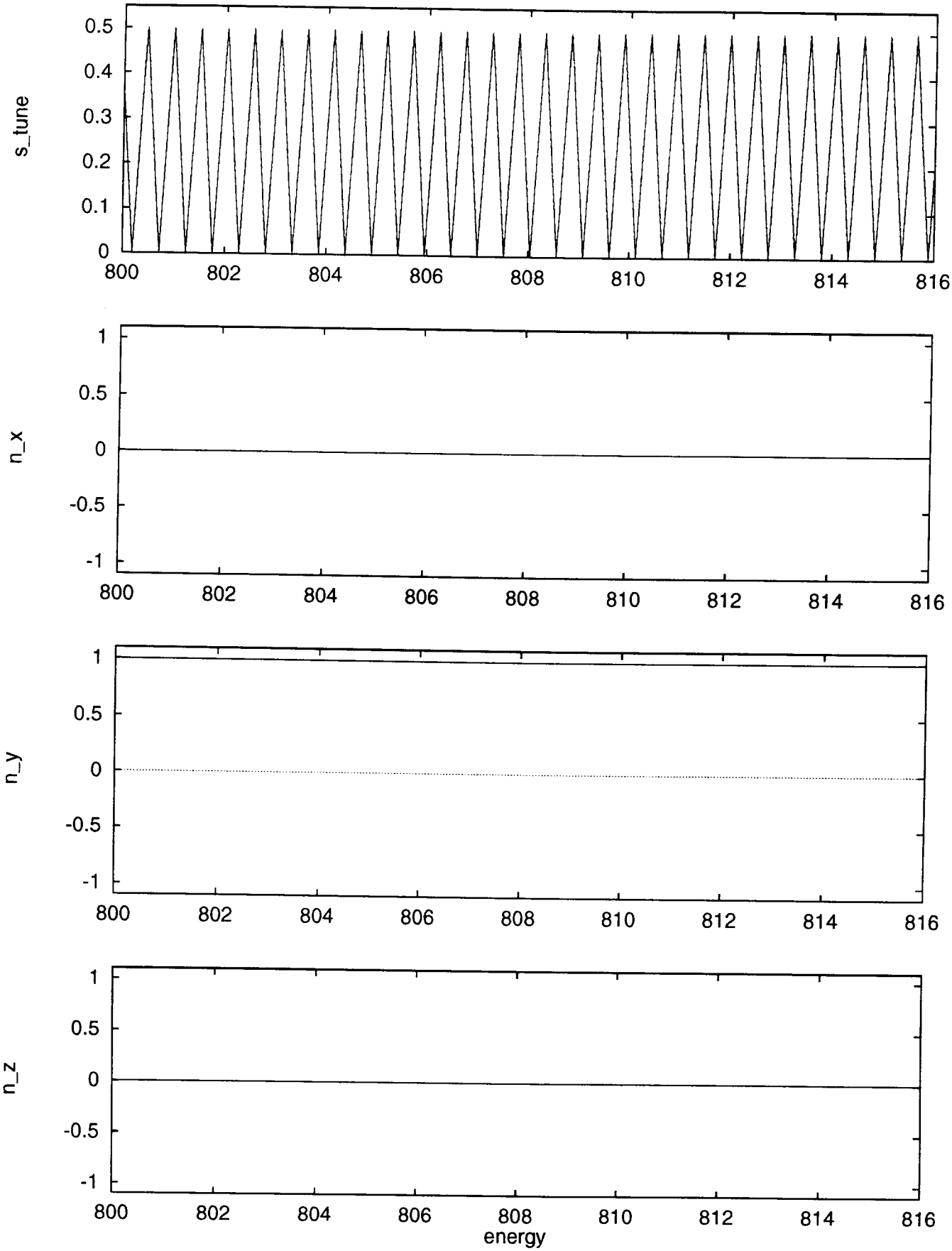

Figure 6: Behaviour of the spin tune and the vector $\vec{n}_0$ with beam energy (GeV) in the flat HERA-p. The view point is the East IP. Here the continuous branches of the spin tune and the vector $\vec{n}_0$ are chosen.

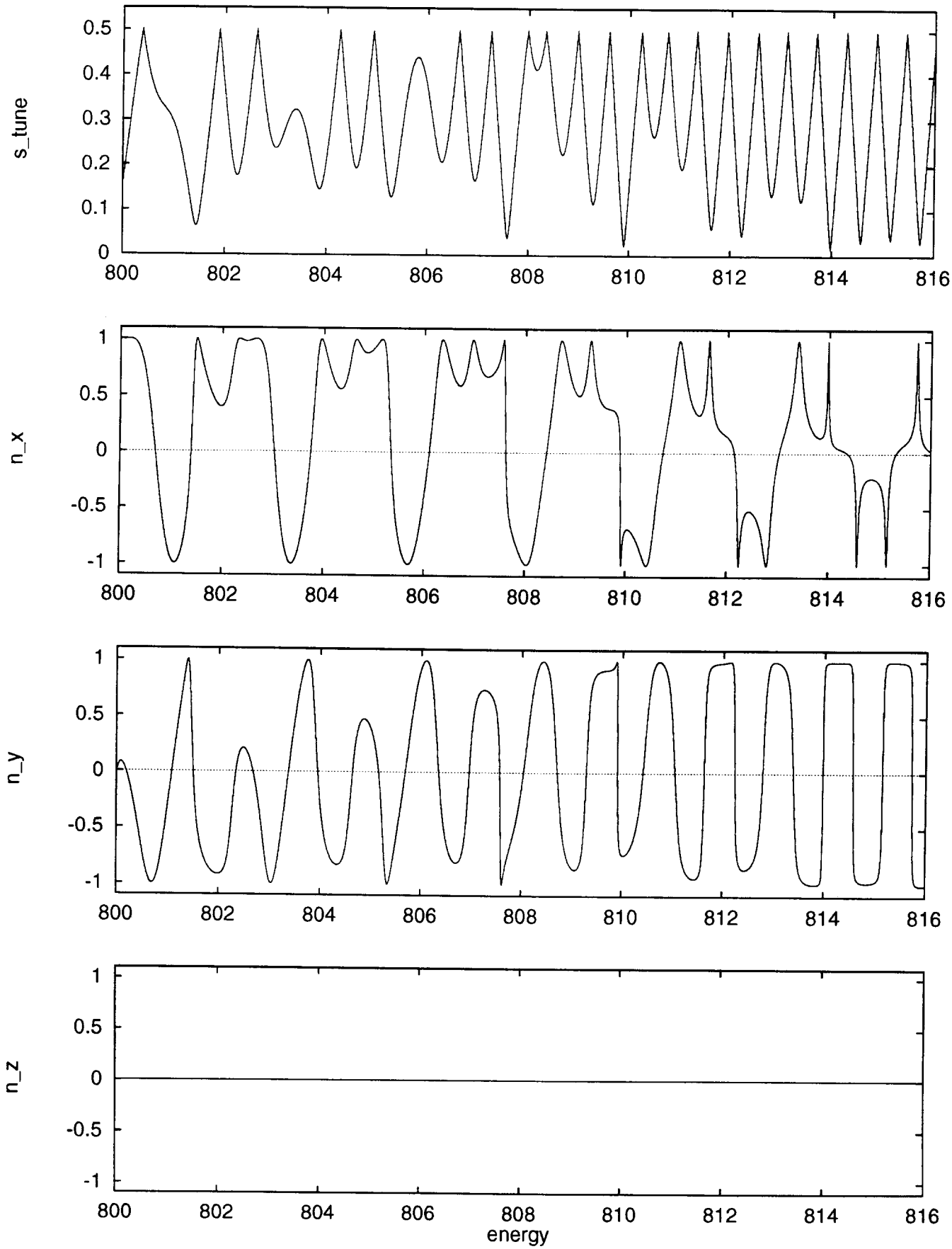

Figure 7: Behaviour of the spin tune and the vector $\vec{n}_0$ with beam energy (GeV) in the nonflat HERA-p. The view point is the East IP. Here the continuous branches of the spin tune and the vector $\vec{n}_0$ are chosen.

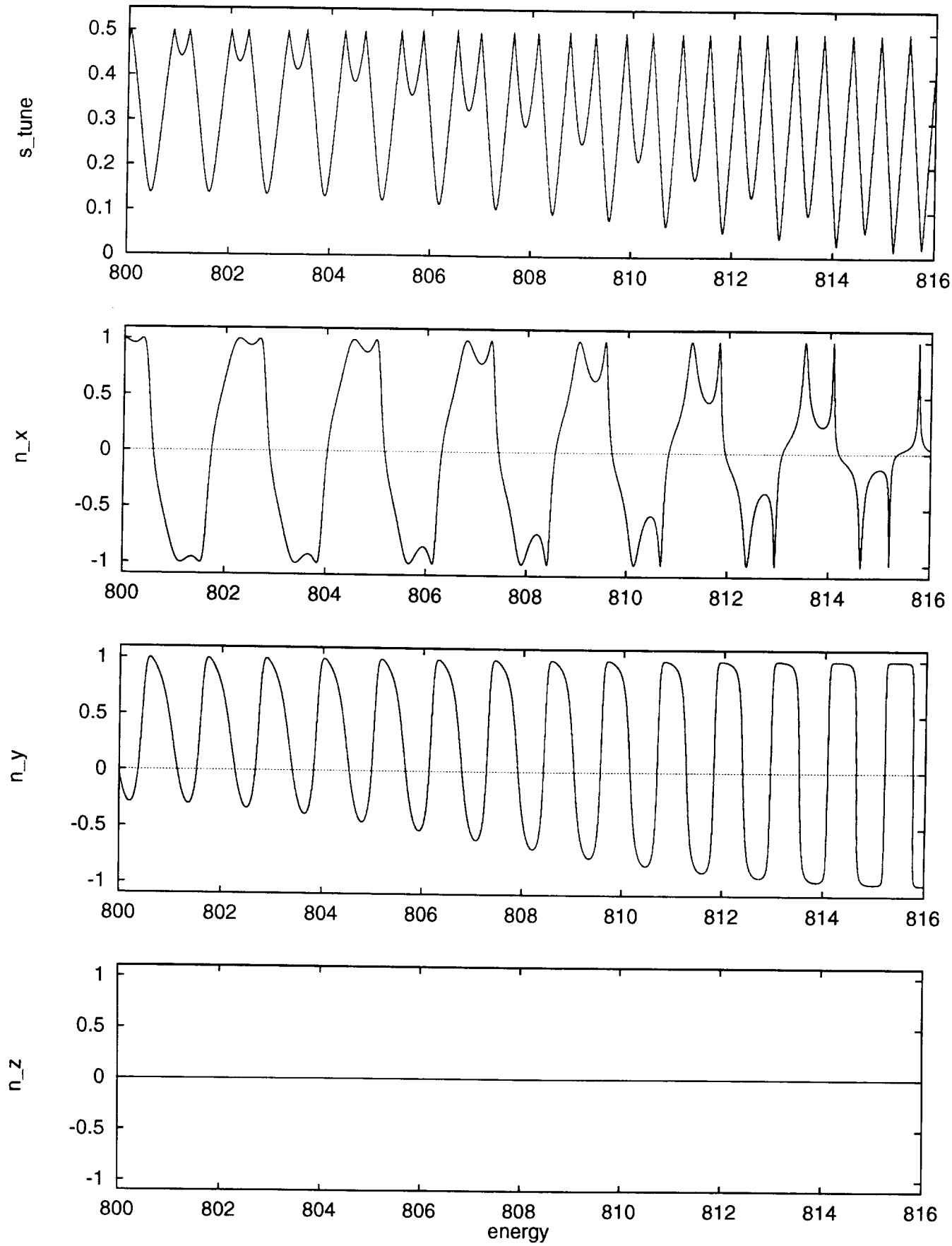

Figure 8: Behaviour of the spin tune and the vector $\vec{n}_0$ with beam energy (GeV) in the nonflat HERA-p (without vertical bends in the East). The view point is the East IP. Here the continuous branches of the spin tune and the vector $\vec{n}_0$ are chosen.

1.6 Siberian Snakes for Nonflat Rings with Mirror Symmetry

We now consider the influence of Siberian Snakes [1]. These are devices which rotate spins around some axis by some fixed angle (very often π). See for example [2].

Consider the mirror symmetrical composition of rotations

$$R(\vec{m}_p, \varphi_p) \circ \ldots \circ R(\vec{m}_1, \varphi_1) \circ R(\vec{m}_1, \varphi_1) \circ \ldots \circ R(\vec{m}_p, \varphi_p) \stackrel{\text{def}}{=} R(\vec{m}, \varphi). \quad (1)$$

The basis of the application of siberian snakes for nonflat rings with mirror symmetrical nonflat sections is the following two theorems proved in [3].

Theorem 1: Let all vectors $\vec{m}_i$, $i = 1, \cdots p$ be orthogonal to some vector $\vec{k}$ then the vector $\vec{m}$ is also orthogonal to the vector $\vec{k}$.

Now introduce a rotation around the vector $\vec{k}$ by an angle π at the point of mirror symmetry of the sequence of rotations (1):

$$R(\vec{m}_p, \varphi_p) \circ \ldots \circ R(\vec{m}_1, \varphi_1) \circ R(\vec{k}, \pi) \circ R(\vec{m}_1, \varphi_1) \circ \ldots \circ R(\vec{m}_p, \varphi_p) \stackrel{\text{def}}{=} R(\vec{m}, \varphi).$$

Theorem 2: Let all vectors $\vec{m}_i$, $i = 1, \ldots p$ be orthogonal to the vector $\vec{k}$. Then the vector $\vec{m}$ is equal to $\vec{k}$ and $\varphi = \pi \ (mod\ 2\pi)$.

Remark: Owing to the conventions adopted in subsection 1.1, in the case when some of the angles $\varphi_i = 0 \ (mod\ 2\pi)$, we choose as the vector $\vec{m}_i$ any vector orthogonal to the vector $\vec{k}$.

According to Theorem 2, any mirror symmetrical section of a nonflat ring which consists of horizontal and vertical bends can be converted into a snake rotating by an angle π around the longitudinal direction by introducing a longitudinal snake (i.e. with $\vec{k}$ chosen so that the rotation is around the longitudinal direction) at the point of mirror symmetry. This opens up wide possibilities for using siberian snakes in a nonflat ring like HERA-p without otherwise changing the lattice.

1.7 Possible Variants for the Placing of Siberian Snakes in Nonflat HERA-p

According the results of the previous section the placing of a longitudinal siberian snake at any interaction point (more precisely at any place between

two nearest bending magnets around this interaction point) makes any mirror symmetrical section with respect to this interaction point equivalent to a longitudinal snake. This could be the basis for the application of siberian snakes in the nonflat HERA-p.

Owing to the group of symmetries (see Fig.1) of the nonflat HERA-p optic the use of from 1 to 8 snakes will make the spin tune (usually 1/2) independent of the energy. $\vec{n}_0$ will also be independent of energy at some point of the ring. As examples, in this paper we consider a few simple variants of snake usage: [2]

1. One longitudinal snake at the West interaction point. In this case the spin tune is 1/2 and we have longitudinal polarization in the East interaction point.

2. Two snakes: one longitudinal snake in the West IP and one radial snake in the East section. The spin tune is equal 1/2 and $\vec{n}_0$ is vertical at the East IP at all energies (Fig.9).

3. Two snakes: one snake at the West IP and one snake in the East IP (snake axis is $\pm 45°$ from the beam direction). The spin tune is equal 1/2 and $\vec{n}_0$ is vertical. This configuration is used only for the flat test model.

4. Three longitudinal snakes: one at the South, the West and the North IP respectively. The spin tune is equal 1/2 and $\vec{n}_0$ is longitudinal at the East IP at all energies.

5. Four snakes: one longitudinal snake at the South, the West and the North IP respectively and one radial snake at the East IP. The spin tune is equal 1/2 and $\vec{n}_0$ is vertical at the East IP at all energies.

6. Four snakes: one snake in each IP (snake axis is $\pm 22.5°$ from the beam direction). The spin tune is equal 1/2 and $\vec{n}_0$ is vertical. This configuration is used only for the flat test model.

[2] In this report we always work with idealized snakes which influence all the spins in the same way independently of their position in phase space and which do not influence the orbit.

7. Four snakes: one longitudinal snake at the West and radial snake at the North, South and East IP respectively. The spin tune is equal 1/2 and $\vec{n}_0$ is vertical at the East IP at all energies.

Naturally, it would not be possible to place snakes right at the IP's in practice. However, by calculating with snakes at the interaction points we maintain a simple layout while still extracting the main features of the spin behaviour. Other snake positioning configurations will be investigated in a future paper.

1.8 Simple Examples of Misalignments

Figs.10-11 show the behaviour of the spin tune ν_s^0 and the vector $\vec{n}_0$ in the nonflat HERA-p without vertical bends in the East with two snakes which have errors. In Fig.10 both snakes have 1° error in the rotation angle. In Fig.11 both snakes have 1° error of the snake axis.

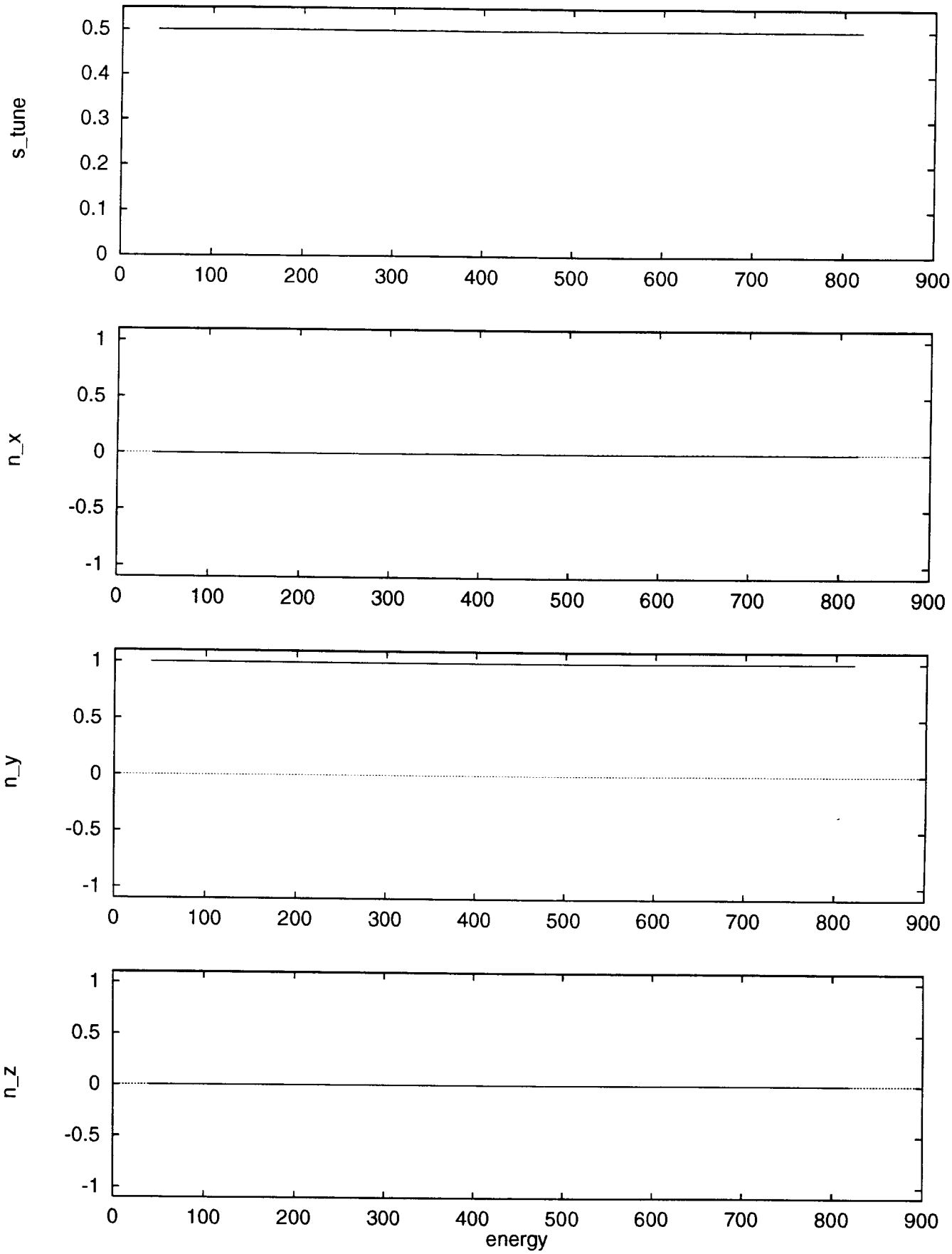

Figure 9: Behaviour of the spin tune and the vector $\vec{n}_0$ with beam energy (GeV) in the nonflat HERA-p (without vertical bends in the East) with two snakes (longitudinal snake in the West and radial snake in the East). The view point is the East IP. Here the continuous branches of the spin tune and the vector $\vec{n}_0$ are chosen.

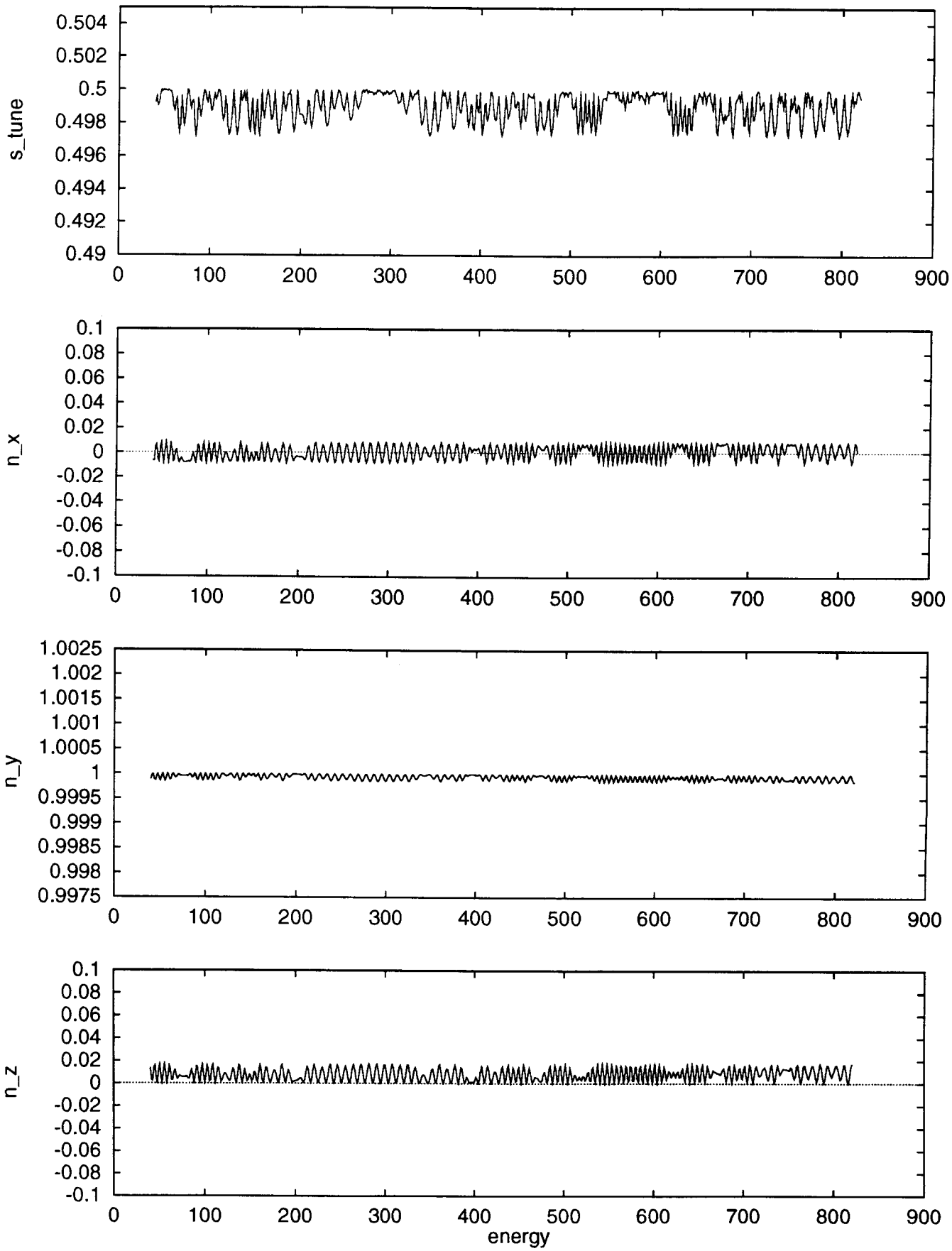

Figure 10: Behaviour of the spin tune and the vector $\vec{n}_0$ with beam energy (GeV) in the nonflat HERA-p (without vertical bends in the East) with two snakes (longitudinal snake in the West and radial snake in the East). Both snakes have 1° error in the rotation angle. The view point is the East IP.

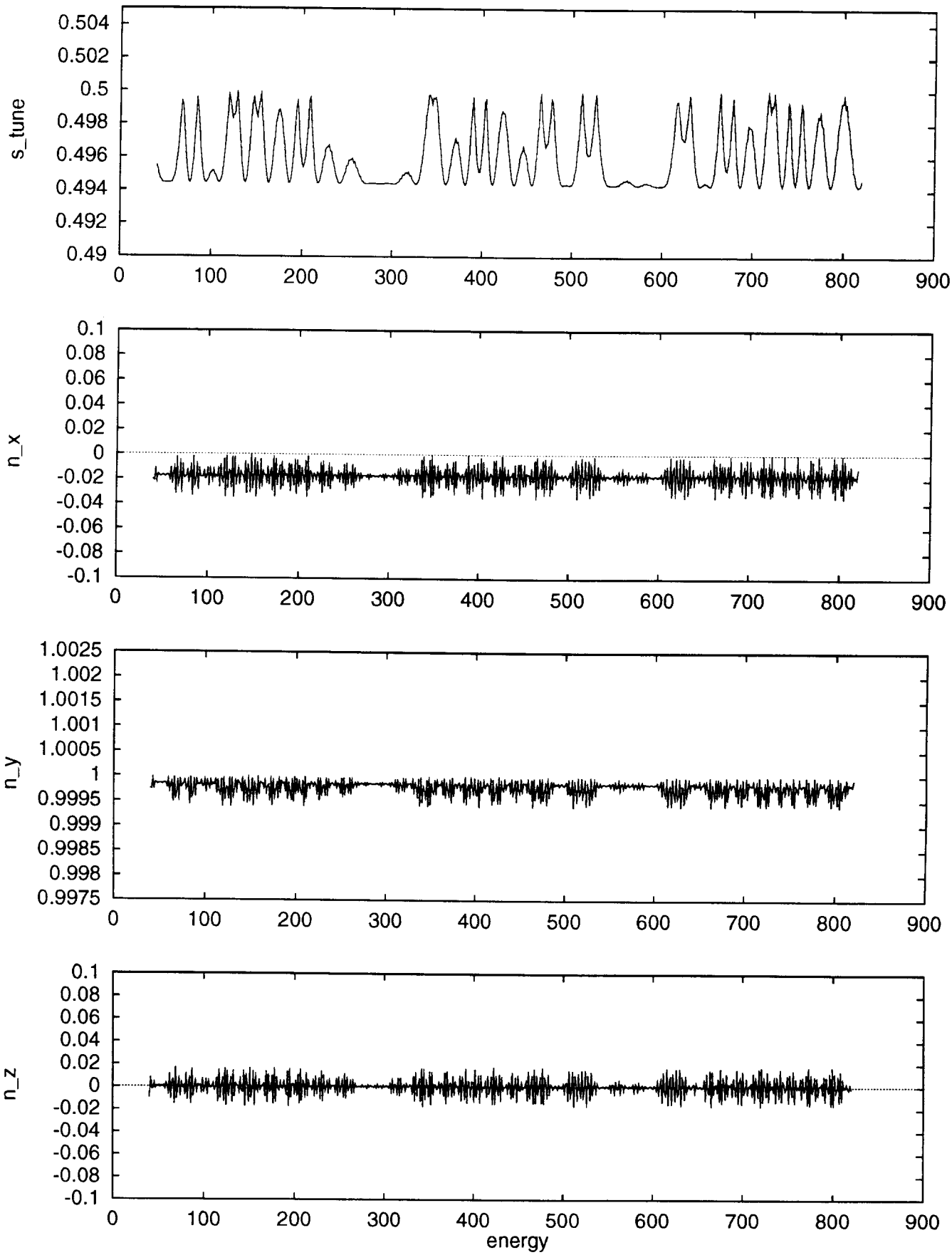

Figure 11: Behaviour of the spin tune and the vector $\vec{n}_0$ with beam energy (GeV) in the nonflat HERA-p (without vertical bends in the East) with two snakes (longitudinal snake in the West and radial snake in the East). Both snakes have 1° error of the direction of the snake axis. The view point is the East IP.

1.9 Behaviour of $\vec{n}_0$ along the Ring

The placing of siberian snakes in the nonflat HERA-p mentioned above guarantees that when there are no imperfections the vector $\vec{n}_0$ at the chosen interaction point will have a certain fixed direction at all energies.

But it is interesting to see how the vector $\vec{n}_0$ varies around the ring. In flat rings with snakes the behaviour of the vector $\vec{n}_0$ is usually fairly simple. It is vertical and rotates by the angle π in the snakes. The behaviour of the vector $\vec{n}_0$ along the nonflat HERA-p ring at two different energies is shown in Figs.12-13. In Fig.12 the energy is chosen so that the spin rotates by an integer number of times in the 60.4 mrad horizontal bends between the vertical bends.

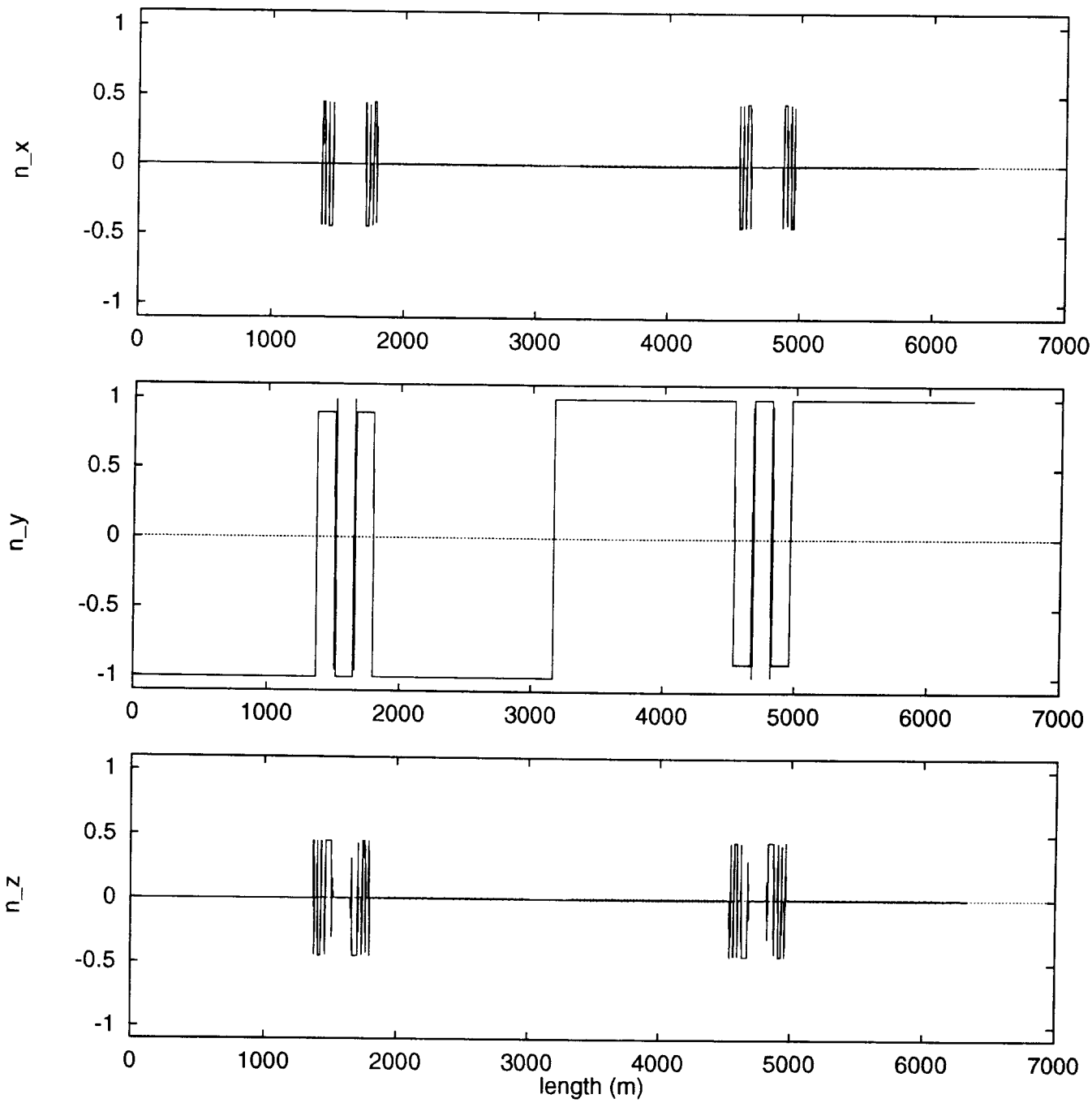

Figure 12: Behaviour of the vector $\vec{n}_0$ along the ring at E = 816.4 Gev in the nonflat HERA-p (without vertical bends in the East) with two snakes (longitudinal snake in the West and radial snake in the East). The view point is the East IP.

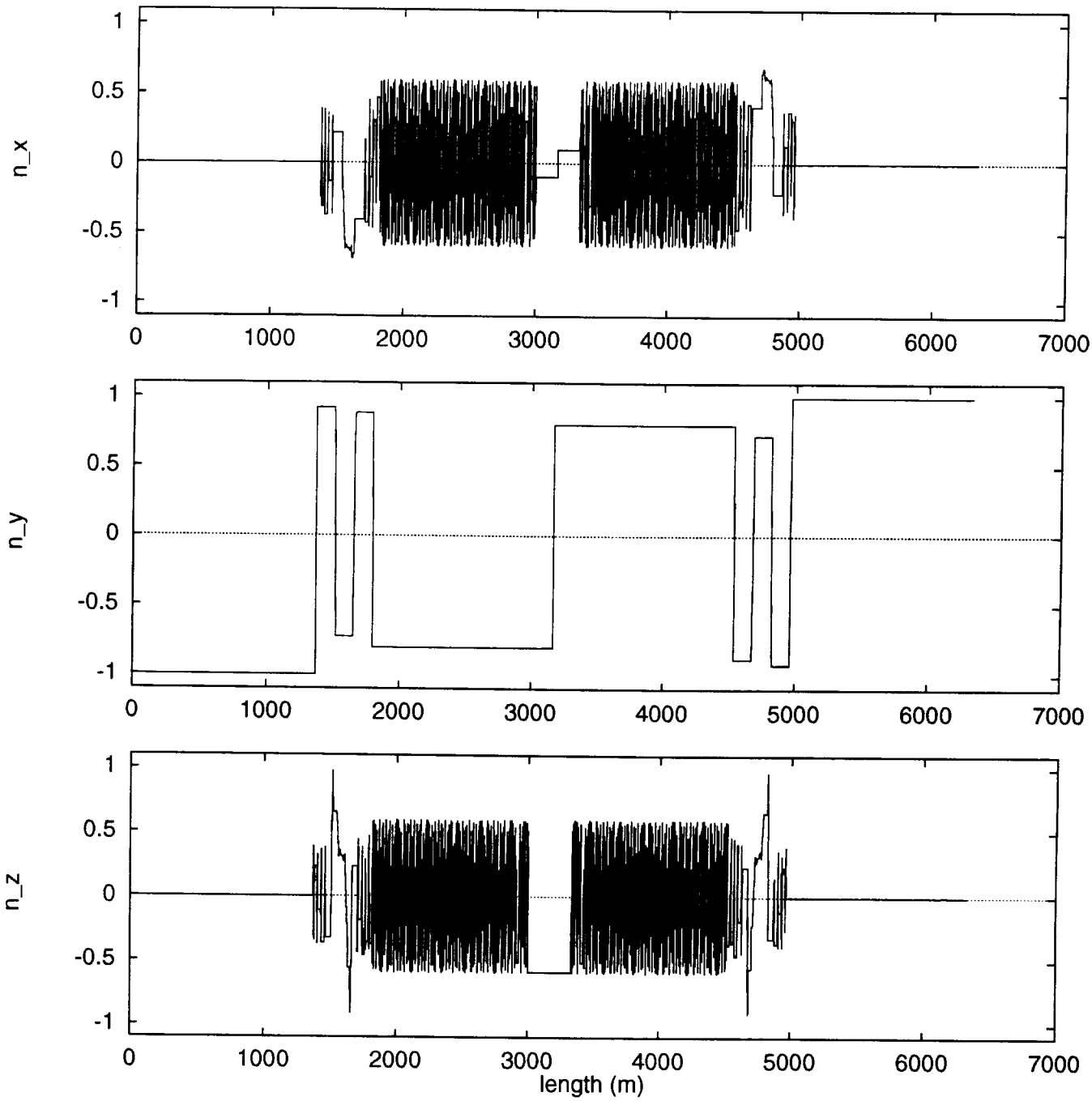

Figure 13: Behaviour of the vector $\vec{n}_0$ along the ring at E = 250 Gev in the nonflat HERA-p (without vertical bends in the East) with two snakes (longitudinal snake in the West and radial snake in the East). The view point is the East IP.

2 Strengths of the Linear Intrinsic Resonances caused by Betatron Oscillations

In addition to the fields in the dipole magnets, the spins experience the off-axis fields in the quadrupoles and in higher multipoles. The resulting additional disturbance can be very strong if there is coherence between the zeroth order spin motion (due to the dipole fields) and the synchrobeta motion characterized by the spin-orbit resonance condition:

$$\nu_s^0 = \pm l_x Q_x \pm l_y Q_y \pm l_z Q_z \qquad (mod\ 1) \tag{2}$$

where the l's are integers and the Q's are respectively the horizontal, vertical and longitudinal tunes of the orbital oscillations.

The order of a resonance is defined as $|l_x| + |l_y| + |l_z|$. Thus the first order resonances are those for which $|l_x| + |l_y| + |l_z| = 1$. The first order resonances for which $|l_x| = 1$ or $|l_y| = 1$ are often called the linear intrinsic resonances. A useful measure of the strength of the intrinsic resonances can be obtained as follows.

2.1 Definition of Linear Spin Resonance Strength associated with Betatron Oscillations

The spin Hamiltonian is:

$$H(\tau, \vec{u}, \vec{s}) = \vec{w}_0(\tau) \cdot \vec{s} + \vec{w}_\varepsilon(\tau, \vec{u}) \cdot \vec{s},$$

where $\vec{u} = (x, p_x, y, p_y, z, p_z)$ is the vector of orbital coordinates and τ is the length along the ring. $\vec{w}_0(\tau + L) \equiv \vec{w}_0(\tau)$ is a periodic vector determining the spin motion along the periodic orbit of the accelerator (L is the total ring length). $\vec{w}_\varepsilon(\tau, \vec{u})$ describes the perturbation of the spin motion due to betatron and synchrotron oscillations around the periodic orbit. z describes the longitudinal separation of the particle from the centre of the bunch, p_z is proportional to the fractional energy deviation of the particle: $p_z = \Delta E/(\beta_0^2 E_0)$. Note that the explicit dependence on z appears in $\vec{w}_\varepsilon$ only in terms of second order due to the rf cavities.

Let $A(\tau, \tau_0)$ be the transfer matrix describing the general solution of the spin motion on the periodic orbit and let $\vec{n}_0(\tau_0)$ be the eigenvector of the

one-turn revolution matrix:

$$A(\tau_0 + L, \tau_0)\ \vec{n}_0(\tau_0) = \vec{n}_0(\tau_0), \quad \mid \vec{n}_0(\tau_0) \mid = 1.$$

Introduce the vector

$$\vec{w}_r(\tau_0, \vec{u}_0) = \lim_{T\to\infty} \frac{1}{T} \int_{\tau_0}^{\tau_0+T} A^{-1}(\tau, \tau_0)\vec{w}_\varepsilon(\tau, \vec{u}(\tau, \tau_0, \vec{u}_0))d\tau \tag{3}$$

where $\vec{u}(\tau, \tau_0, \vec{u}_0)$ is the solution of the linearized equations of the orbital oscillations.

Divide $\vec{w}_r$ into two parts: $\parallel$ and $\perp$ to $\vec{n}_0(\tau_0)$:

$$(\vec{w}_r(\tau_0, \vec{u}_0) \cdot \vec{n}_0(\tau_0))\ \vec{n}_0(\tau_0)\ ,$$

$$\vec{v}_r(\tau_0, \vec{u}_0) = \vec{w}_r(\tau_0, \vec{u}_0) - (\vec{w}_r(\tau_0, \vec{u}_0) \cdot \vec{n}_0(\tau_0))\ \vec{n}_0(\tau_0)$$

It is easy to see that the norm of the vector $\vec{v}_r$ and the projection of the vector $\vec{w}_r$ on the vector $\vec{n}_0$ do not depend on the choice of τ_0.

The resonance strength is defined as [8]

$$\varepsilon_{\mathbf{r}}(\vec{u}_0) = \frac{L}{2\pi} \mid \vec{v}_r(0, \vec{u}_0) \mid .$$

The spin tune shift is defined as:

$$\lambda_{\mathbf{r}}(\vec{u}_0) = \frac{L}{2\pi}\vec{w}_r(0, \vec{u}_0) \cdot \vec{n}_0(0).$$

In the case when the synchrotron frequency is very small compared to the other frequencies in the system (as in the case of HERA-p) it is not necessary to carry out the averaging in (3) along trajectories of the 6-D linearized equations of the orbital motion. Instead, it is sufficient to average along the trajectories of the 4-D linearized equations of the betatron motion at fixed z, p_z.

Remark: In general, the spin tune shift is nonzero even if we are not on resonance. We will need it for the later investigations.

2.2 Effects which are Included in the Resonance Strength Calculations

In these calculations we take $\vec{w}_\varepsilon(\tau, \vec{u})$ in the form:

$$\vec{w}_\varepsilon(\tau, \vec{u}) = -(1 + \gamma_0 G)(\vec{a}_\varepsilon(\tau, \vec{u}) + p_z \vec{b}_\varepsilon(\tau)).$$

where

$$a_\varepsilon^x = \left(k - \alpha^2 + \tan(\xi)\left(\alpha' - h'\right)\right) y,$$

$$a_\varepsilon^y = \left(k + h^2 + \tan(\xi)\left(\alpha' - h'\right)\right) x,$$

$$a_\varepsilon^z = \frac{(1 - \gamma_0)G(hp_y - \alpha p_x) + (1 + G)\left(h'y - \alpha' x\right)}{1 + \gamma_0 G},$$

$$b_\varepsilon^x = \left(k - \alpha^2 + \tan(\xi)\left(\alpha' - h'\right)\right) D_y + \frac{(1 + \gamma_0^{-1} G)\alpha}{1 + \gamma_0 G},$$

$$b_\varepsilon^y = \left(k + h^2 + \tan(\xi)\left(\alpha' - h'\right)\right) D_x - \frac{(1 + \gamma_0^{-1} G)h}{1 + \gamma_0 G},$$

$$b_\varepsilon^z = \frac{(1 - \gamma_0)G(hD_{p_y} - \alpha D_{p_x}) + (1 + G)\left(h' D_y - \alpha' D_x\right)}{1 + \gamma_0 G},$$

and γ_0 is the Lorentz factor. $G = (g - 2)/2$ quantifies the anomalous spin g factor. h and α are the curvatures in the horizontal and vertical directions respectively and k is the quadrupole strength. $D_x, D_y, D_{p_x}, D_{p_y}$ are dispersion functions. $\xi(\tau)$ is the edge angle for a rectangular magnet.

The above expressions for $\vec{a}_\varepsilon$ and $\vec{b}_\varepsilon$ indicate that we include only terms linear in the orbit motion and that the cavities are neglected.

It is easy to see from the above expressions that in the case of first order spin-orbit resonances due to betatron oscillations the resonance strengths do not depend on z and p_z and that in the case where p_z is fixed the spin tune shift is proportional to p_z.

In the case of the flat ring ($\alpha = 0$) and no synchrotron oscillations the definition of the resonance strength given above transforms into the definition used in the program DEPOL [4]. Test calculations have shown better than 1% agreement between the results obtained, using the long term averaging (3) and the program DEPOL.

2.3 Spin Resonance Strengths for Flat and Nonflat HERA-p

The resonance strengths for first order Q_x and Q_y resonances for flat and nonflat HERA-p are shown in Fig.14.

For Figs.14-21 there are no snakes in the ring.

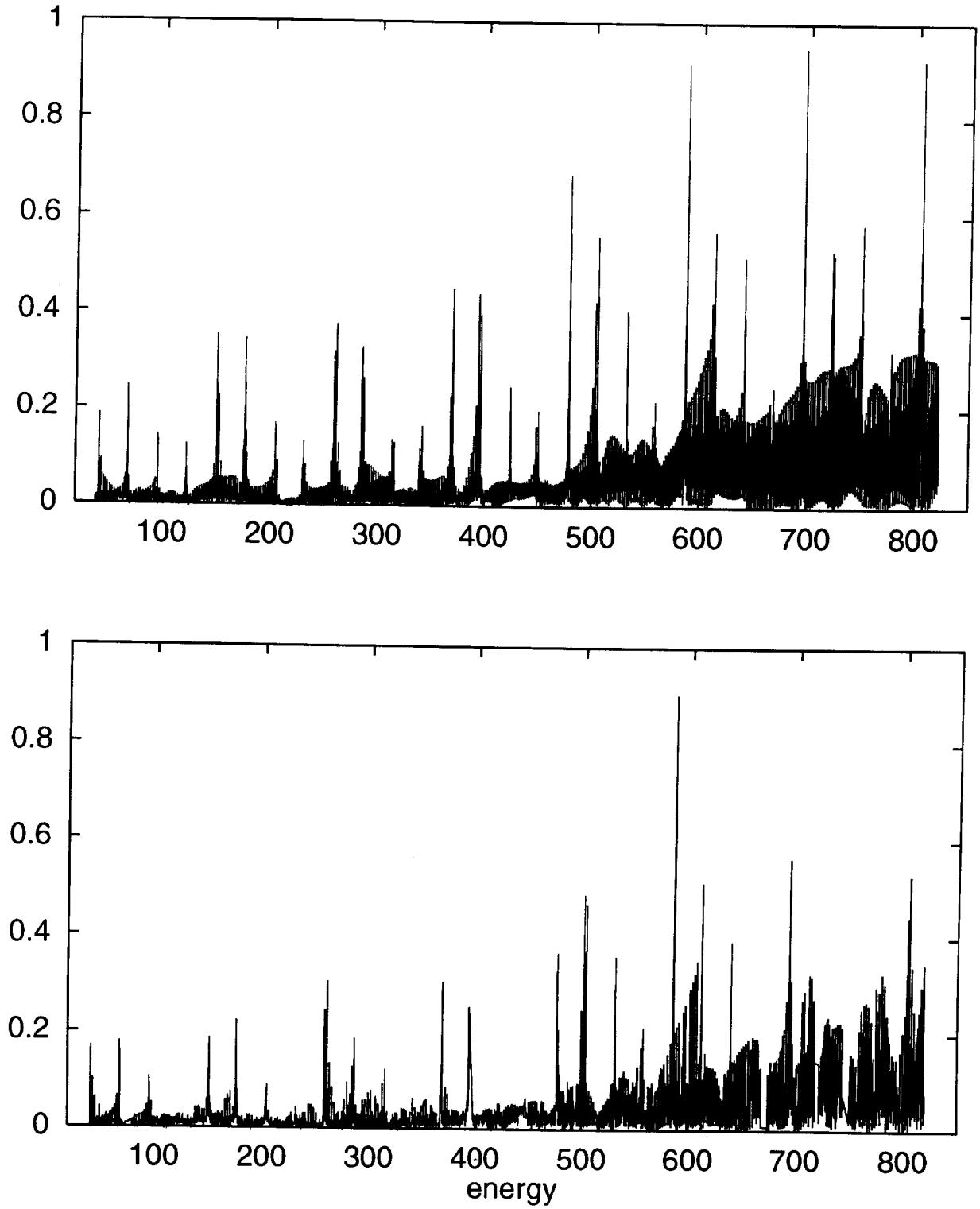

Figure 14: Strengths of linear intrinsic spin resonances with betatron oscillations calculated with help of averaging method. Top: for flat HERA-p. Bottom: for nonflat HERA-p. Tracking of N = 1 particle for 50 turns. Emittances: $\varepsilon_x = \varepsilon_y = 10 \cdot 10^{-6}\ \pi\ m \cdot rad.$

2.4 Spin Tune Modulation due to Synchrotron Oscillations

For the effects included above the spin tune shift can be written as

$$\lambda_r(\vec{u}) = \lambda_0 \cdot p_z$$

where λ_0 is constant for the fixed energy E_0 ($\gamma = \gamma_0$). The spin tune shift λ_r is important even if we are not exactly at the resonances defined by

$$\nu_s^0 = \pm l_x Q_x \pm l_y Q_y \ \ (mod\ 1)$$

because if $\lambda_r \neq 0$, the modulated spin tune

$$\nu_s^0 + \lambda_r$$

may satisfy the resonance conditions for some values of p_z. This means that we may have periodic crossing of spin resonances due to synchrotron oscillations. As in NMR this can cause spin flip. The direction of the spin tune shift depends on the sign of p_z. Fig.15 shows the result of a tracking calculation [3] where we have two vertical betatron (Q_y) resonances lying to the left and right of ν_s^0 at distances $\Delta\nu_s^0 = -0.14$ and $\Delta\nu_s^0 = 0.44$, respectively. During one period (approximately 1600 turns) of synchrotron oscillation the spin feels the effect of both of these resonances. But the furthest resonance has a weaker effect. For details see Fig.15 where the behaviour of the spin of two particles in the flat HERA-p is shown. The upper picture shows the behaviour of the particle which has $z = -z_{max}$ at the start and after a quarter of a synchrotron period has $p_z = -1.6 \cdot 10^{-4}$. In this case this particle crosses the nearest resonance first. After three quarters of a synchrotron period when $p_z = 1.6 \cdot 10^{-4}$, this particle crosses the other resonance. The lower picture shows the opposite situation, when initially $z = z_{max}$. This particle first crosses the furthest resonance and then the nearest resonance.

[3] Some details of the tracking algorithm and the references needed are given in section 3.2.

Fig.16 shows the same effect for the nonflat HERA-p.

Such periodic crossing of resonances may lead the initially polarized beam to become fully depolarized after several synchrotron periods. This situation is shown in Fig.17. [4] The top figure is the ensemble average $< \vec{s} \cdot \vec{n}_0 >$ of $\vec{s} \cdot \vec{n}_0$. The bottom figure is the dispersion of the spins, $D\vec{s}$, defined as the ensemble average of $| \vec{s} \cdot \vec{n}_0 - < \vec{s} \cdot \vec{n}_0 > |$.

A decrease of the value of longitudinal emittance weakens this effect and in principle it completely disappears if the longitudinal emittance is small enough. Fig.18 shows the spin motion at two values of longitudinal emittances. The lower picture is for the characteristic longitudinal emittance for HERA-p. Now the effect is not so evident as before, but if we look more carefully, we can see that small depolarization takes place even after three periods of the synchrotron oscillations. This characteristic value of the longitudinal emittance will be used in all the calculations that follow.

In the captions of figures we write the longitudinal emittance in the units which are used in the tracking code. The value $\varepsilon_z = 1.5 \cdot 10^{-5}\, m \cdot rad$ corresponds to $\varepsilon_z = 0.04\, eV \cdot s$.

[4] In all multiparticle tracking simulations discussed in this report, the particles are initially distributed uniformly along the perimeters of the phase space ellipses corresponding to the chosen emittances and with the spins initially set parallel to $\vec{n}_0$. In this paper the term 'emittance', when applied to the transverse motion means the adiabatically invariant emittance.

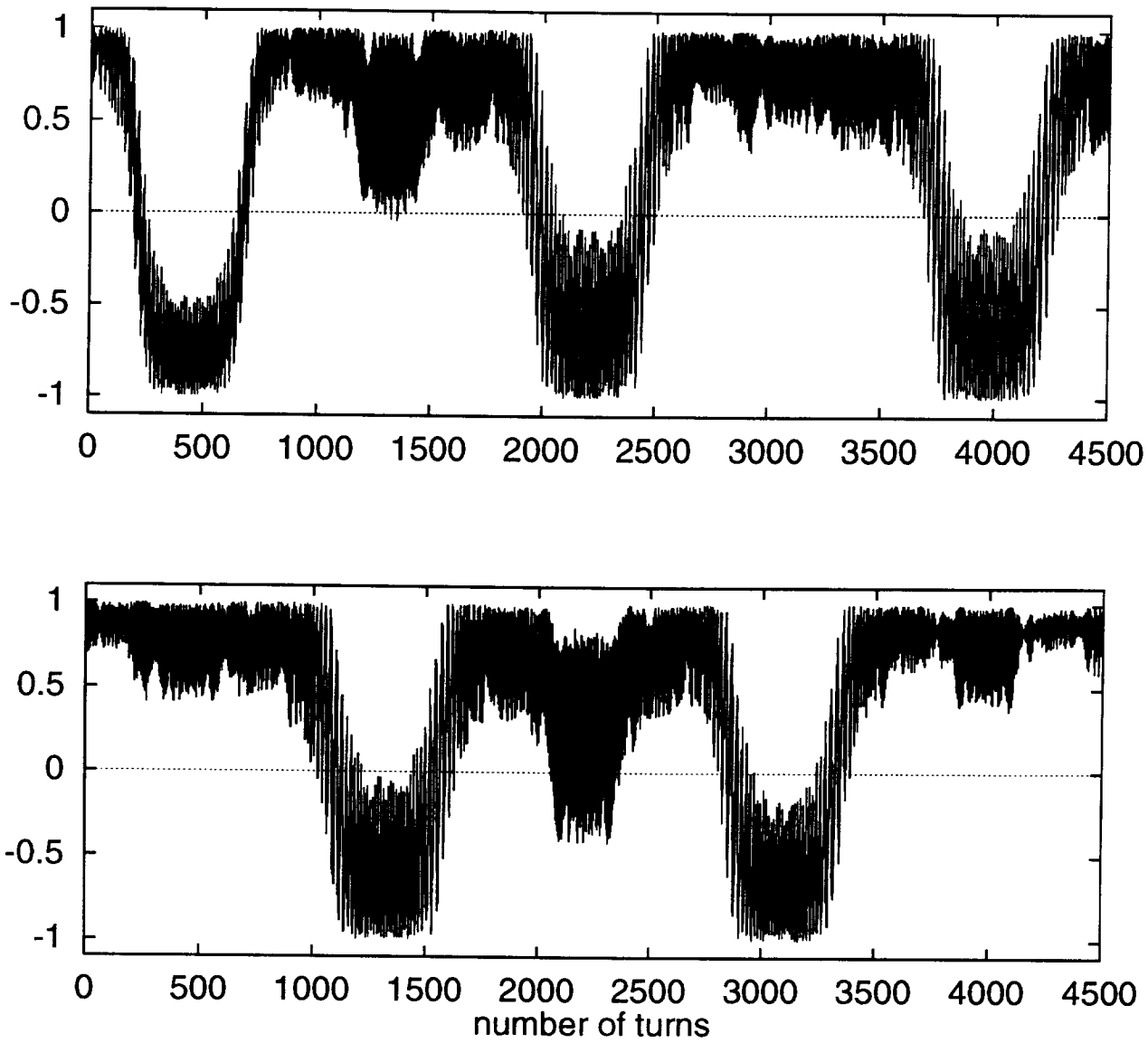

Figure 15: Spin flipping due to spin tune modulation by synchrotron oscillations in the flat HERA-p at E = 820 GeV. The view point is the East IP. Tracking of N = 1 particle for 4500 turns. The vertical axis: $< \vec{s} \cdot \vec{n}_0 >$. Emittances: $\varepsilon_x = 4.0 \cdot 10^{-6}\, \pi\, m \cdot rad$, $\varepsilon_y = 4.0 \cdot 10^{-6}\, \pi\, m \cdot rad$, $\varepsilon_z = 5.0 \cdot 10^{-5}\, m \cdot rad$ $((\Delta p/p_0)_{max} = 1.6 \cdot 10^{-4})$. Top: $z_0 = -z_{max}$, $p_{z0} = 0.0$. Bottom: $z_0 = z_{max}$, $p_{z0} = 0.0$.

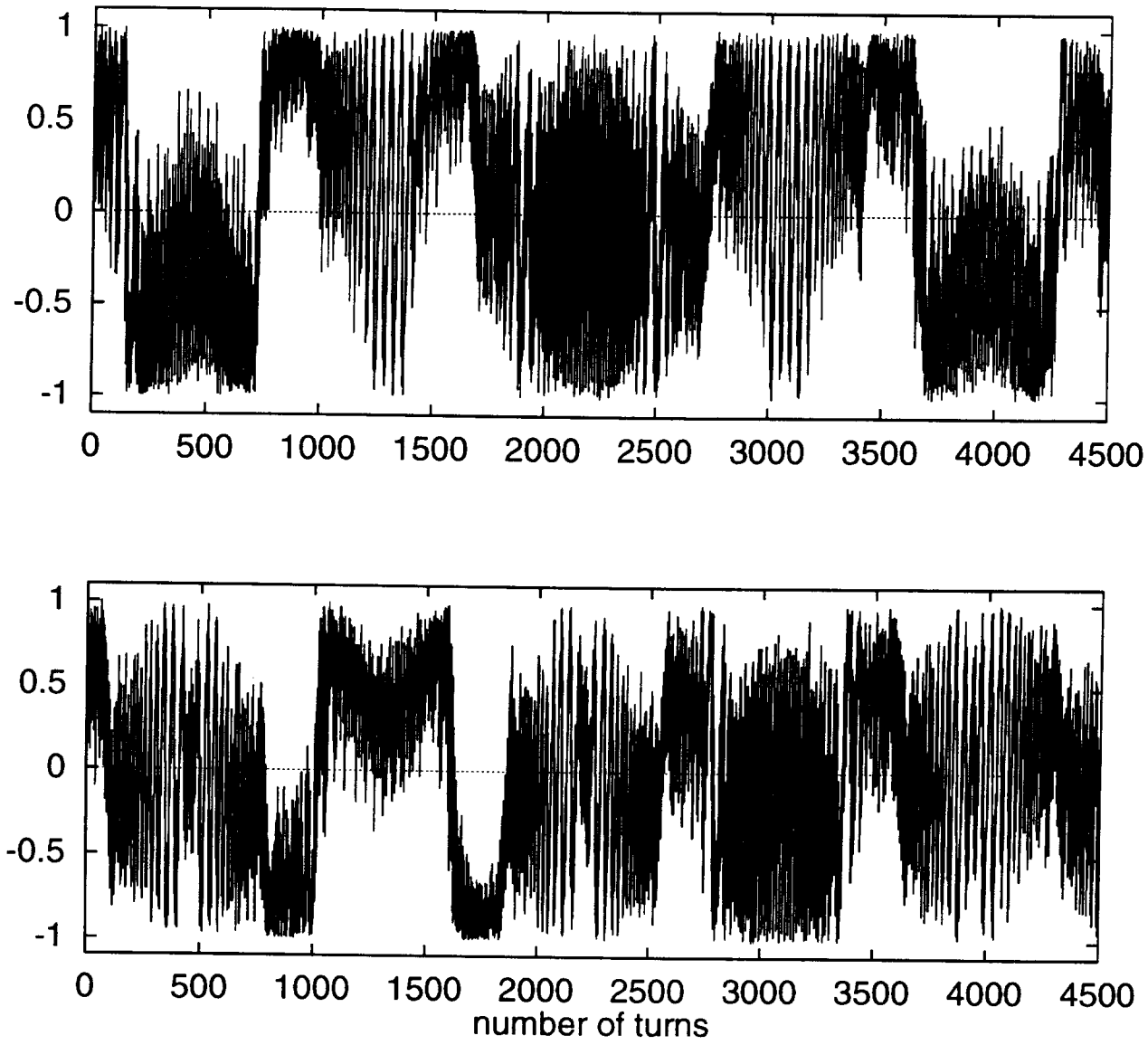

Figure 16: Spin flipping due to spin tune modulation by synchrotron oscillations in the nonflat HERA-p at E = 820 GeV. The view point is the East IP. Tracking of N = 1 particle for 4500 turns. The vertical axis: $< \vec{s} \cdot \vec{n}_0 >$. Emittances: $\varepsilon_x = 4.0 \cdot 10^{-6}\, \pi\, m \cdot rad$, $\varepsilon_y = 4.0 \cdot 10^{-6}\, \pi\, m \cdot rad$, $\varepsilon_z = 5.0 \cdot 10^{-5}\, m \cdot rad$ $((\Delta p/p_0)_{max} = 1.6 \cdot 10^{-4})$. Top: $z_0 = -z_{max}$, $p_{z0} = 0.0$. Bottom: $z_0 = z_{max}$, $p_{z0} = 0.0$.

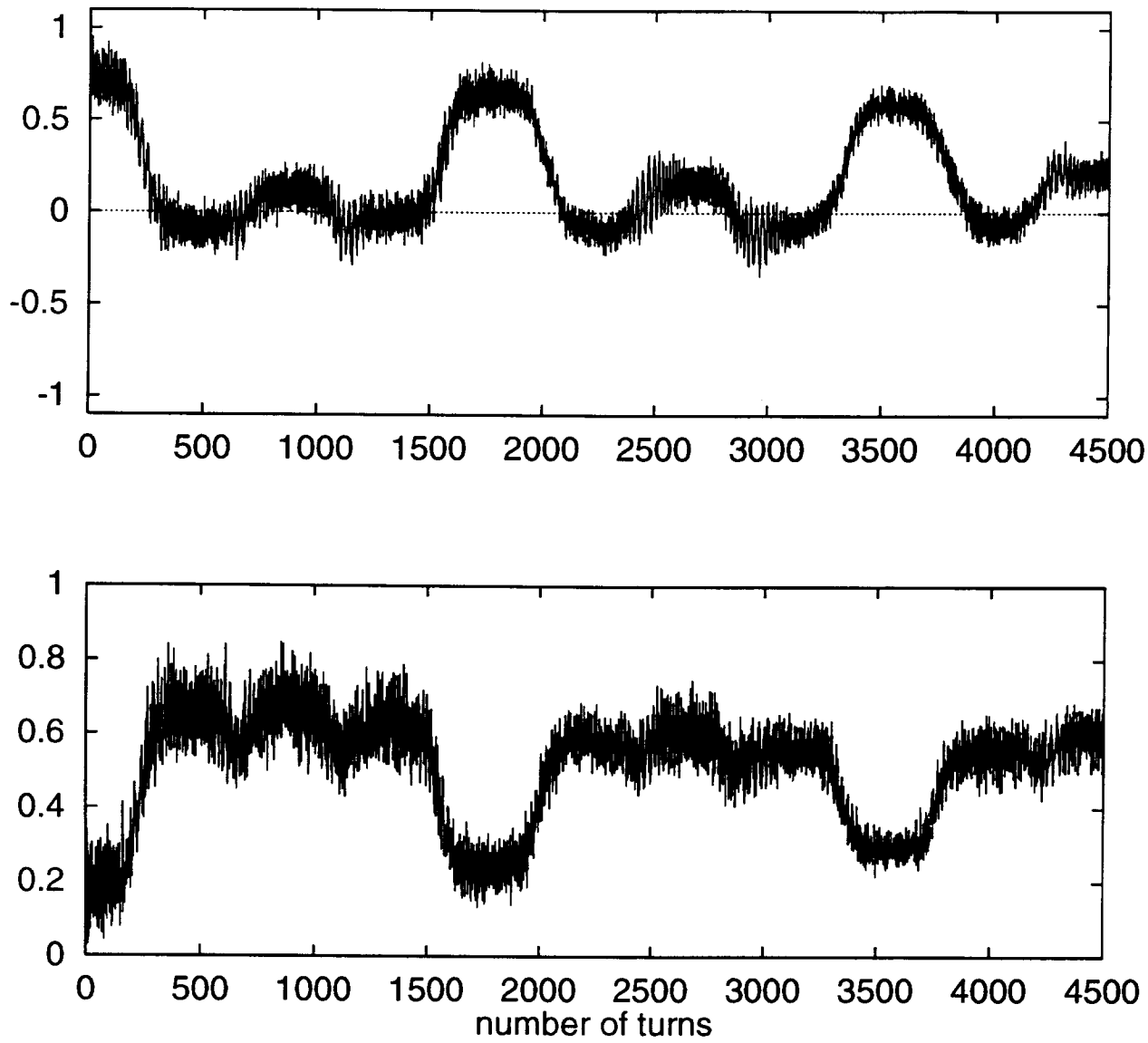

Figure 17: Flat HERA-p at E = 820 GeV. The view point is the East IP. Tracking of N = 64 particles for 4500 turns. Top: $< \vec{s} \cdot \vec{n}_0 >$. Bottom: $D\vec{s}$. Emittances: $\varepsilon_x = 4.0 \cdot 10^{-6}\,\pi\, m \cdot rad$, $\varepsilon_y = 4.0 \cdot 10^{-6}\,\pi\, m \cdot rad$, $\varepsilon_z = 5.0 \cdot 10^{-5} m \cdot rad$.

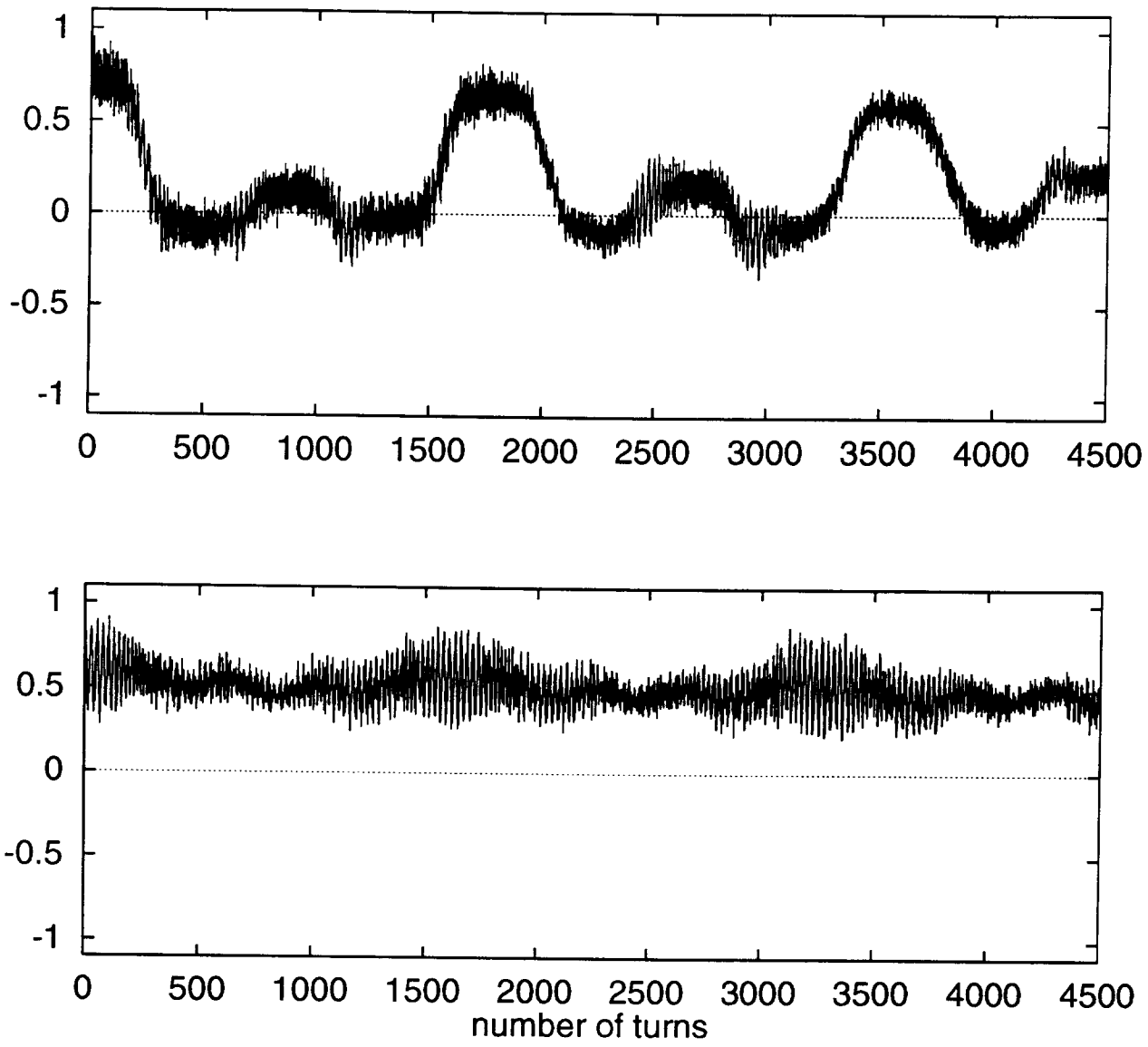

Figure 18: Flat HERA-p at E = 820 GeV for different values of longitudinal emittances. The view point is the East IP. Tracking of N = 64 particles for 4500 turns. The vertical axis: $< \vec{s} \cdot \vec{n}_0 >$. Emittances: $\varepsilon_x = 4.0 \cdot 10^{-6}\, \pi\, m \cdot rad$, $\varepsilon_y = 4.0 \cdot 10^{-6}\, \pi\, m \cdot rad$. Top: $\varepsilon_z = 5.0 \cdot 10^{-5} m \cdot rad$. Bottom: $\varepsilon_z = 1.5 \cdot 10^{-5} m \cdot rad$.

Figs.19-20 show the spin motion in the nonflat HERA-p with and without vertical bends in the East, respectively. The optic of the nonflat HERA-p at the energy considered is very close to the first order spin resonances $Q_x+\nu_s^0 = 0.002$ and $Q_y + \nu_s^0 = 0.024$ (the fractional part of the spin tune is 0.7357). We see fast depolarization during the first few turns (Fig.19). In the case of the optic without vertical bends in the East (in this case the fractional part of the spin tune is 0.4807) we do not observe such depolarization during the first few turns (Fig.20). But in both cases (Figs.19-20), already after about 400 turns, the slow oscillatory behaviour of $< \vec{s} \cdot \vec{n}_0 >$ is dominated by the spin tune modulation which in turn is driven by the synchrotron oscillations [5]. This is confirmed by inspection of Fig.21 where the spin motion is studied for zero longitudinal emittance and without the effects of RF cavities on spin-orbit motion.

In all further calculations the 'nonflat HERA-p' will have no vertical bends in the East.

[5] For the optic without vertical bends in the East we have slightly different betatron and spin tunes and we are not so close to spin resonances as for Fig.19.

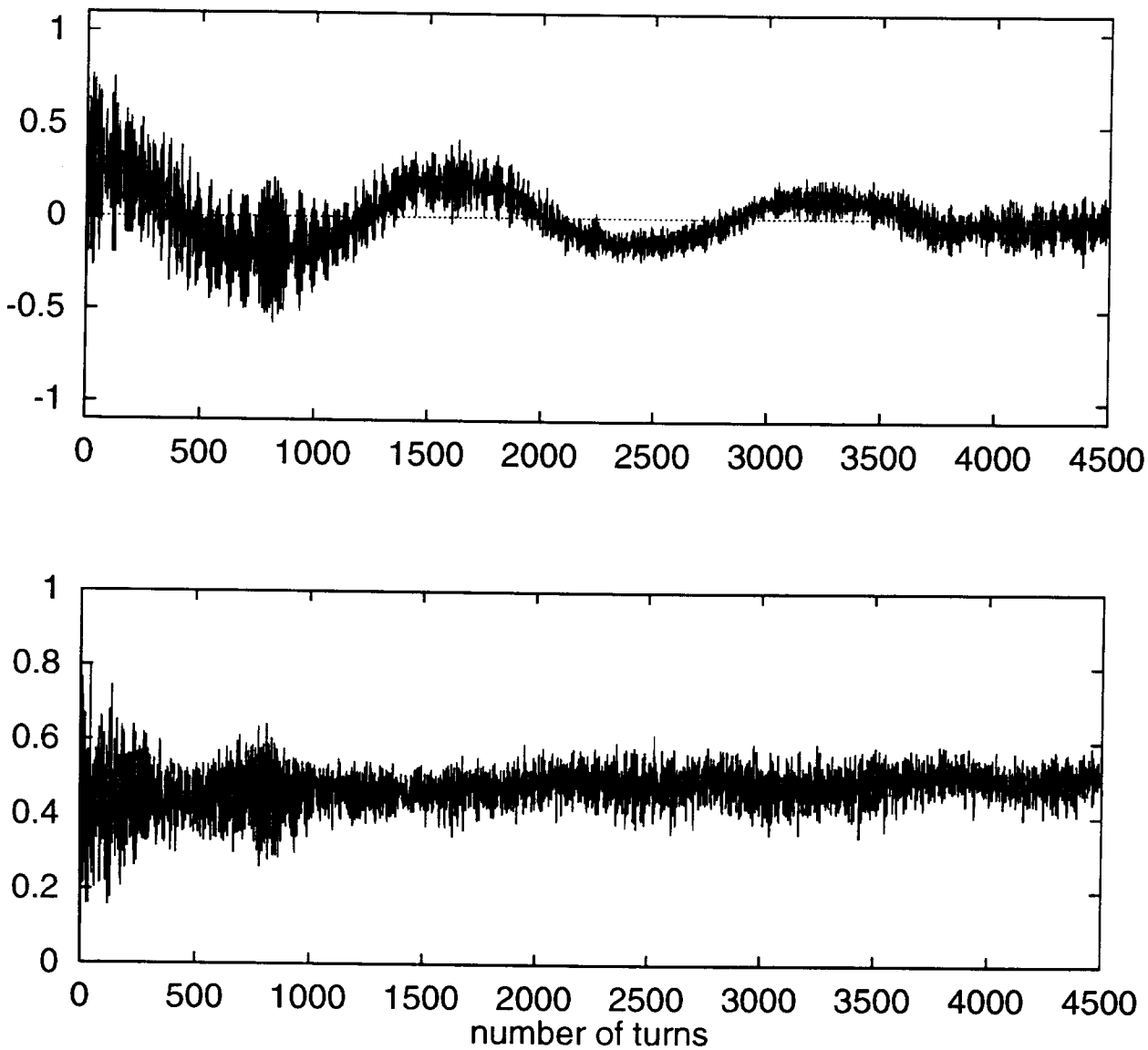

Figure 19: Nonflat HERA-p at E = 820 GeV. The view point is the East IP. Tracking of N = 64 particles for 4500 turns. Top: $< \vec{s} \cdot \vec{n}_0 >$. Bottom: $D\vec{s}$. Emittances: $\varepsilon_x = 4.0 \cdot 10^{-6}\, \pi\, m \cdot rad$, $\varepsilon_y = 4.0 \cdot 10^{-6}\, \pi\, m \cdot rad$, $\varepsilon_z = 1.5 \cdot 10^{-5} m \cdot rad$.

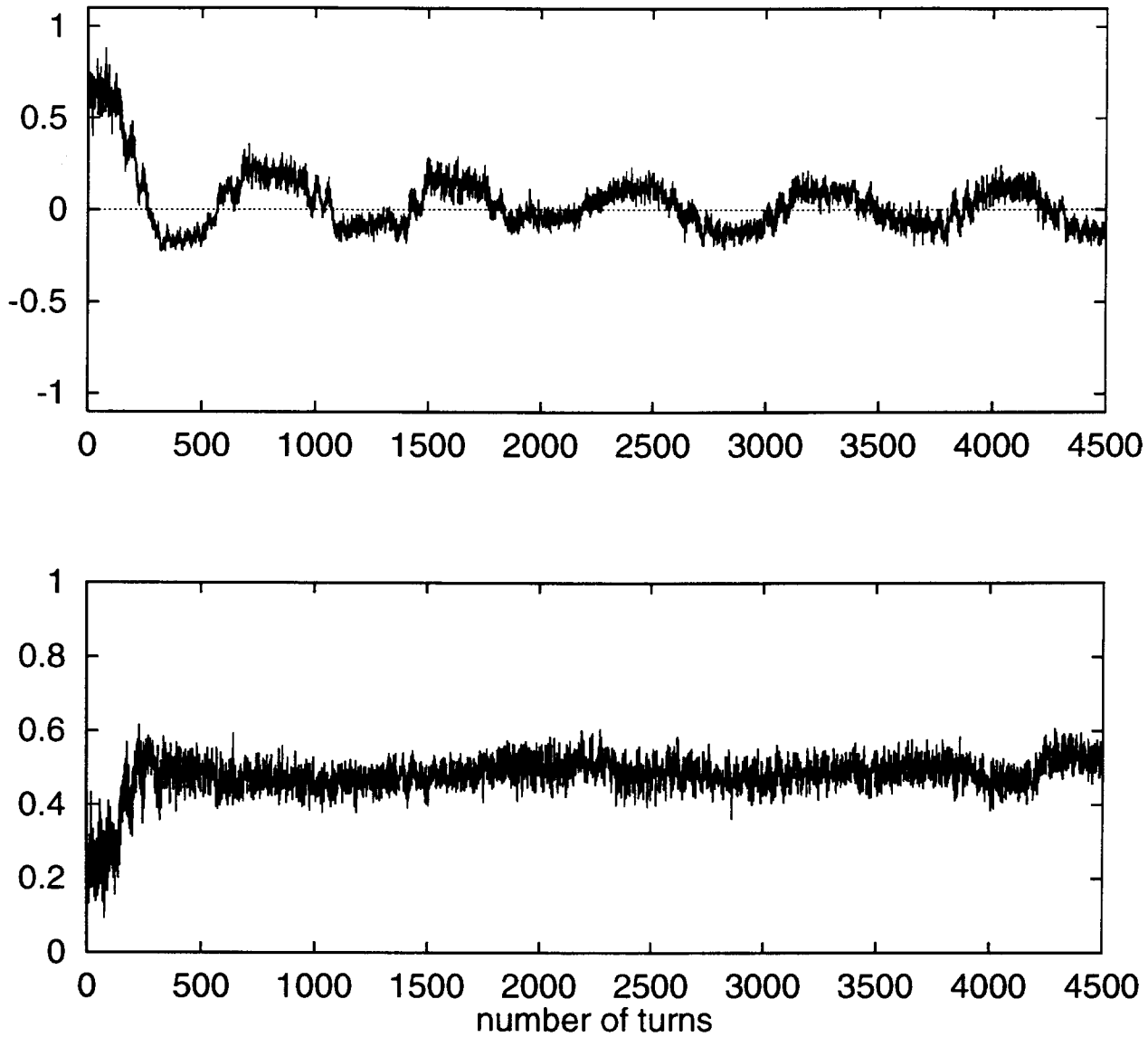

Figure 20: Nonflat HERA-p (without vertical bend in the East) at E = 820 GeV. The view point is the East IP. Tracking of N = 64 particles for 4500 turns. Top: $< \vec{s} \cdot \vec{n}_0 >$. Bottom: $D\vec{s}$. Emittances: $\varepsilon_x = 4.0 \cdot 10^{-6}\, \pi\, m \cdot rad$, $\varepsilon_y = 4.0 \cdot 10^{-6}\, \pi\, m \cdot rad$, $\varepsilon_z = 1.5 \cdot 10^{-5} m \cdot rad$.

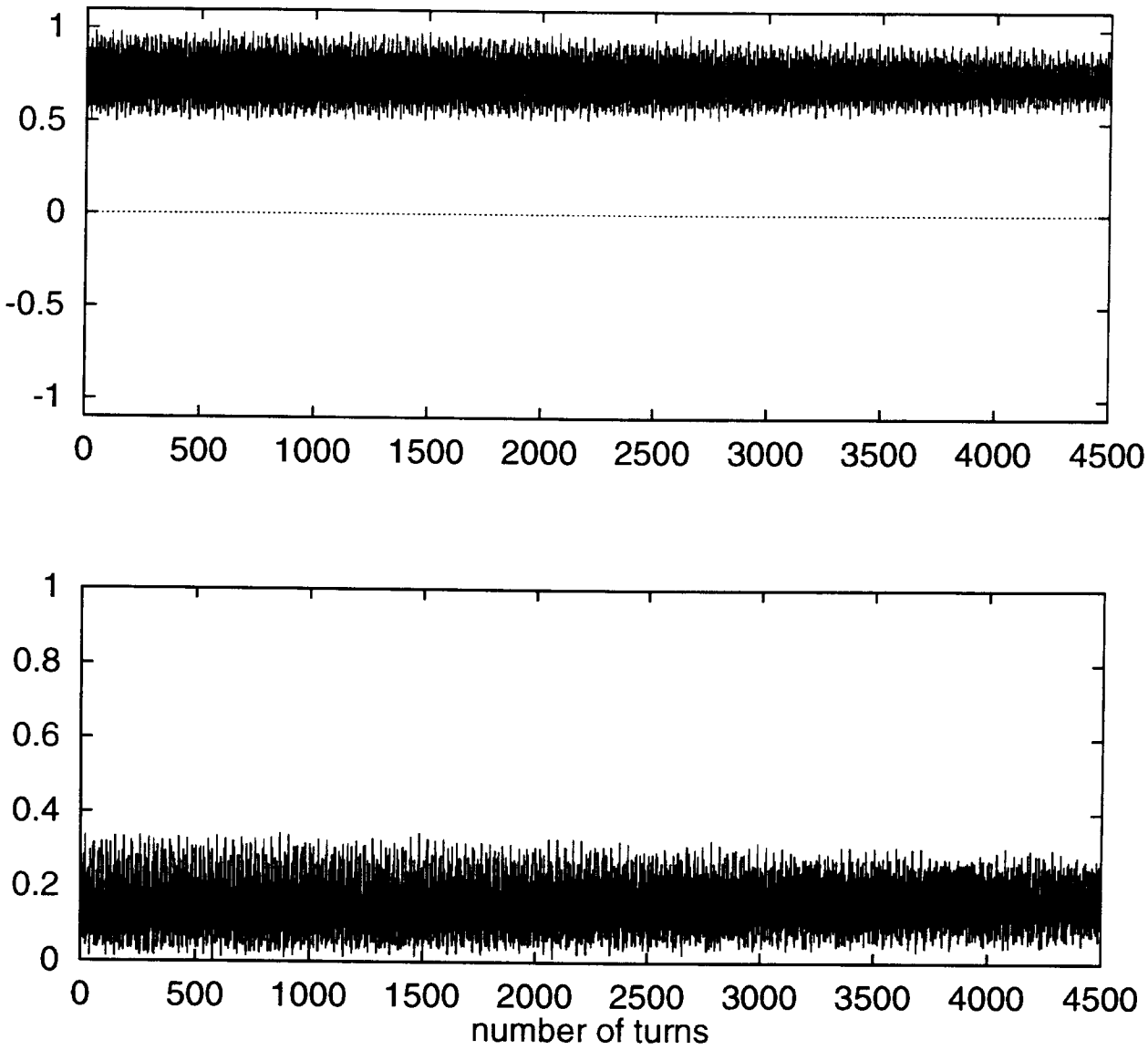

Figure 21: Nonflat HERA-p (without vertical bend in the East) at E = 820 GeV. The view point is the East IP. Tracking of N = 64 particles for 4500 turns. Top: $< \vec{s} \cdot \vec{n}_0 >$. Bottom: $D\vec{s}$. Emittances: $\varepsilon_x = 4.0 \cdot 10^{-6}\, \pi\, m \cdot rad$, $\varepsilon_y = 4.0 \cdot 10^{-6}\, \pi\, m \cdot rad$, $\varepsilon_z = 0.0$. There are no RF cavities.

3 Behaviour of Proton Spin Motion in HERA-p with Snakes

3.1 The Normal Form Method and its Applicability at High Energies

When viewing the motion 'stroboscopically' at a fixed point in the ring (for example, the interaction point of a physics experiment), it is convenient to view the motion in terms of a one-turn map instead of in terms of the differential equations of motion. The one-turn map is defined by the response of the system for one turn:

$$\begin{cases} \vec{u}_f = \vec{F}(\vec{u}_i) \\ \vec{S}_f = A(\vec{u}_i) \cdot \vec{S}_i \end{cases} \tag{4}$$

where $\vec{S}$ is a classical spin vector, $\vec{F}(\vec{0}) = \vec{0}$ (coordinates $\vec{u}$ are displacement from the periodic orbit) and $A(\vec{u})$ is a 3×3 matrix. The subscripts i and f label the beginning and end of the stretch of ring under consideration.

An important concept for the understanding of the geometry of the motion of spin vectors is that of the spin dependent (adiabatic) invariant function introduced in [5] and which in the case when the orbital motion is integrable leads to the well known Derbenev-Kondratenko vector $\vec{n}$ [6].

The function $V(\vec{u}, \vec{S})$ is called an invariant function of the map (4) if

$$V(\vec{u}, \vec{S}) = V(F(\vec{u}), A(\vec{u}) \cdot \vec{S}) \tag{5}$$

Due to the fact that the map (4) is linear with respect to spin variables, we can take $V(\vec{u}, \vec{S})$ only in the form:

$$V(\vec{u}, \vec{S}) = \vec{n}(\vec{u}) \cdot \vec{S} \tag{6}$$

Equation (6) for the function (5) becomes:

$$A(\vec{u}) \cdot \vec{n}(\vec{u}) = \vec{n}(\vec{F}(\vec{u})) \tag{7}$$

If $\mid \vec{n}(\vec{0}) \mid \neq 0$, the function (7) is called nondegenerate. In this case we can choose $\mid \vec{n}(\vec{u}) \mid = 1$.

The existence of a nondegenerate invariant function gives us a relatively simple geometric picture of the behaviour of the spin vector: the projection of the vector $\vec{S}$ on the vector $\vec{n}(\vec{u})$ is conserved during map iterations.

What is the most general way to find the invariant function? It is to guess it for some simple situation, and then try to reduce the real problem to the simpler one by a coordinate transformation. This technique is called the normal form method and allows us to obtain the vector $\vec{n}(\vec{u})$ in the form of a Taylor series with respect to orbit variables $\vec{u}$ (see [5] for details). Unfortunately, the Taylor series used for the coordinate transformations in the method of normal forms are usually not convergent. This means that in practice we can only obtain the adiabatic invariants by cutting off the Taylor series at some order of nonlinearity. In this case the parameter is the vector $\vec{u}$ and the approximation works better if emittances are smaller. So once one has an approximation to the vector $\vec{n}$, it is necessary to define the value of the emittance for which this approximation is applicable.

The three groups of figures (Figs.22-24, Figs.25-27, Figs.28-30) summarize calculations of $\vec{n}$ for various cases: for the flat test HERA-p without snakes, for the flat HERA-p with two snakes (longitudinal snake in the West and radial snake in the East) and for the flat HERA-p with four snakes (snake axis is $\pm 22.5°$ from the beam direction). What do the figures of each group show? The first two figures represent the dependence of the maximum, the average value and the minimum [6] of the vector norm $\mid \vec{n}_k \mid$ on the emittances for different orders k of truncation of the Taylor series for $\vec{n}$. The deviation of the norm of $\vec{n}$ from unity is a useful indication of the validity of the approximation. The third figure of each group shows the dependence of the spin tune ν_j ($j = int(k/2)$) on the invariants of the orbital oscillations (in the case of linear orbit motion we use the transverse emittances). If we fix the highest order for the truncation at $k = 5$ we can obtain only two correction terms to the spin tune. In the calculations we have changed the horizontal emittance ε_x from zero to the value $4.0 \cdot 10^{-6}\ m \cdot rad$. At the same time we change the vertical and longitudinal emittances as functions of ε_x according to the rules:

$$\varepsilon_y = \varepsilon_x, \quad \varepsilon_z = 1.5 \cdot 10^{-5} * (\varepsilon_x / 4.0 \cdot 10^{-6}).$$

[6] For fixed emittances we distribute the particles uniformly in phase and calculate the maximum, the average and the minimum values as the functions of phases.

Clearly, the Taylor method can lead to large, nonphysical deviations of the norm from unity. Thus care is needed when interpreting results of Taylor expansion calculations of $\vec{n}$ and the spin tune spread.

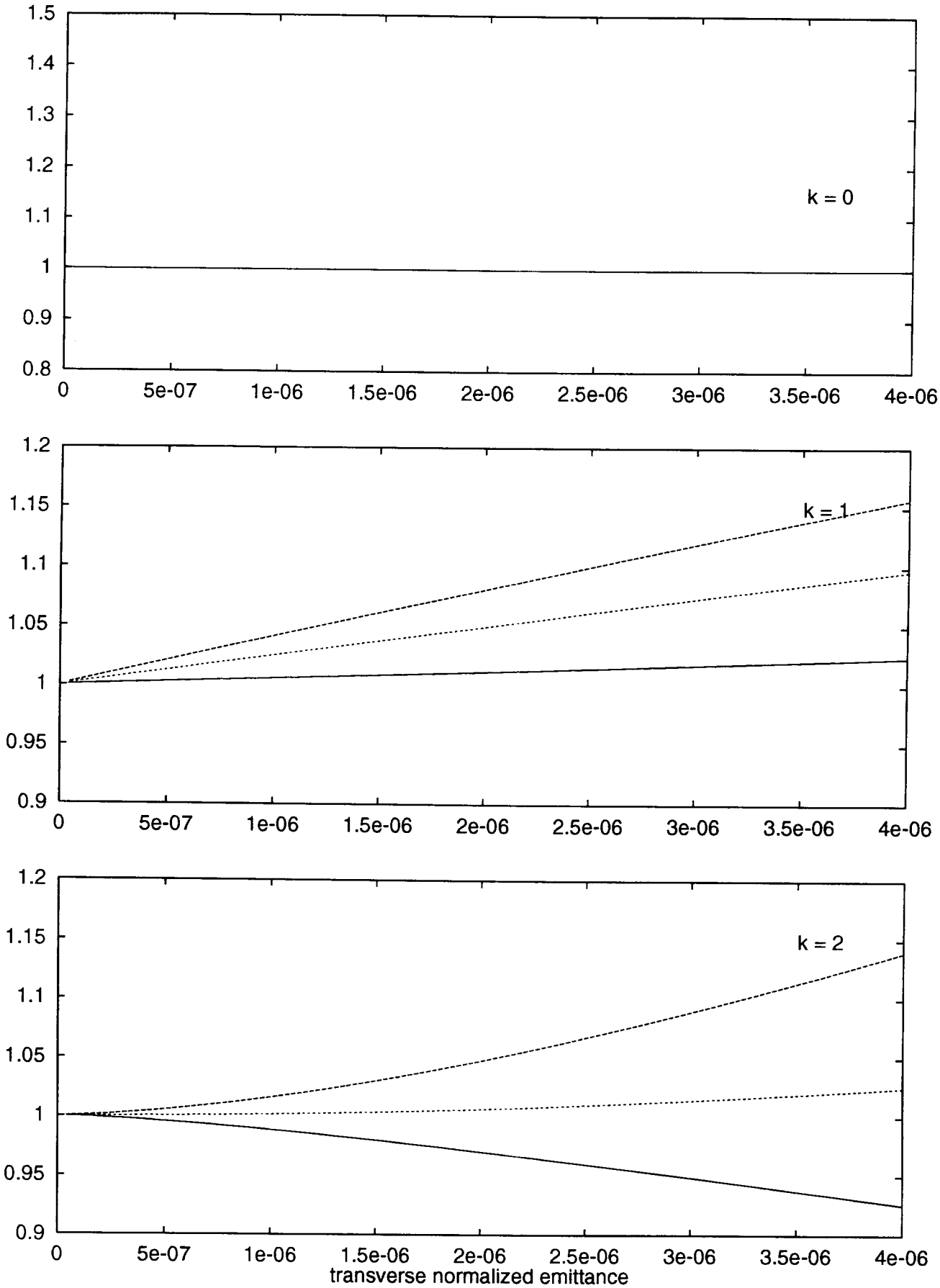

Figure 22: Flat HERA-p at E = 820 GeV. The view point is the East IP. The dependence of the maximum , the average value and the minimum of the vector norm $| \vec{n}_k |$ on the value of transverse emittance.

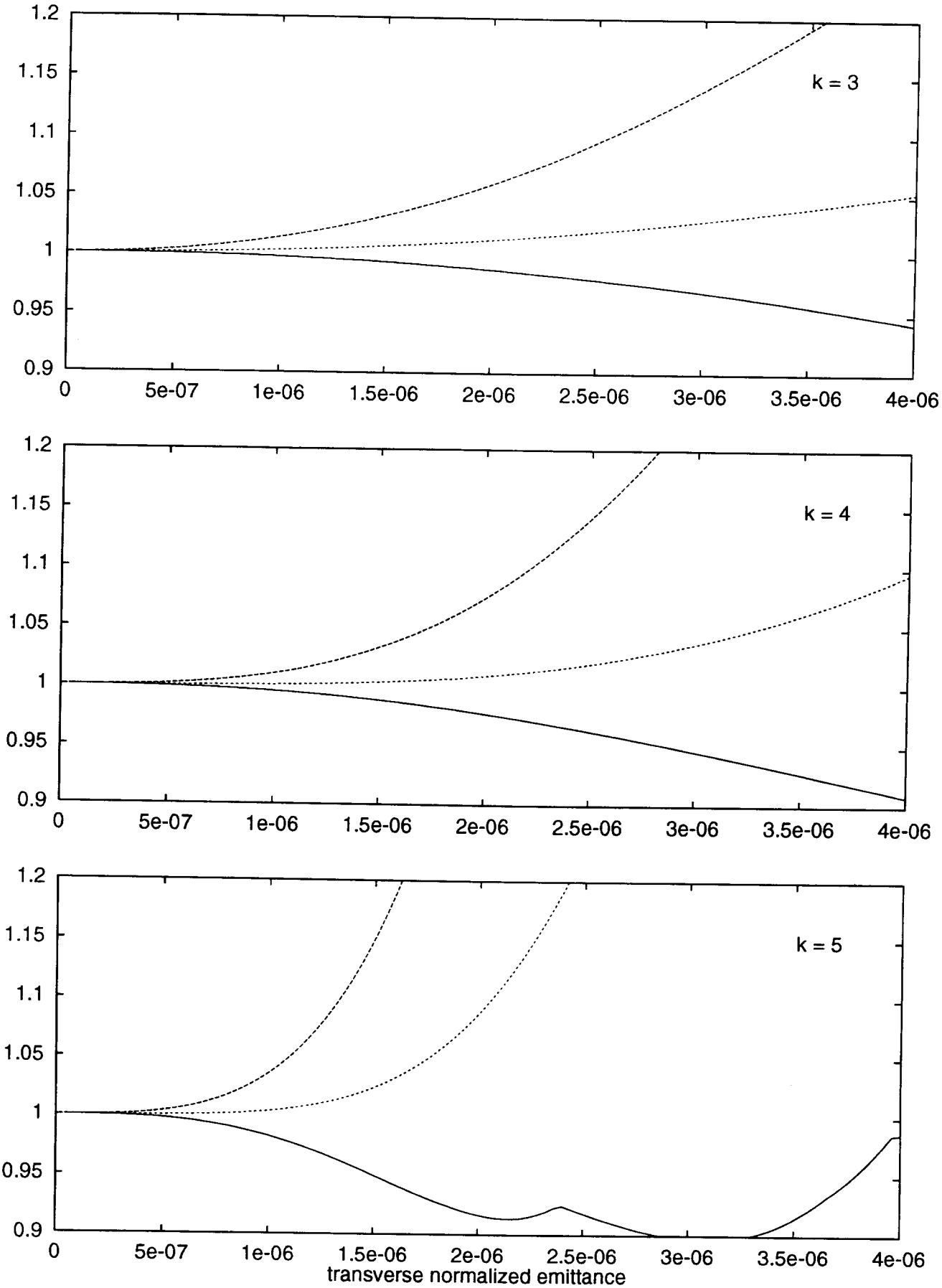

Figure 23: Flat HERA-p at E = 820 GeV. The view point is the East IP. The dependence of the maximum , the average value and the minimum of the vector norm $| \vec{n}_k |$ on the value of transverse emittance.

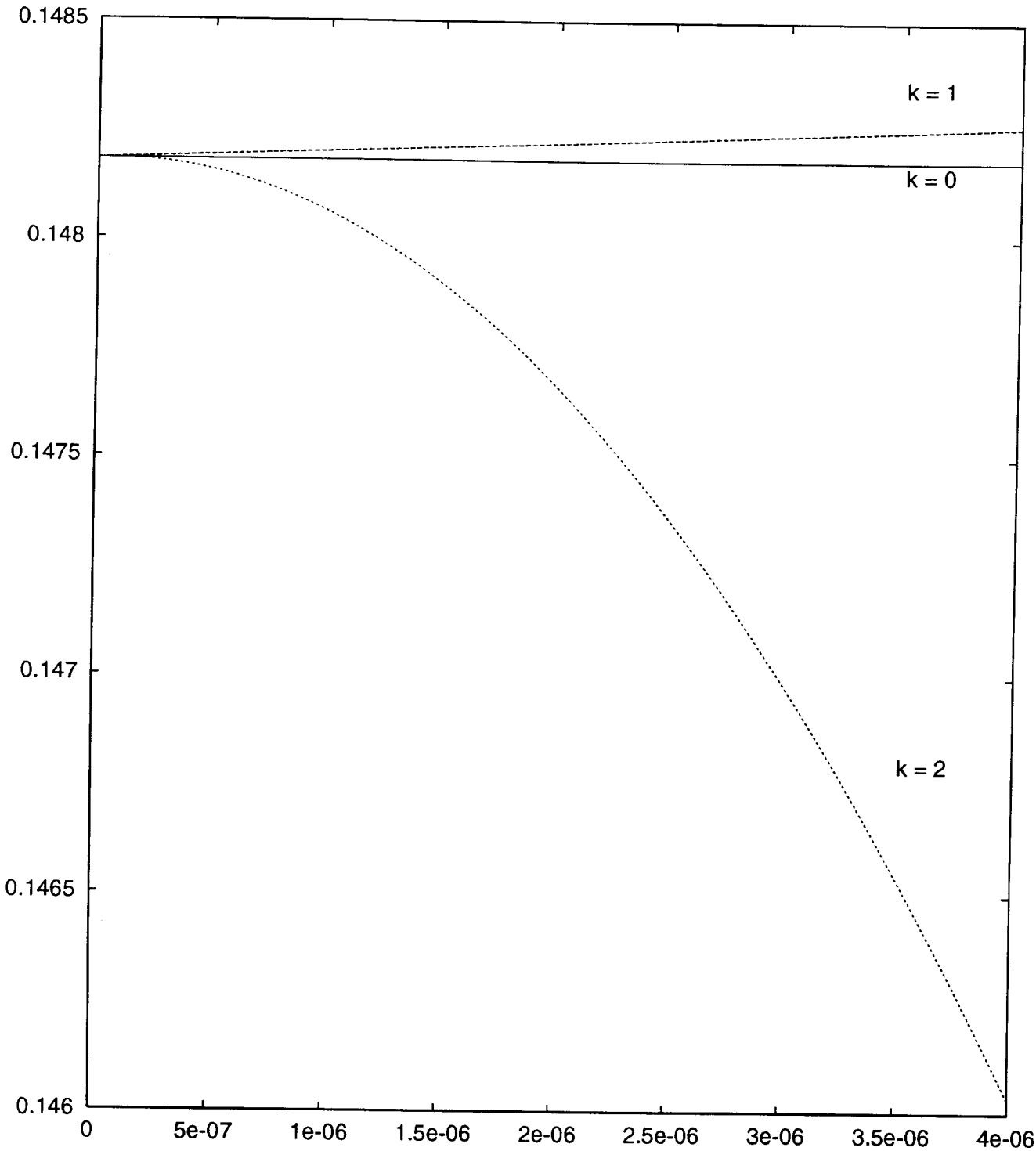

Figure 24: Flat HERA-p at E = 820 GeV. The dependence of the spin tune ν_k on the value of transverse emittance.

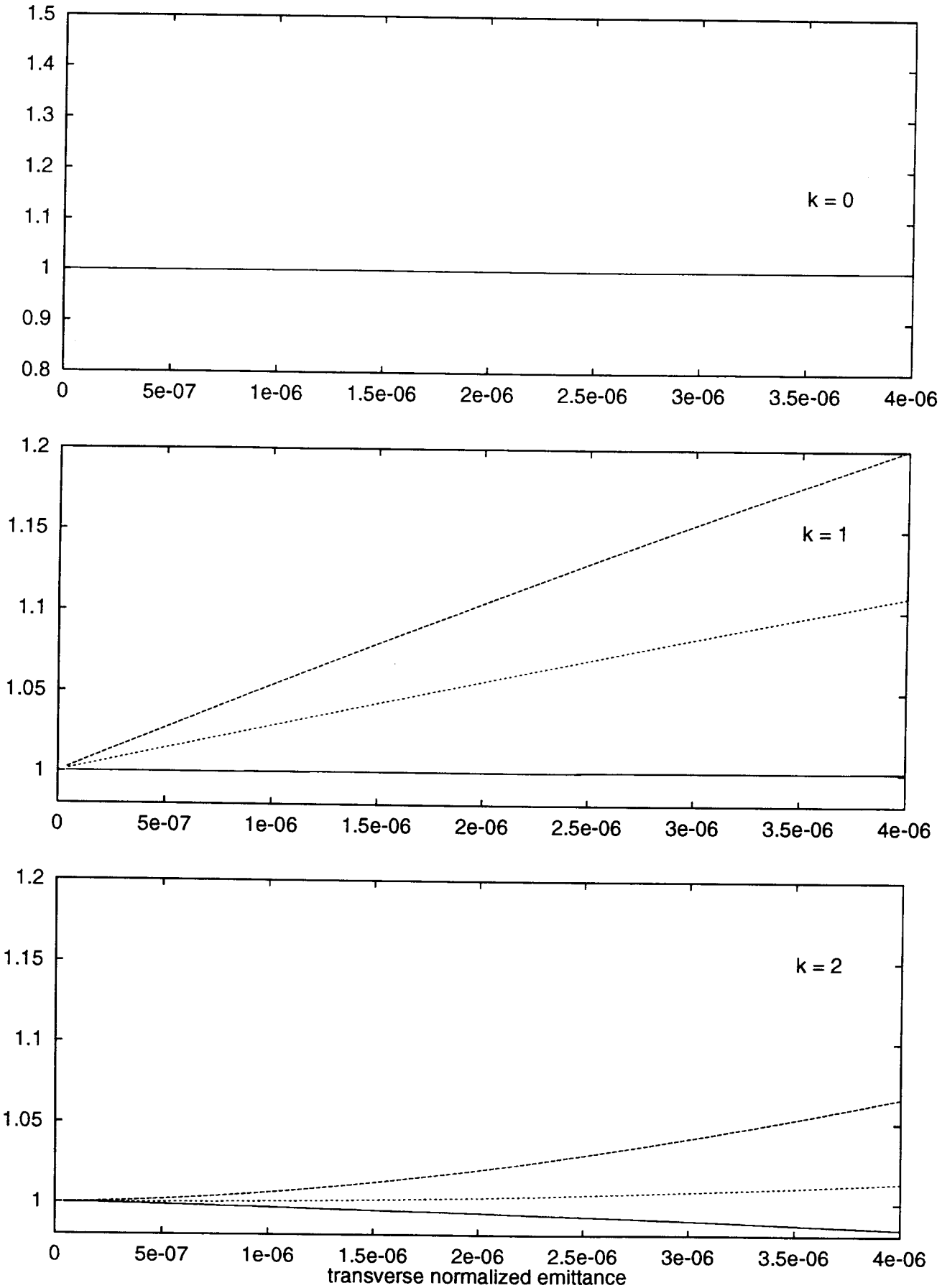

Figure 25: Flat HERA-p with two snakes at E = 820 GeV. The view point is the East IP. The dependence of the maximum , the average value and the minimum of the vector norm $|\vec{n}_k|$ on the value of transverse emittance.

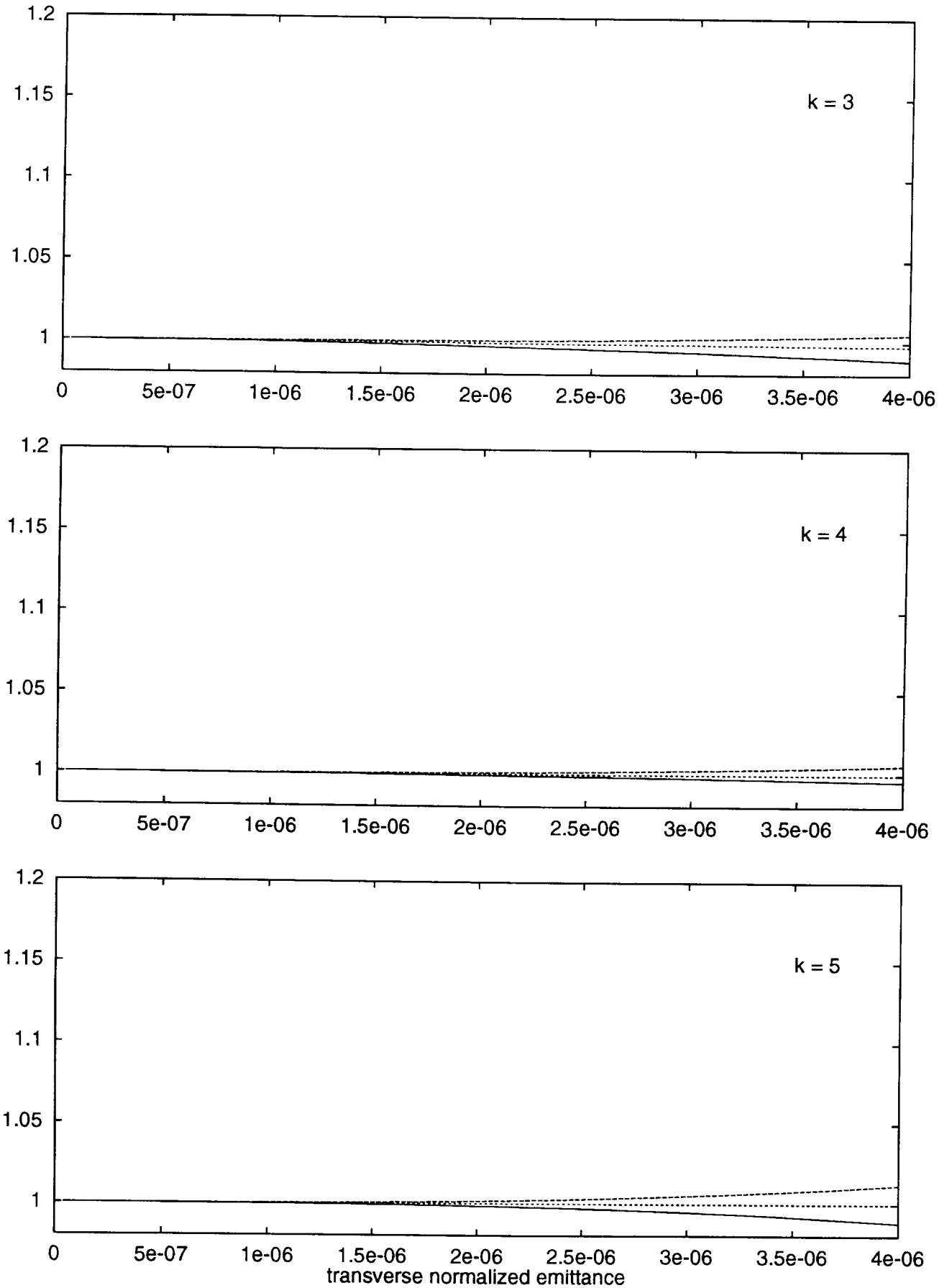

Figure 26: Flat HERA-p with two snakes at E = 820 GeV. The view point is the East IP. The dependence of the maximum , the average value and the minimum of the vector norm $\mid \vec{n}_k \mid$ on the value of transverse emittance.

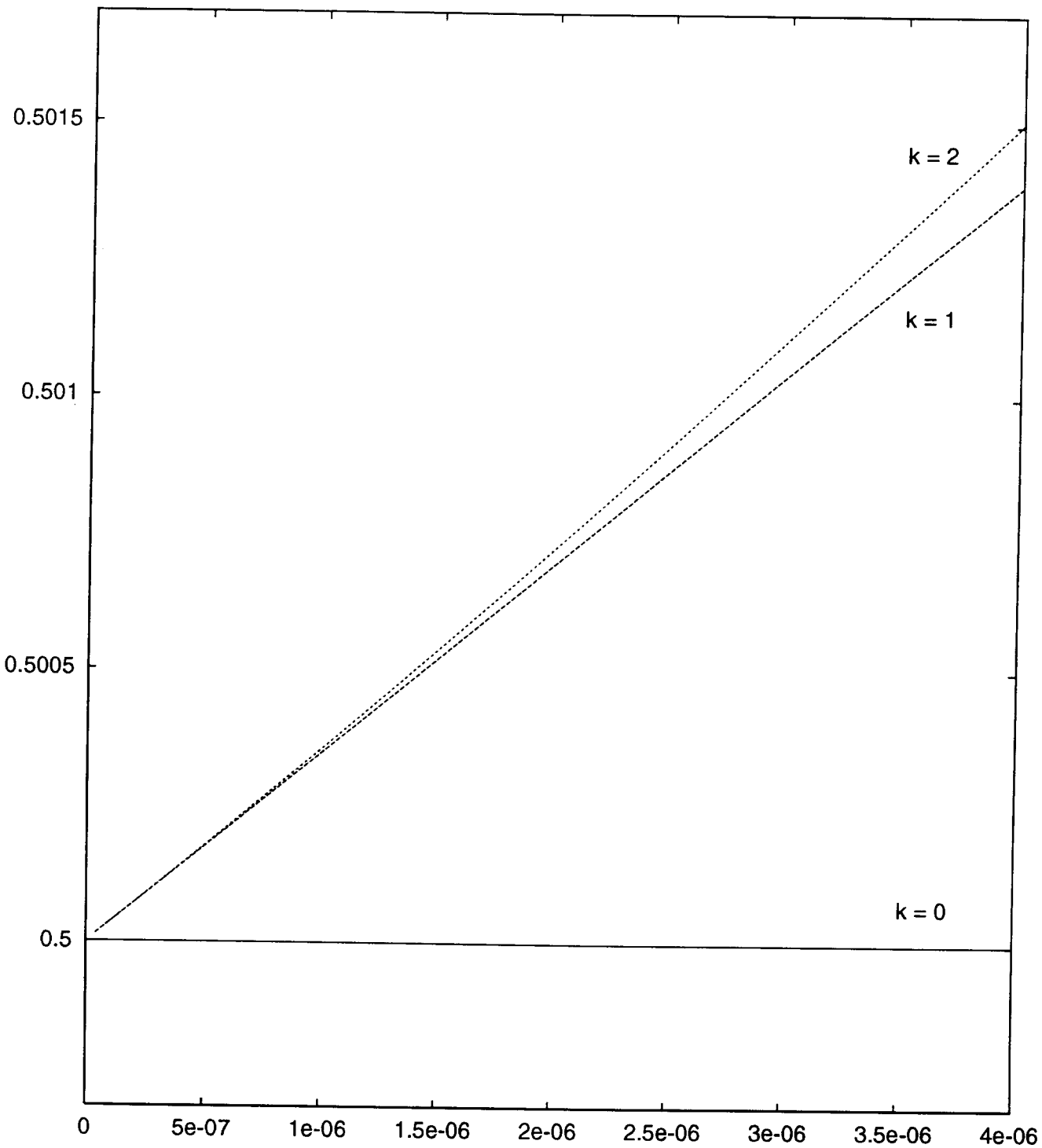

Figure 27: Flat HERA-p with two snakes at E = 820 GeV. The dependence of the spin tune ν_k on the value of transverse emittance.

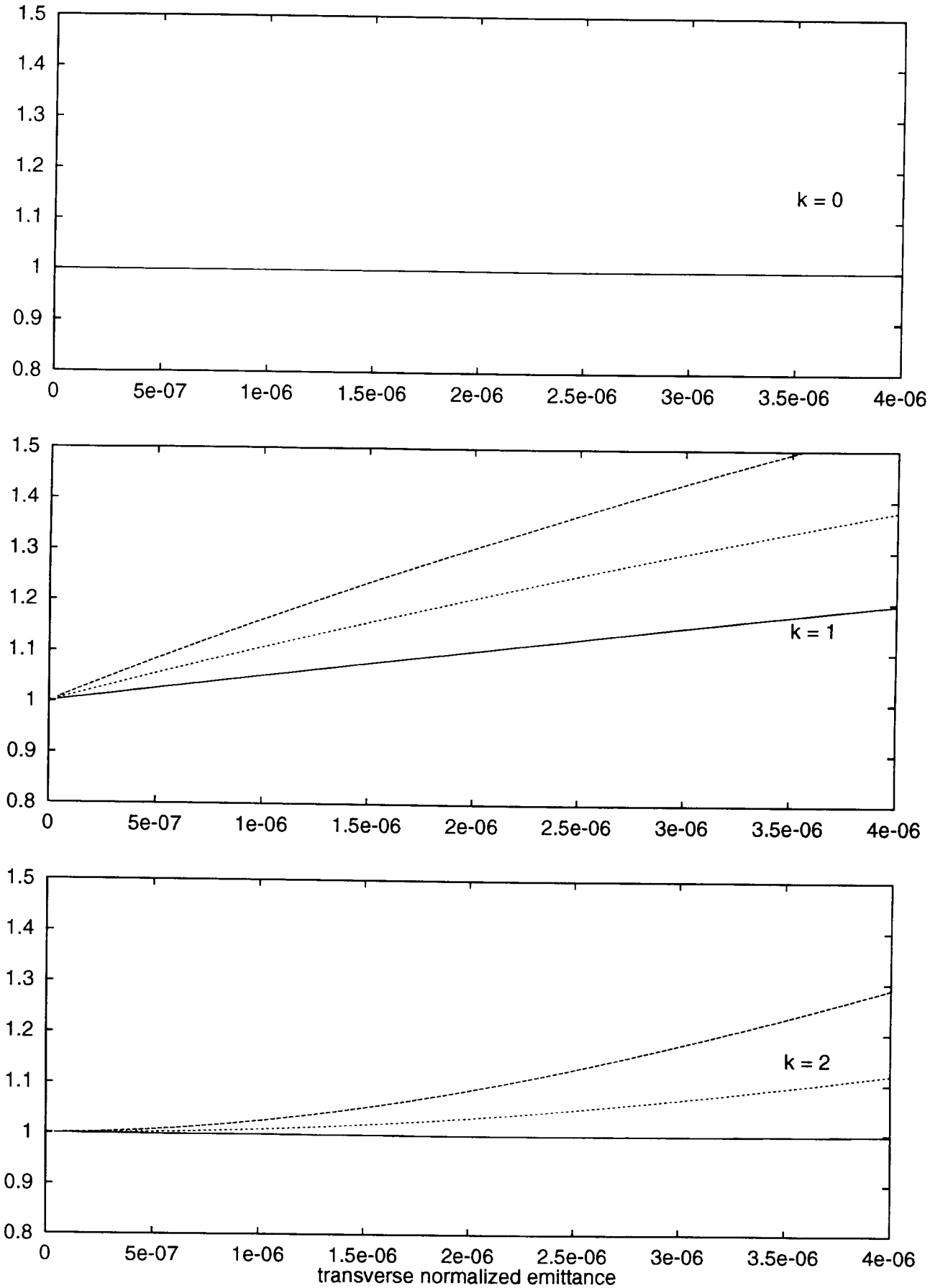

Figure 28: Flat HERA-p with 4 snakes at E = 814.8 GeV. The view point is the East IP. The dependence of the maximum , the average value and the minimum of the vector norm $\mid \vec{n}_k \mid$ on the value of transverse emittance.

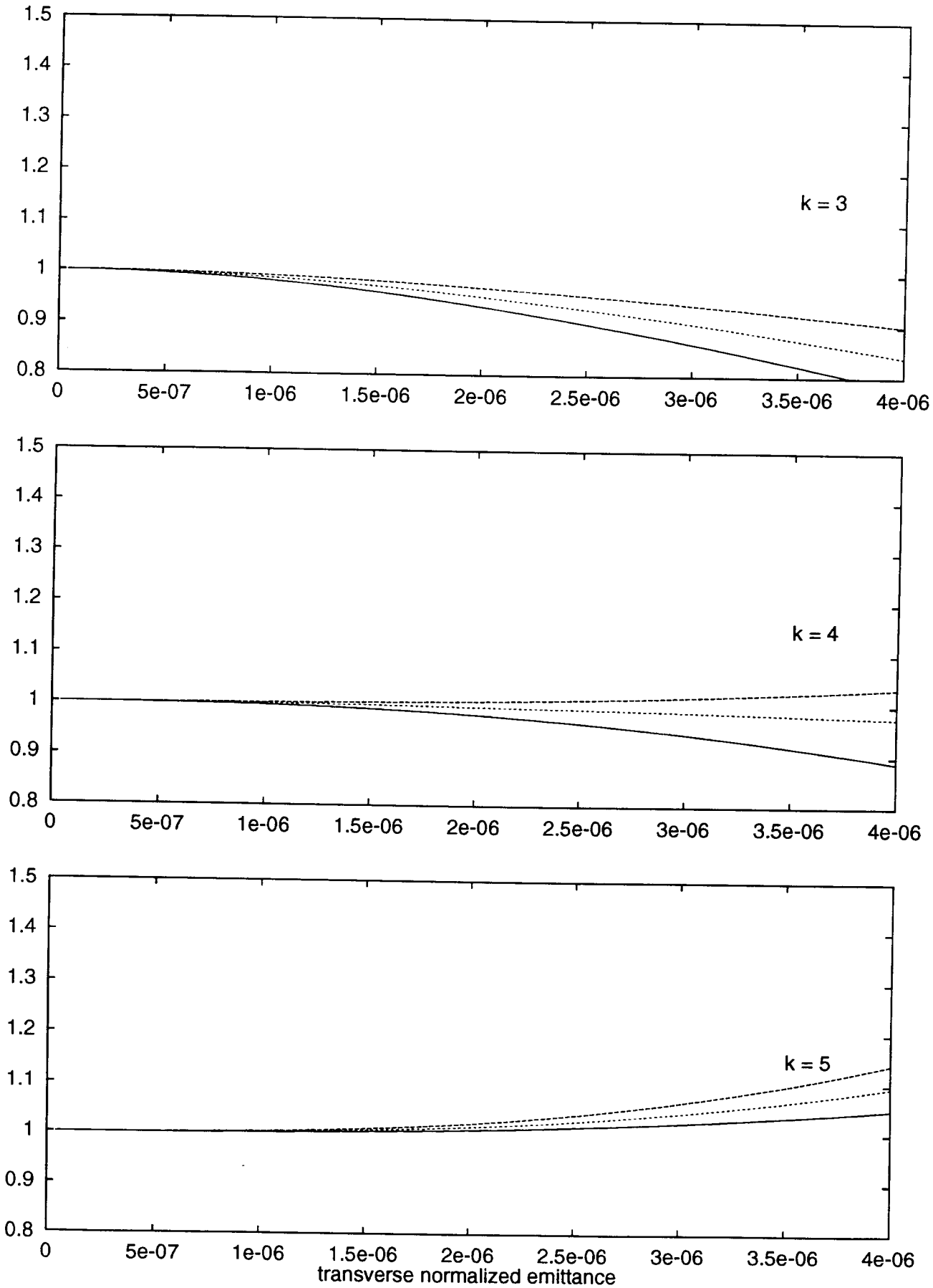

Figure 29: Flat HERA-p with 4 snakes at E = 814.8 GeV. The view point is the East IP. The dependence of the maximum , the average value and the minimum of the vector norm $| \vec{n}_k |$ on the value of transverse emittance.

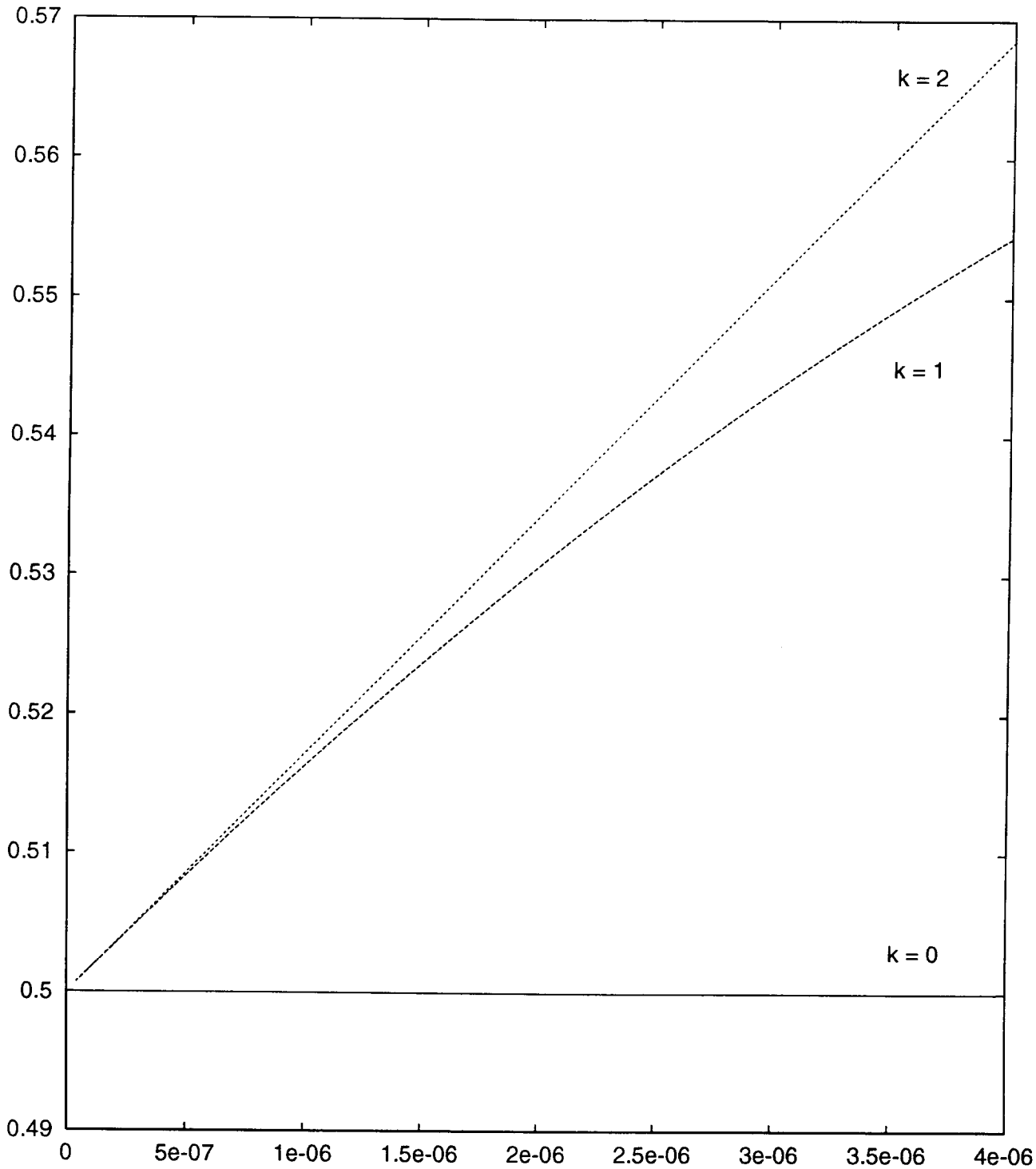

Figure 30: Flat HERA-p with 4 snakes at E = 814.8 GeV. The dependence of the spin tune ν_k on the value of transverse emittance.

3.2 Method of Numerical Integration

To track particles with spin we use a method of numerical integration which is symplectic with respect to the 6-D orbit motion and orthogonal with respect to the 3-D spin motion (see details in a[7]-[9]). The orbit Hamiltonian contains all terms up to order 3 with respect to coupled synchro-betatron motion and the spin part of the Hamiltonian contains all terms up to order 2 with respect to the orbital variables for all elements. Thus sextupole effects are included in both the spin and the orbital motion. Besides that, of course, we use the terms of high order for octupoles and other multipoles.

The number of numerical integration steps needed per element was investigated and we concluded that to obtain high speed for the calculations without essential loss of the precision it is enough to have one integration step per element except for dipoles. These were divided into pieces not more than 1.5 m long.

3.3 One Snake

Figs.31-32 show the spin behaviour in the flat and nonflat HERA-p with one longitudinal snake in the West section. The view point is the East IP. Clearly, the snake has essentially stabilized the spin motion and strongly suppressed the tendency for spin flip by spin tune modulation.

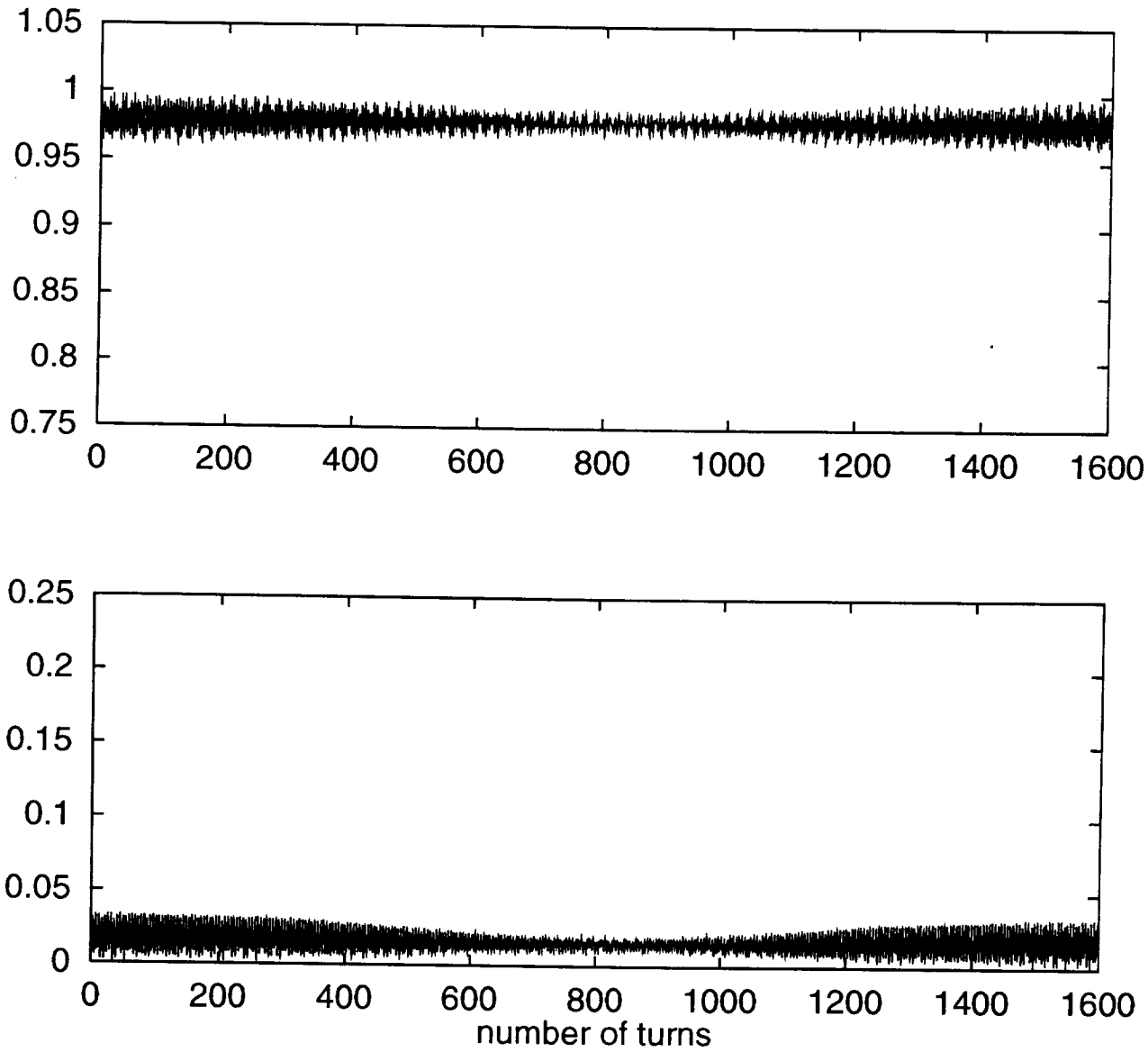

Figure 31: Flat HERA-p at E = 820 GeV with one longitudinal snake in the West. The view point is the East IP. Tracking of N = 64 particles for 1600 turns. Top: $< \vec{s} \cdot \vec{n}_0 >$. Bottom: $D\vec{s}$. Emittances: $\varepsilon_x = 4.0 \cdot 10^{-6}\, \pi\, m \cdot rad$, $\varepsilon_y = 4.0 \cdot 10^{-6}\, \pi\, m \cdot rad$, $\varepsilon_z = 1.5 \cdot 10^{-5} m \cdot rad$.

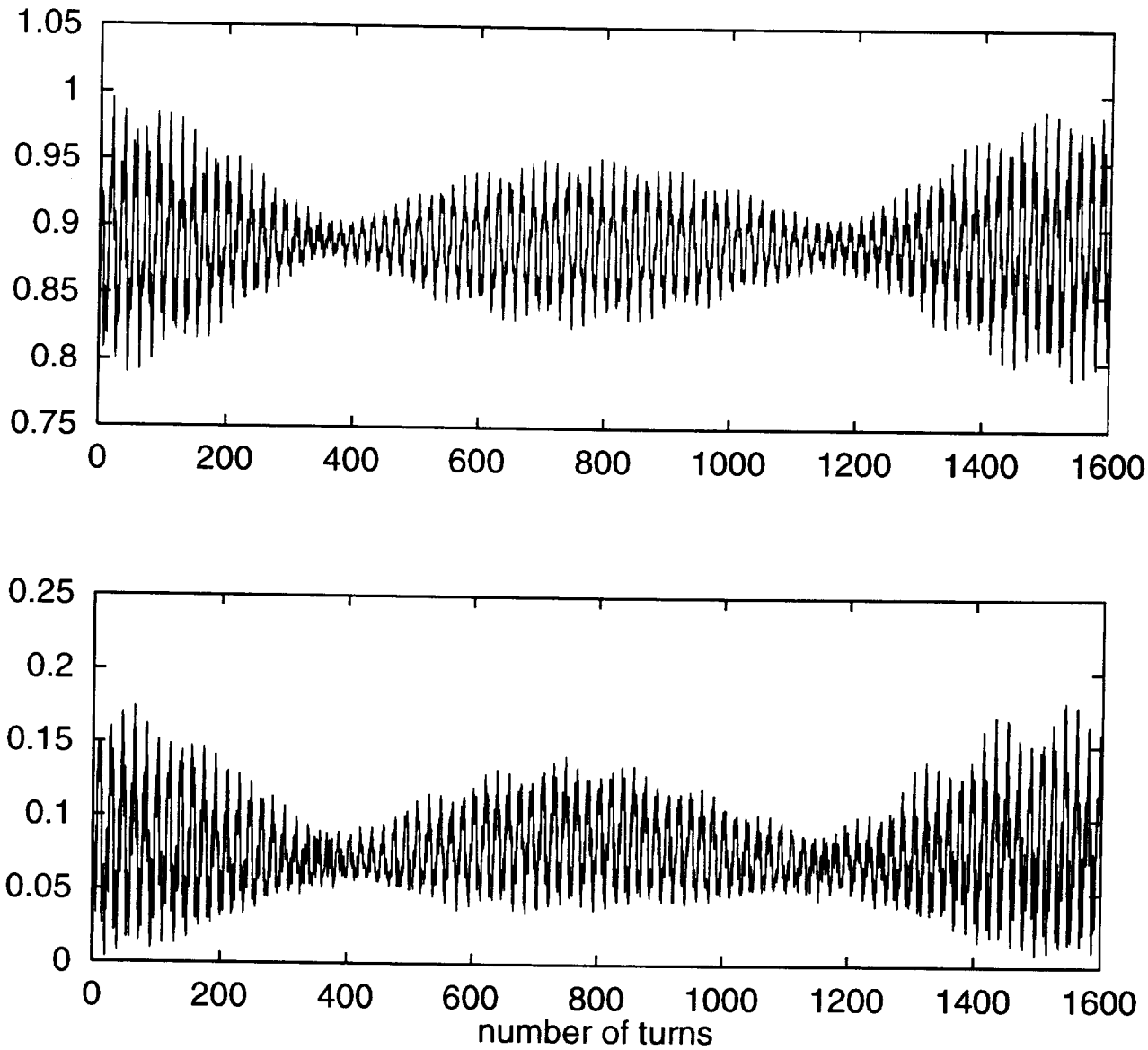

Figure 32: Nonflat HERA-p at E = 820 GeV with one longitudinal snake in the West. The view point is the East IP. Tracking of N = 64 particles for 1600 turns. Top: $< \vec{s} \cdot \vec{n}_0 >$. Bottom: $D\vec{s}$. Emittances: $\varepsilon_x = 4.0 \cdot 10^{-6}\, \pi\, m \cdot rad$, $\varepsilon_y = 4.0 \cdot 10^{-6}\, \pi\, m \cdot rad$, $\varepsilon_z = 1.5 \cdot 10^{-5} m \cdot rad$.

3.4 Two Snakes

Figs.33-43 show the spin motion in the flat and nonflat HERA-p with two snakes.

Before proceeding we wish to understand the extent to which the results of calculations depend on the number of particles. In all of these tracking simulations we used a small number of particles (with the spins initially set parallel to $\vec{n}_0$), usually 64. One could suspect that the relatively large modulation of $< \vec{s} \cdot \vec{n}_0 >$ and $D\vec{s}$ as a function of the number of turns is due to the small number of particles and that the modulation would be smaller if the number of particles were increased. However, this is not the case (at least for the tracking results which are given in this paper). Compare Figs.33-35 where the number of particles takes the values 64, 125 and 1000 respectively.

Returning to Fig.33 we see strong modulation of the spin motion. This is no surprise, since we are viewing a quasiperiodic motion stroboscopically. But of course, it is very interesting to understand which effect dominates: the linear betatron oscillations, the synchrotron oscillations or a nonlinear effect.

Figs.33,36,37 show the spin motion in the same optic with the same snakes (the flat HERA-p with one longitudinal snake in the West and one radial snake in the East) for various conditions: taking into account all effects (Fig.33), for a longitudinal emittance $\varepsilon_z = 0$ without the effects of RF cavities on the spin-orbit motion (Fig.36) and for the transverse emittances two times smaller than the initial value (Fig.37). We see that the removal of the synchrotron oscillations makes little difference except that the modulation has more regular behaviour (see Figs.33,36). However, on decreasing the transverse emittances the modulations take on another form, but the maximum range of fast oscillations is decreased linearly. We therefore conclude that slow modulations are caused by nonlinear effects of betatron motion, but at the same time the short time behaviour appears to depend linearly on the emittances. To see the approximate linear dependence of this short time behaviour on emittances we compare the behaviour of the spin dispersion functions in Figs.38-39 [7] where the results are shown for emittances differing by a factor of two. Such simultaneous linear and nonlinear behaviour may be explained using the concept of quasi-nondegenerate invariant functions

[7]Note that in Figs.38-39 we study the polarization along the ring and not only turn by turn.

introduced in [10].

It is interesting also to look at the sensitivity of the short term spin behaviour to changes in the orbital, spin tunes and the energy. Numerical results have shown us that the dependence on the shift of orbital tunes is small (see, for example, Fig.40) but that the behaviour is very sensitive to the shift of the spin tune (see, for example, Fig.41). The spin behaviour for this snake configuration but for another energy is shown in Fig.48.

It would be useful to study all the phenomena just mentioned using the Fourier transformation of the tracking results. This question will be discussed in future papers.

As further examples, Figs.42-43 show the spin behaviour in the flat HERA-p with two snakes of another type (the snake axis is $\pm 45°$ away from the beam) and in the nonflat HERA-p (longitudinal in the West and radial in the East). We see the another shape for the modulations, but the mean polarization is approximately the same.

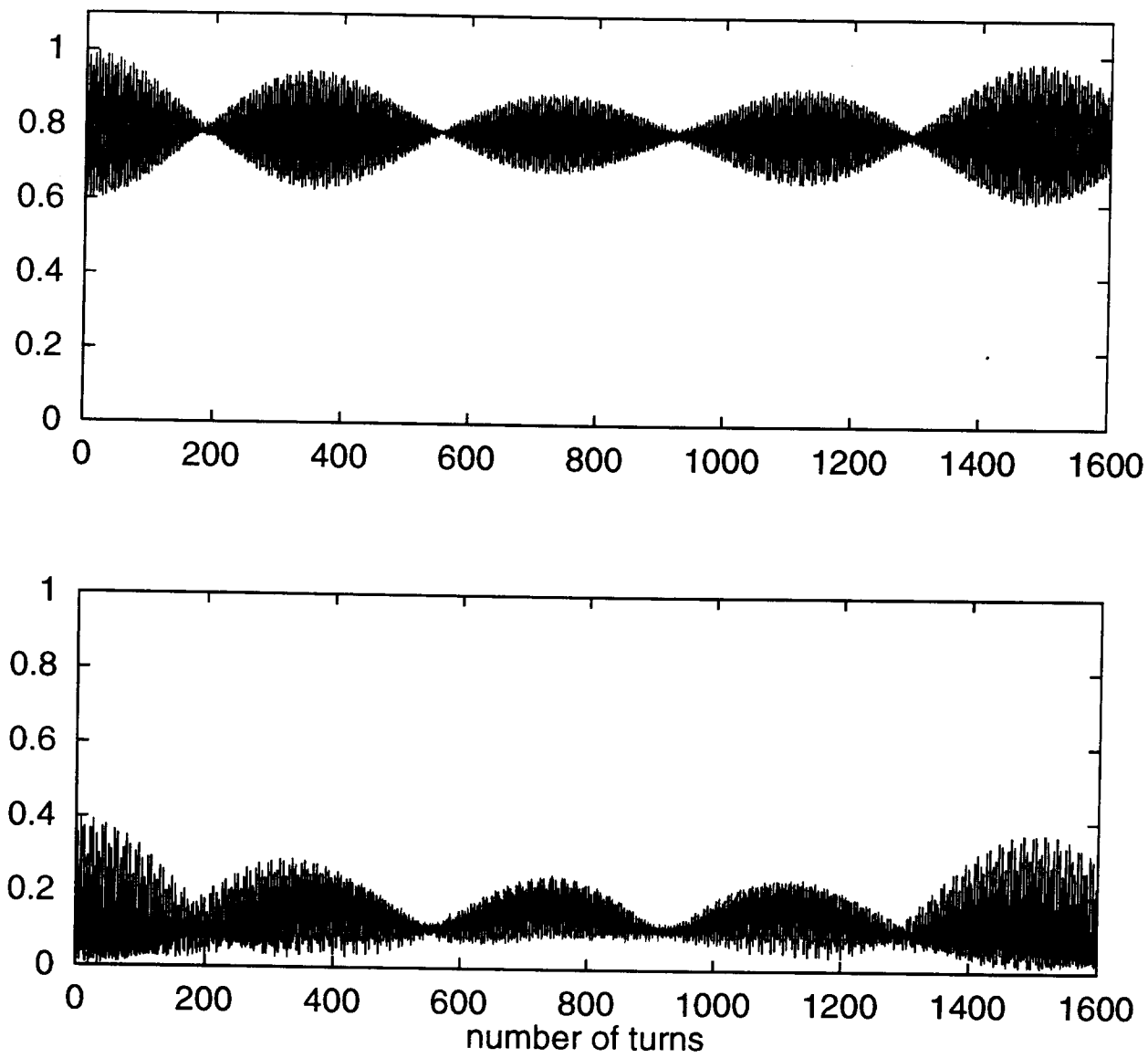

Figure 33: Flat HERA-p at E = 820 GeV with two snakes (longitudinal snake in the West and radial snake in the East). The view point is the East IP. Tracking of N = 64 particles for 1600 turns. Top: $< \vec{s} \cdot \vec{n}_0 >$. Bottom: $D\vec{s}$. Emittances: $\varepsilon_x = 4.0 \cdot 10^{-6}\, \pi\, m \cdot rad$, $\varepsilon_y = 4.0 \cdot 10^{-6}\, \pi\, m \cdot rad$, $\varepsilon_z = 1.5 \cdot 10^{-5} m \cdot rad$.

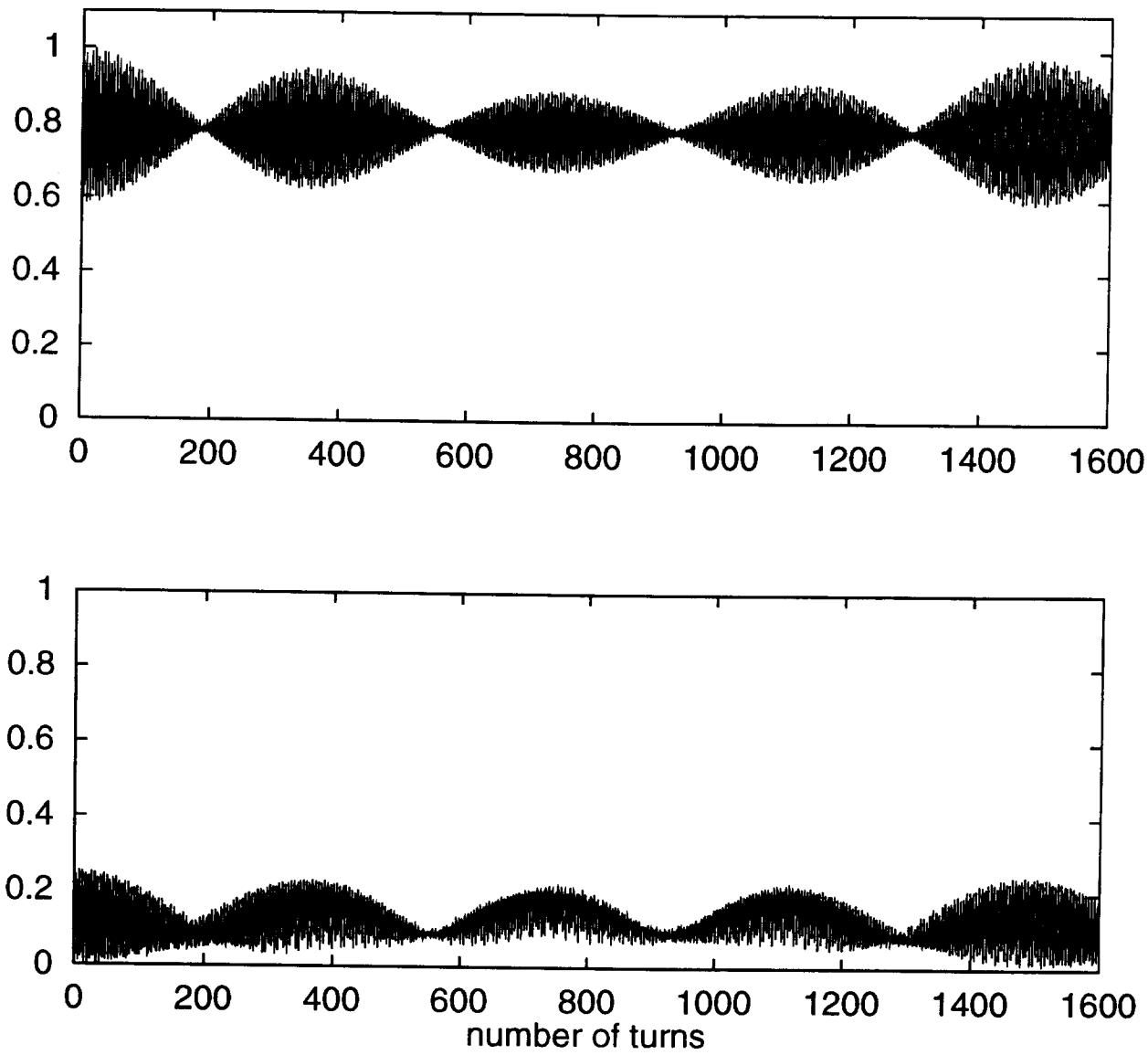

Figure 34: Flat HERA-p at E = 820 GeV with two snakes (longitudinal snake in the West and radial snake in the East). The view point is the East IP. Tracking of N = 125 particles for 1600 turns. Top: $< \vec{s} \cdot \vec{n}_0 >$. Bottom: $D\vec{s}$. Emittances: $\varepsilon_x = 4.0 \cdot 10^{-6}\, \pi\, m \cdot rad$, $\varepsilon_y = 4.0 \cdot 10^{-6}\, \pi\, m \cdot rad$, $\varepsilon_z = 1.5 \cdot 10^{-5} m \cdot rad$.

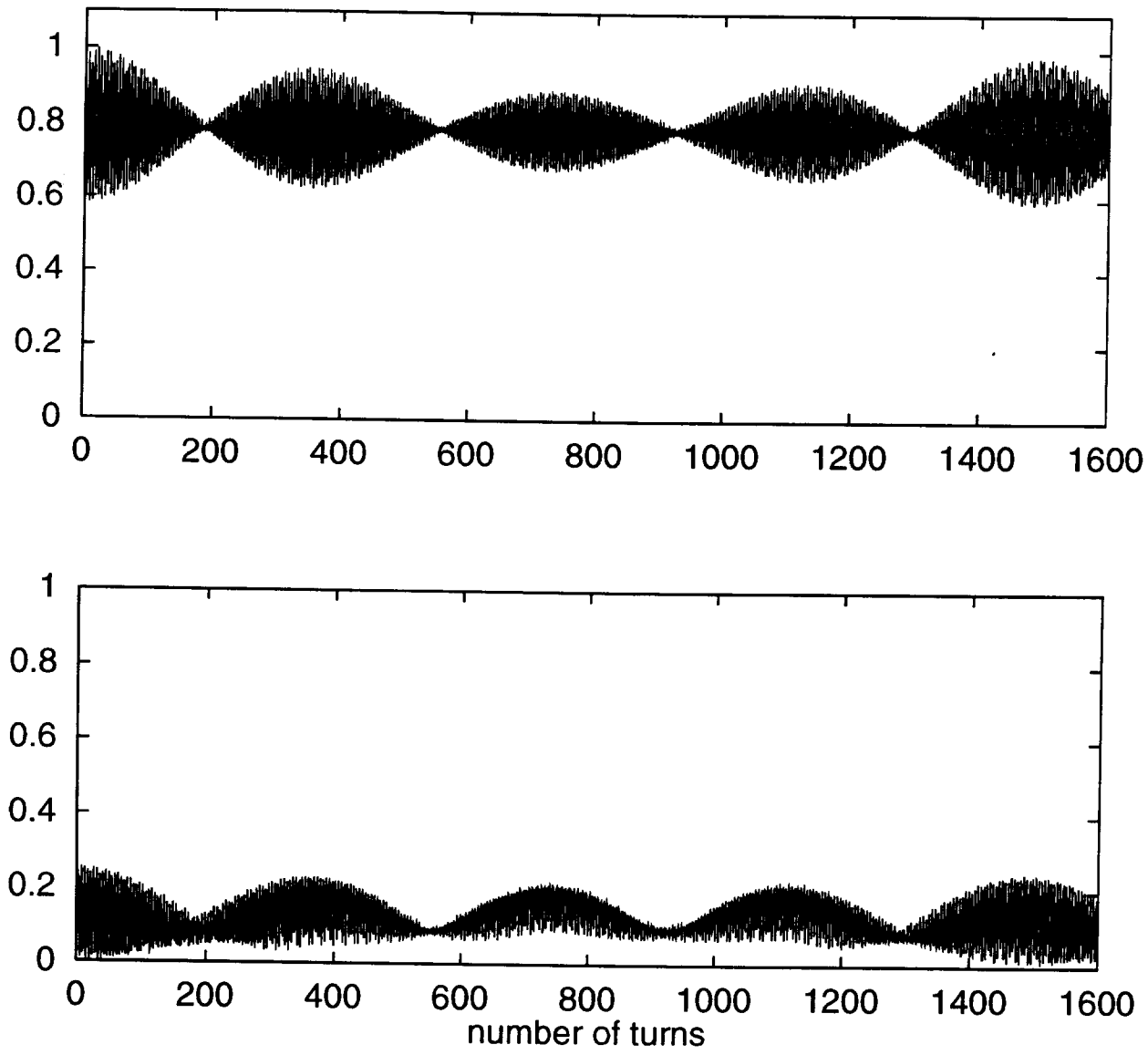

Figure 35: Flat HERA-p at E = 820 GeV with two snakes (longitudinal snake in the West and radial snake in the East). The view point is the East IP. Tracking of N = 1000 particles for 1600 turns. Top: $< \vec{s} \cdot \vec{n}_0 >$. Bottom: $D\vec{s}$. Emittances: $\varepsilon_x = 4.0 \cdot 10^{-6}\, \pi\, m \cdot rad$, $\varepsilon_y = 4.0 \cdot 10^{-6}\, \pi\, m \cdot rad$, $\varepsilon_z = 1.5 \cdot 10^{-5} m \cdot rad$.

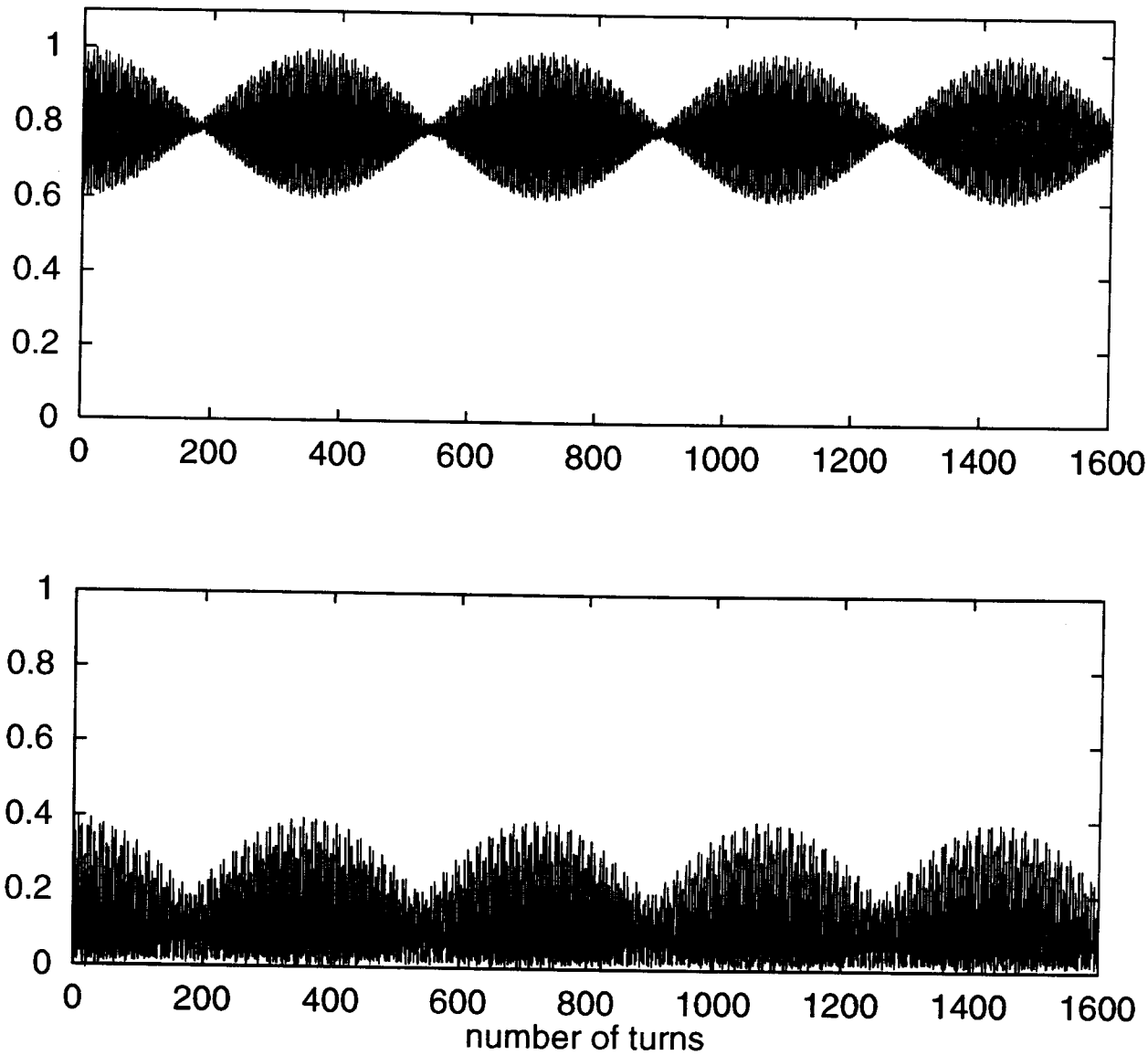

Figure 36: Flat HERA-p at E = 820 GeV with two snakes (longitudinal snake in the West and radial snake in the East). The view point is the East IP. Tracking of N = 64 particles for 1600 turns. Top: $< \vec{s} \cdot \vec{n}_0 >$. Bottom: $D\vec{s}$. Emittances: $\varepsilon_x = 4.0 \cdot 10^{-6}\, \pi\, m \cdot rad$, $\varepsilon_y = 4.0 \cdot 10^{-6}\, \pi\, m \cdot rad$, $\varepsilon_z = 0.0$. There are no RF cavities.

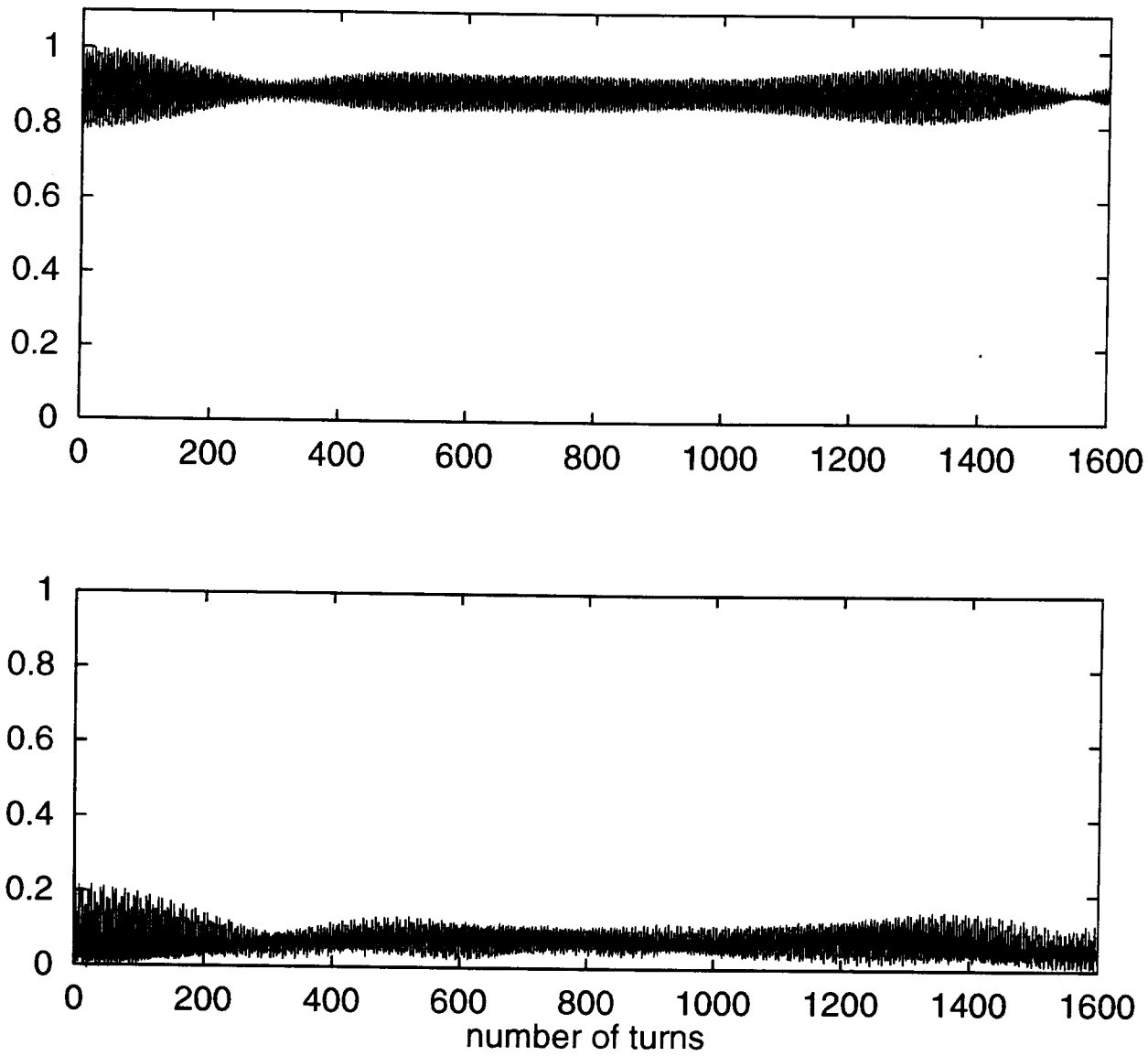

Figure 37: Flat HERA-p at E = 820 GeV with two snakes (longitudinal snake in the West and radial snake in the East). The view point is the East IP. Tracking of N = 64 particles for 1600 turns. Top: $< \vec{s} \cdot \vec{n}_0 >$. Bottom: $D\vec{s}$. Emittances: $\varepsilon_x = 2.0 \cdot 10^{-6}\, \pi\, m \cdot rad$, $\varepsilon_y = 2.0 \cdot 10^{-6}\, \pi\, m \cdot rad$, $\varepsilon_z = 1.5 \cdot 10^{-5}\, m \cdot rad$.

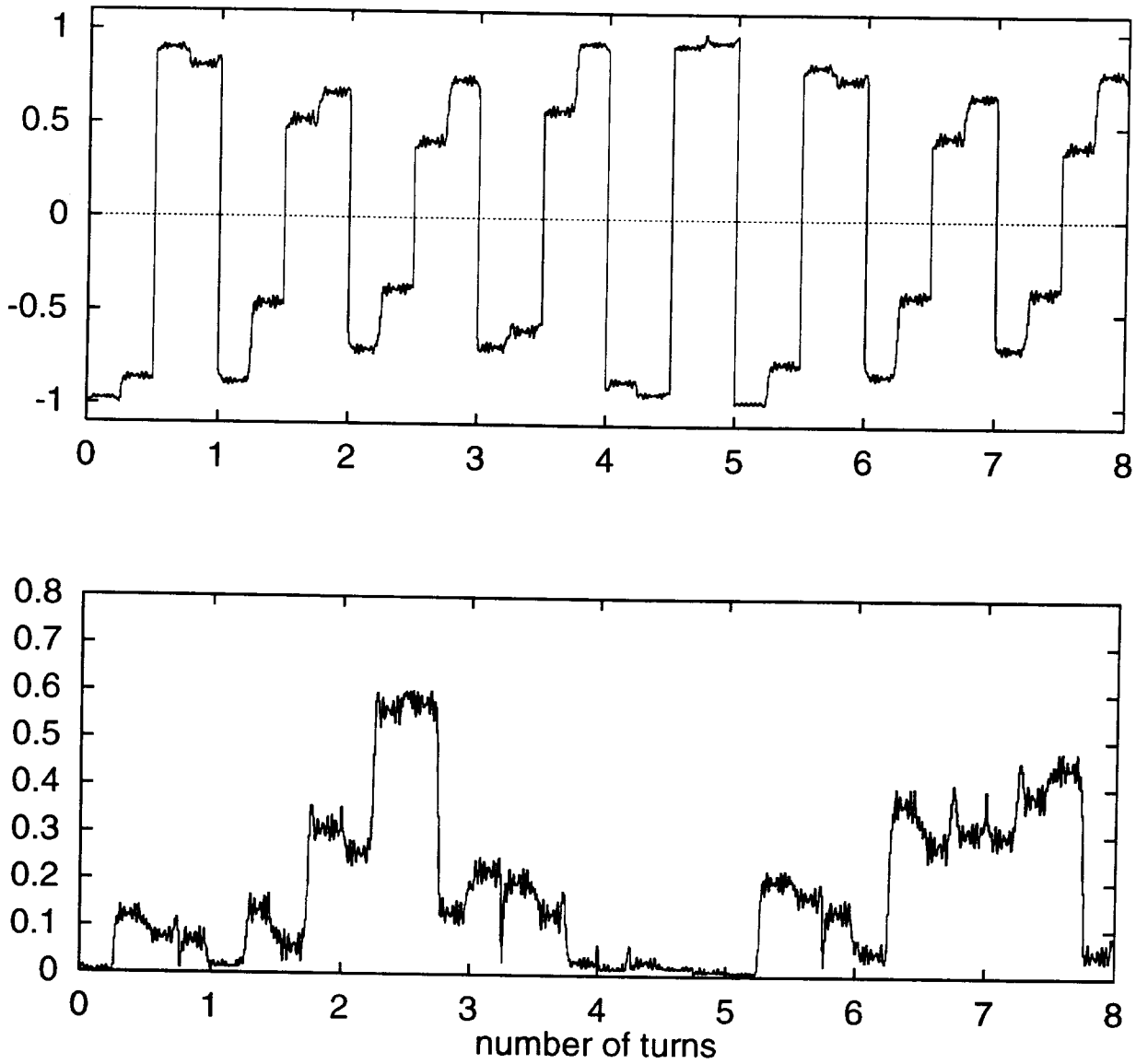

Figure 38: Behaviour of the polarization along the ring during 8 turns. The length of the ring has been scaled to unity. Flat HERA-p at E = 820 GeV with two snakes (longitudinal snake in the West and radial snake in the East). The start point is the East IP. Tracking of N = 64 particles for 8 turns. Top: $< \vec{s} \cdot \vec{n}_0 >$. Bottom: $D\vec{s}$. Emittances: $\varepsilon_x = 4.0 \cdot 10^{-6}\, \pi\, m \cdot rad$, $\varepsilon_y = 4.0 \cdot 10^{-6}\, \pi\, m \cdot rad$, $\varepsilon_z = 1.5 \cdot 10^{-5} m \cdot rad$.

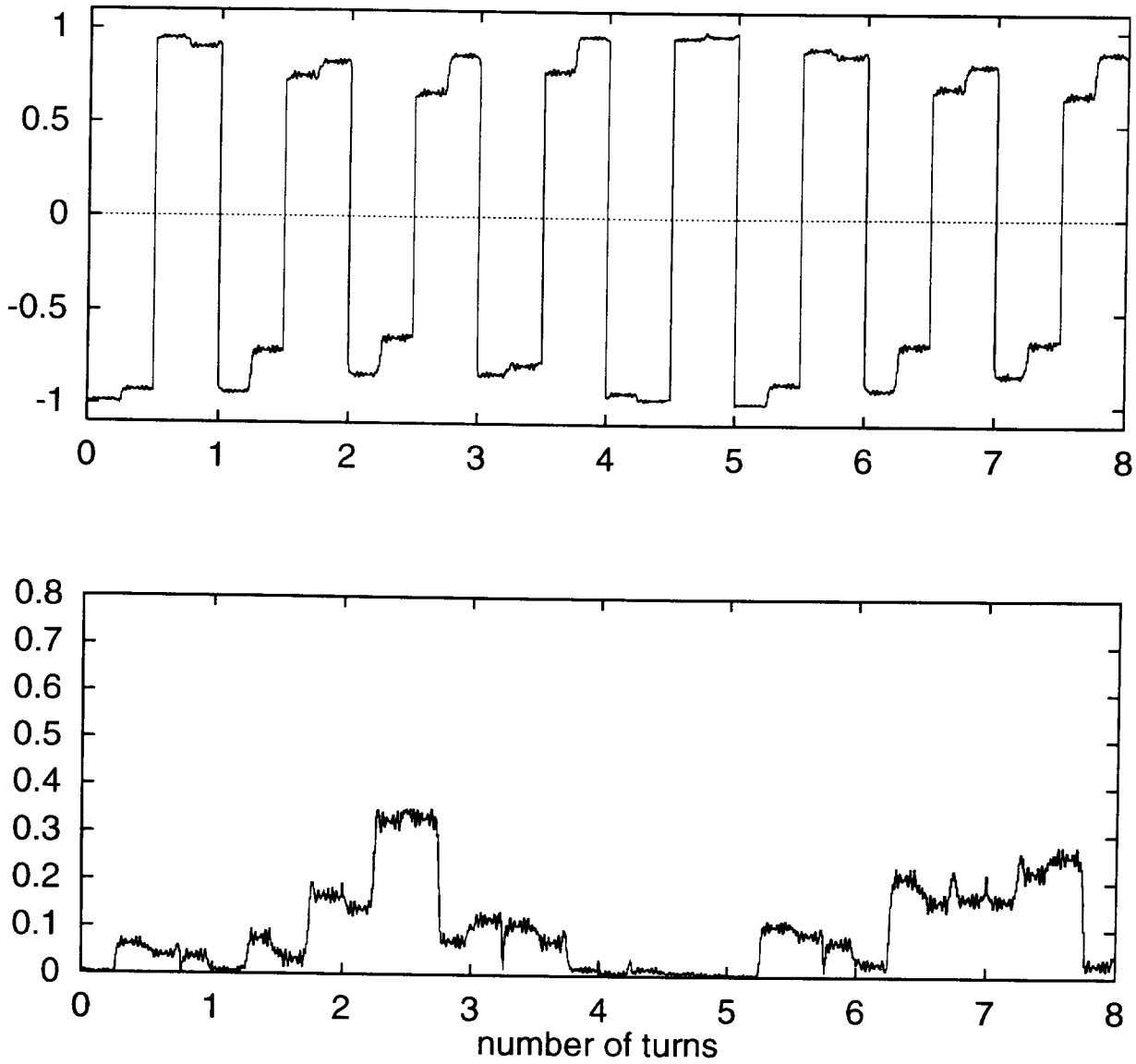

Figure 39: Behaviour of the polarization along the ring during 8 turns. The length of the ring has been scaled to unity. Flat HERA-p at E = 820 GeV with two snakes (longitudinal snake in the West and radial snake in the East). The start point is the East IP. Tracking of N = 64 particles for 8 turns. Top: $< \vec{s} \cdot \vec{n}_0 >$. Bottom: $D\vec{s}$. Emittances: $\varepsilon_x = 2.0 \cdot 10^{-6}\, \pi\, m \cdot rad$, $\varepsilon_y = 2.0 \cdot 10^{-6}\, \pi\, m \cdot rad$, $\varepsilon_z = 1.5 \cdot 10^{-5} m \cdot rad$.

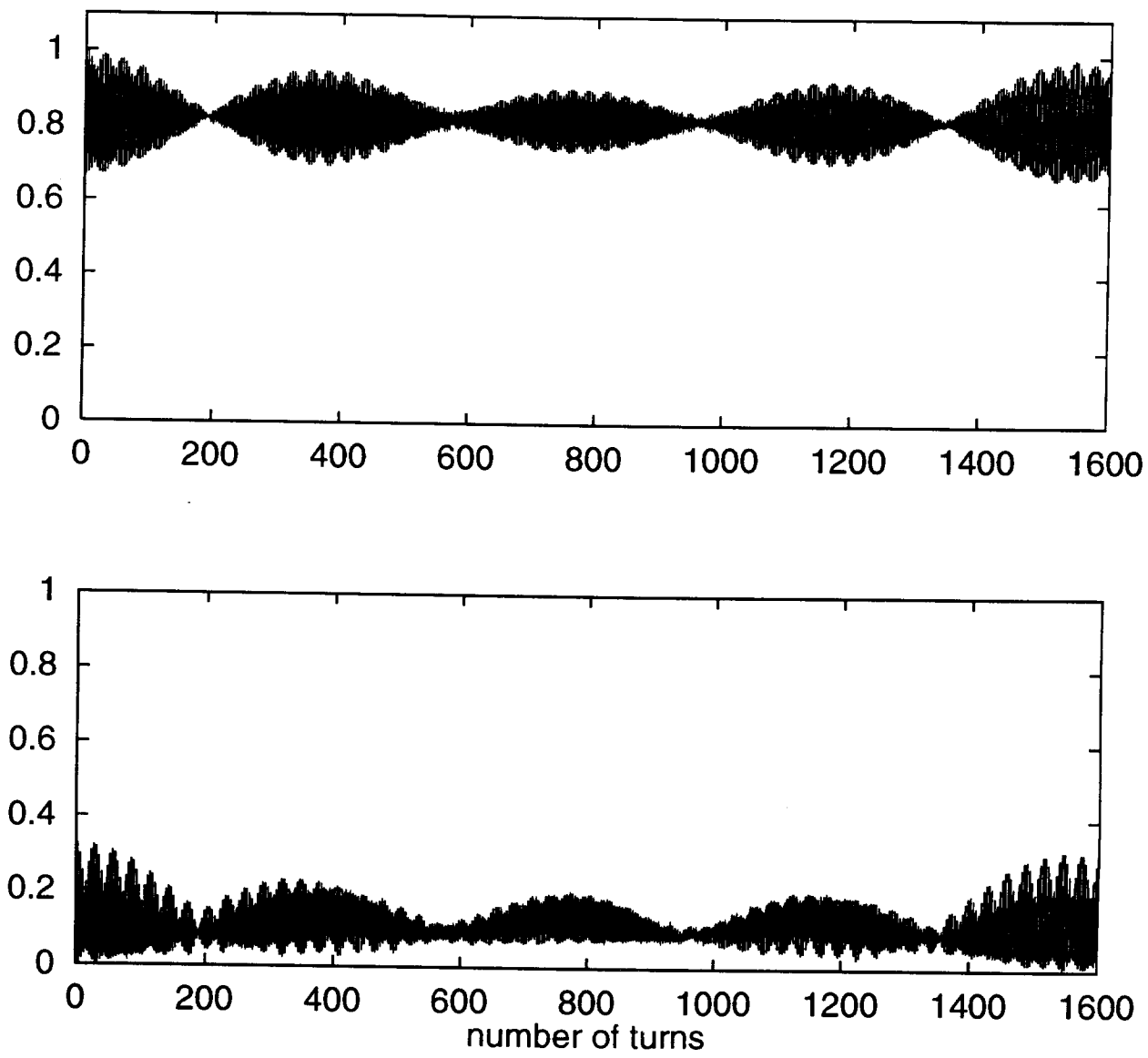

Figure 40: Flat HERA-p at E = 820 GeV with two snakes (longitudinal snake in the West and radial snake in the East) and with shifted vertical betatron tune: $\Delta\nu_y^0 = 0.03$. The view point is the East IP. Tracking of N = 64 particles for 1600 turns. Top: $< \vec{s} \cdot \vec{n}_0 >$. Bottom: $D\vec{s}$. Emittances: $\varepsilon_x = 4.0 \cdot 10^{-6}\, \pi\, m \cdot rad$, $\varepsilon_y = 4.0 \cdot 10^{-6}\, \pi\, m \cdot rad$, $\varepsilon_z = 1.5 \cdot 10^{-5} m \cdot rad$.

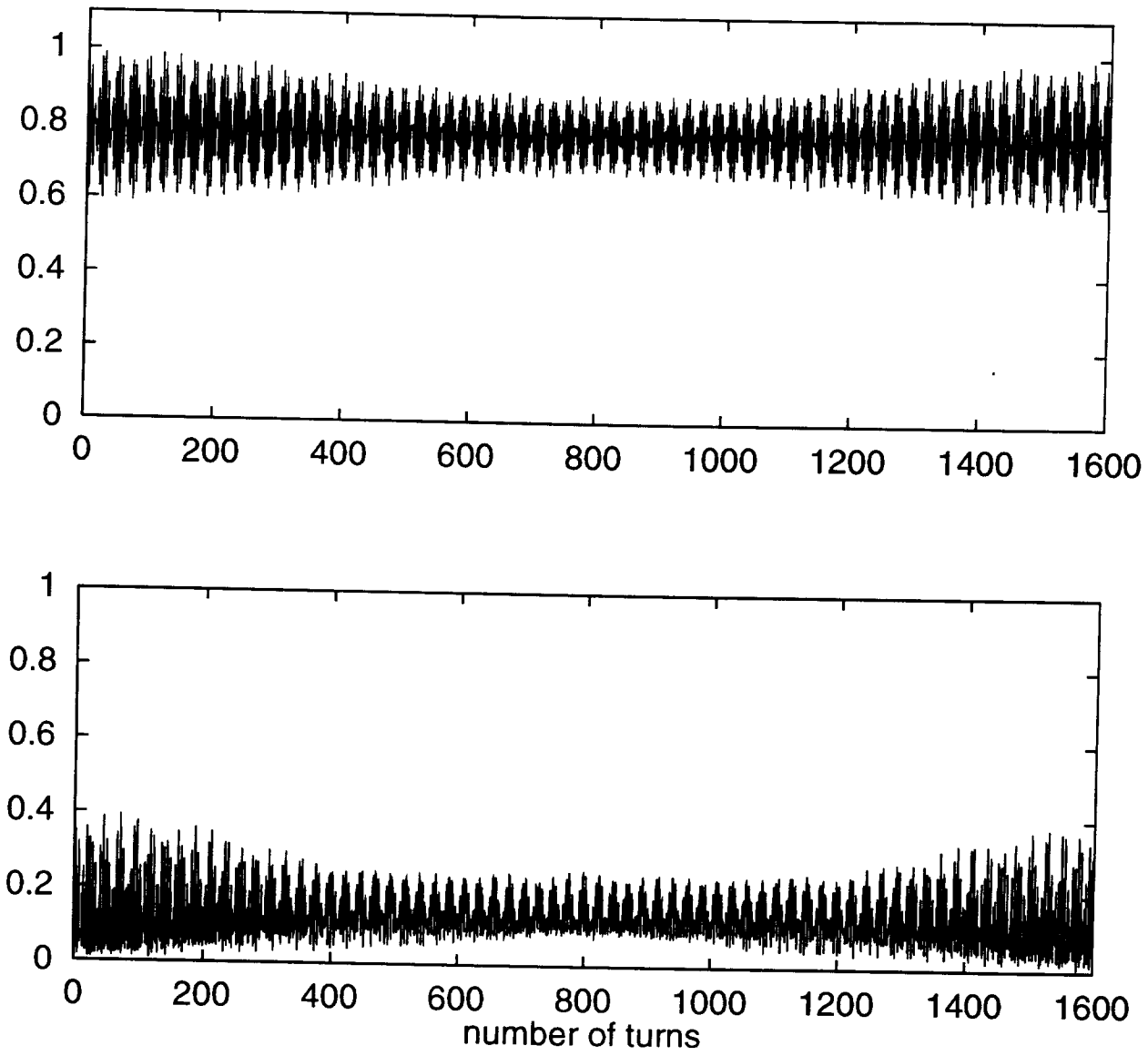

Figure 41: Flat HERA-p at E = 820 GeV with two snakes (longitudinal snake in the West and radial snake in the East) and with an additional spin rotation in the East chosen to give $\Delta\nu_s^0 = 0.022272$. The view point is the East IP. Tracking of N = 64 particles for 1600 turns. Top: $< \vec{s} \cdot \vec{n}_0 >$. Bottom: $D\vec{s}$. Emittances: $\varepsilon_x = 4.0 \cdot 10^{-6}\,\pi\, m \cdot rad$, $\varepsilon_y = 4.0 \cdot 10^{-6}\,\pi\, m \cdot rad$, $\varepsilon_z = 1.5 \cdot 10^{-5} m \cdot rad$.

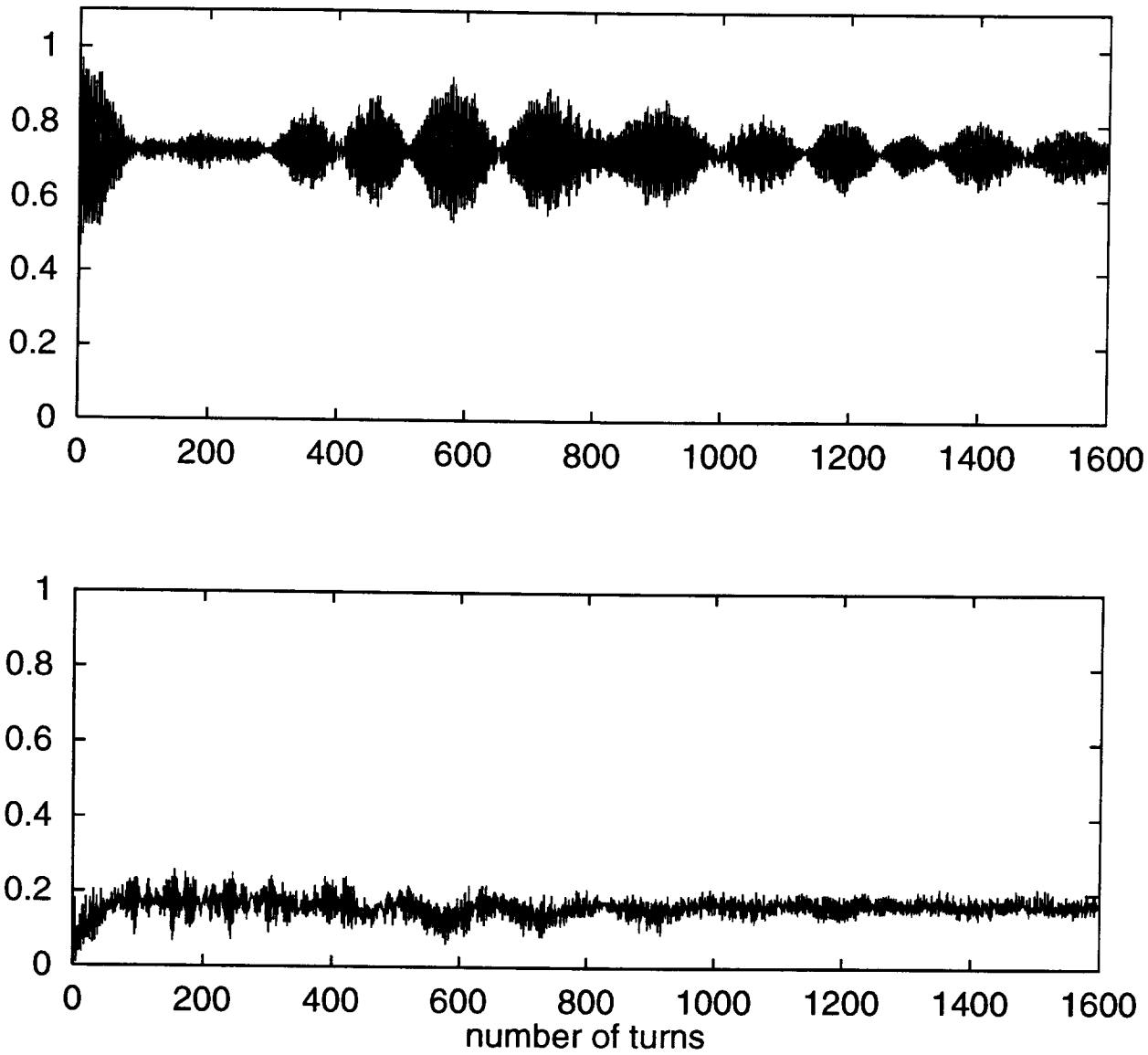

Figure 42: Flat HERA-p at E = 820 GeV with two snakes in the West and in the East (snake axis is ±45° from the beam direction). The view point is the East IP. Tracking of N = 64 particles for 1600 turns. Top: $< \vec{s} \cdot \vec{n}_0 >$. Bottom: $D\vec{s}$. Emittances: $\varepsilon_x = 4.0 \cdot 10^{-6}\, \pi\, m \cdot rad$, $\varepsilon_y = 4.0 \cdot 10^{-6}\, \pi\, m \cdot rad$, $\varepsilon_z = 1.5 \cdot 10^{-5}\, m \cdot rad$.

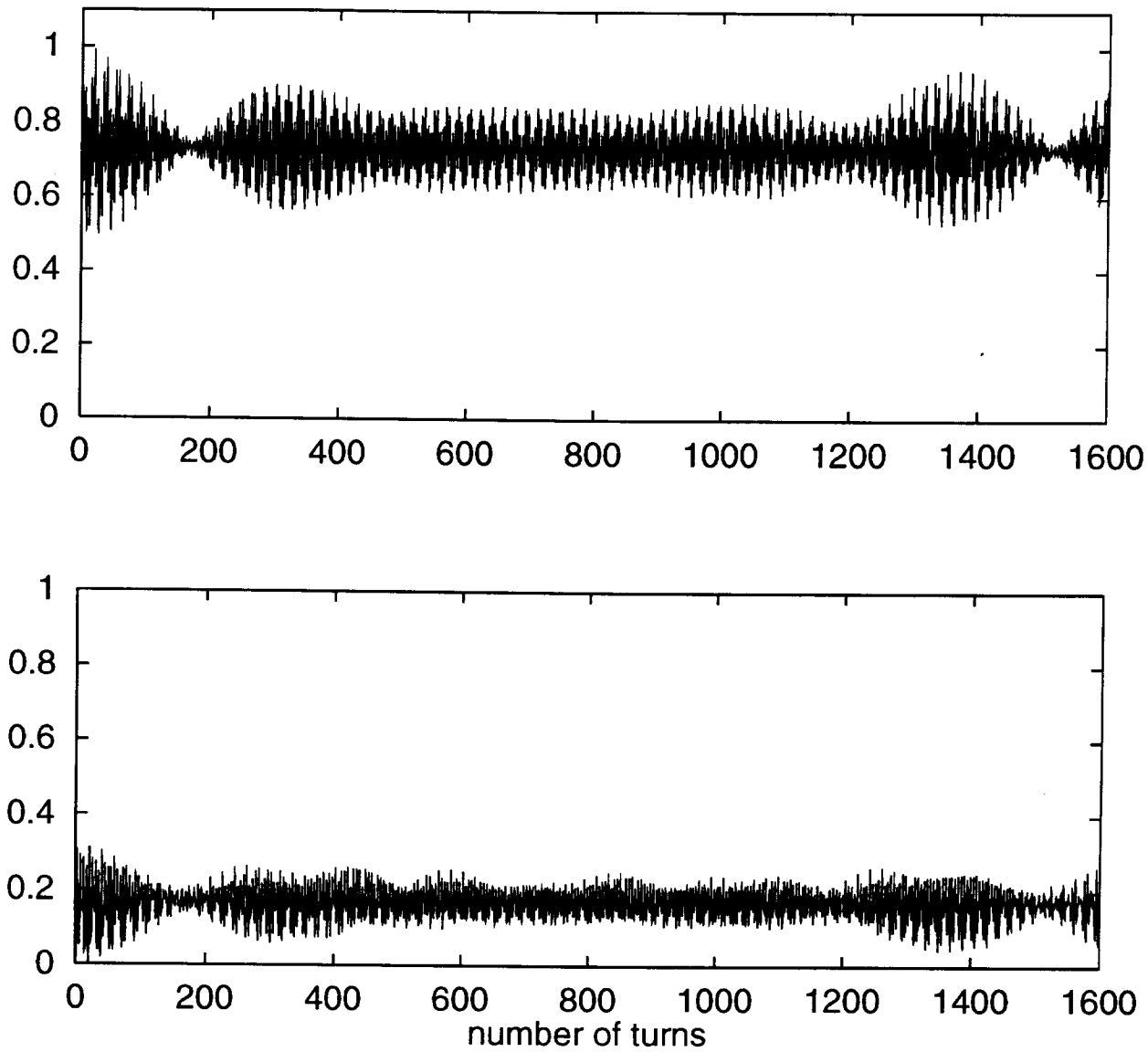

Figure 43: Nonflat HERA-p (without vertical bends in the East) at E = 820 GeV with two snakes (longitudinal snake in the West and radial snake in the East). The view point is the East IP. Tracking of N = 64 particles for 1600 turns. Top: $< \vec{s} \cdot \vec{n}_0 >$. Bottom: $D\vec{s}$. Emittances: $\varepsilon_x = 4.0 \cdot 10^{-6}\, \pi\, m \cdot rad$, $\varepsilon_y = 4.0 \cdot 10^{-6}\, \pi\, m \cdot rad$, $\varepsilon_z = 1.5 \cdot 10^{-5}\, m \cdot rad$.

3.5 Three Snakes

Figs.44-45 show the spin behaviour in the flat and nonflat HERA-p with a longitudinal snake in the South, West and North sections. The view point is the East IP. Compared to the case of one longitudinal snake (Figs.31-32) we do not see very much change of the polarization behaviour.

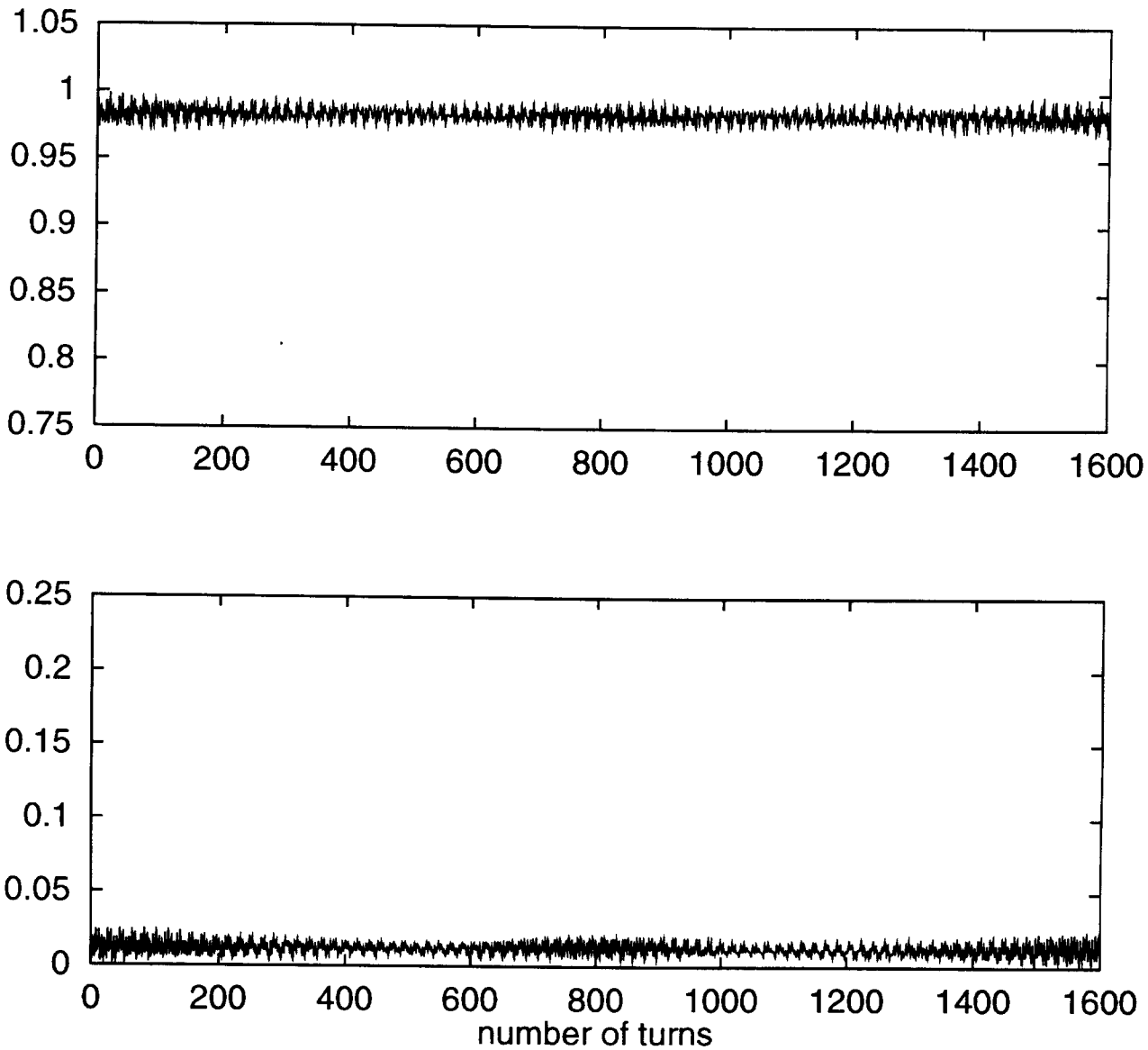

Figure 44: Flat HERA-p at E = 820 GeV with 3 longitudinal snakes in the South, the West and the North. The view point is the East IP. Tracking of N = 64 particles for 1600 turns. Top: $< \vec{s} \cdot \vec{n}_0 >$. Bottom: $D\vec{s}$. Emittances: $\varepsilon_x = 4.0 \cdot 10^{-6}\, \pi\, m \cdot rad$, $\varepsilon_y = 4.0 \cdot 10^{-6}\, \pi\, m \cdot rad$, $\varepsilon_z = 1.5 \cdot 10^{-5}\, m \cdot rad$.

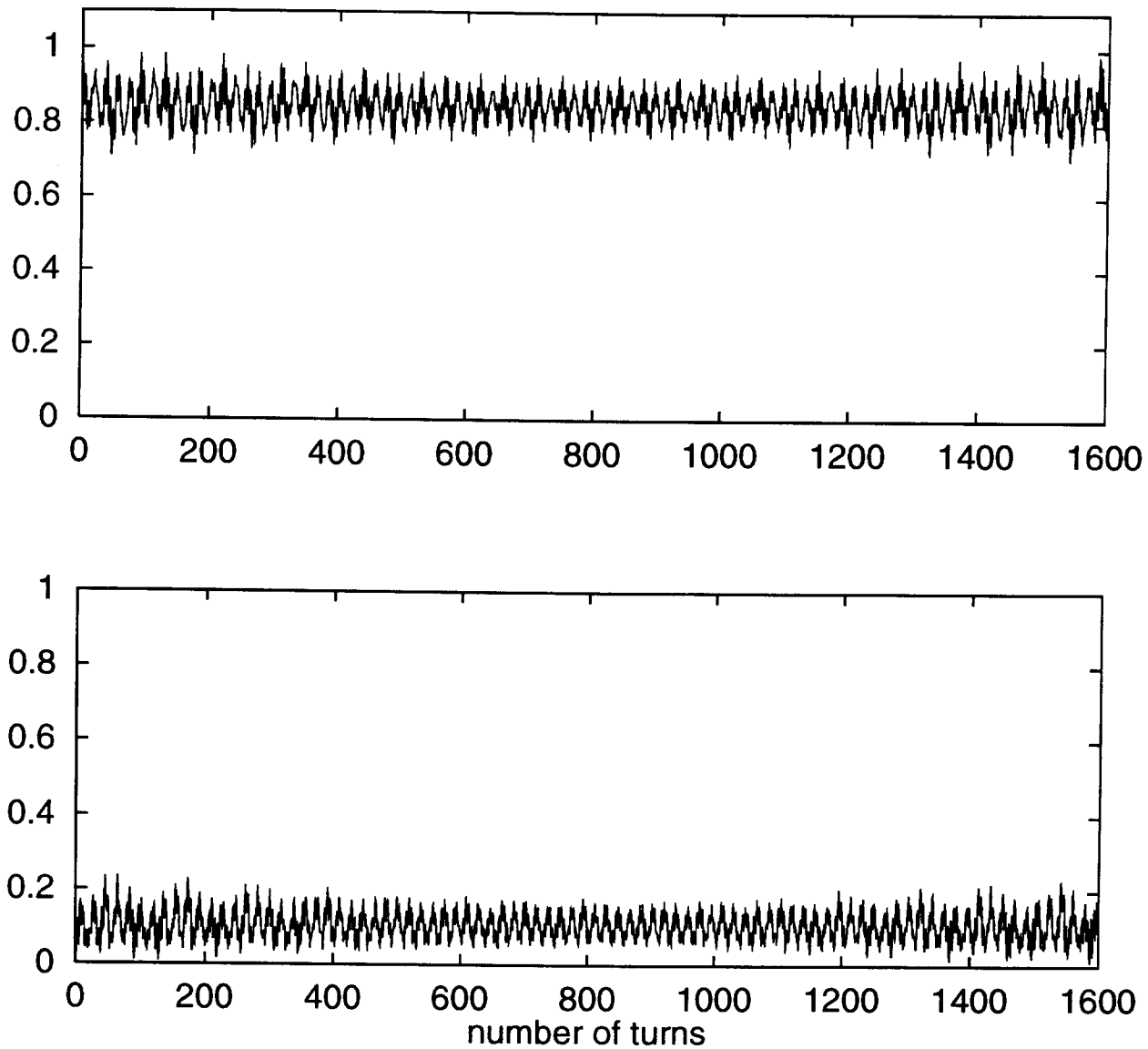

Figure 45: Nonflat HERA-p at E = 820 GeV with 3 longitudinal snakes in the South, the West and the North. The view point is the East IP. Tracking of N = 64 particles for 1600 turns. Top: $< \vec{s} \cdot \vec{n}_0 >$. Bottom: $D\vec{s}$. Emittances: $\varepsilon_x = 4.0 \cdot 10^{-6}\, \pi\, m \cdot rad$, $\varepsilon_y = 4.0 \cdot 10^{-6}\, \pi\, m \cdot rad$, $\varepsilon_z = 1.5 \cdot 10^{-5}\, m \cdot rad$.

3.6 Four Snakes

The tracking calculations for the flat and nonflat HERA-p with four snakes give us results which depend on the distribution of the snake types.

First, we present the case when the placing of siberian snakes in the ring causes a large spin tune spread for some energies with the result that some particles cross high order spin resonances. Fig.46 shows the spin behaviour in the flat HERA-p with four snakes (snake axis is $\pm 22.5°$ from the beam direction; one snake near the centre of each straight section) at the energy $E_0 = 820\ GeV$. The situation already does not look too good, but nevertheless we have a stable mean value of the polarization (approximately 75%). On changing the energy to $E_0 = 814.8\ GeV$ we have fast depolarization of the beam for the same snake configuration (see Fig.47). In this case the tune spread is near 0.07 for the characteristic emittances and the nearest resonances are $2Q_y - \nu_s^0 = 0.077$, $Q_x + Q_y - \nu_s^0 = 0.054$, $2Q_x - \nu_s^0 = 0.03$. The dependence of the maximum, the average value and the minimum of the norm $\mid \vec{n}_k \mid$ and the spin tune on values of transverse emittances for this case are shown in Figs.28-30. At this energy $E_0 = 814.8\ GeV$, the variant with two snakes looks much better (see Fig.48).

Another example of four snake placement is shown in Figs.49-52. The difference between the promising results (Figs.51-52) and not so optimistic situation (Figs.49-50) is only due to the usage of two radial or longitudinal snakes, respectively, in the North and the South interaction points. In principle, without breaking the mirror symmetry, we can use any two equivalent snakes (with arbitrary rotation angle and axis, may be depending on energy) at these points. This gives us the additional possibilities for the future optimization.

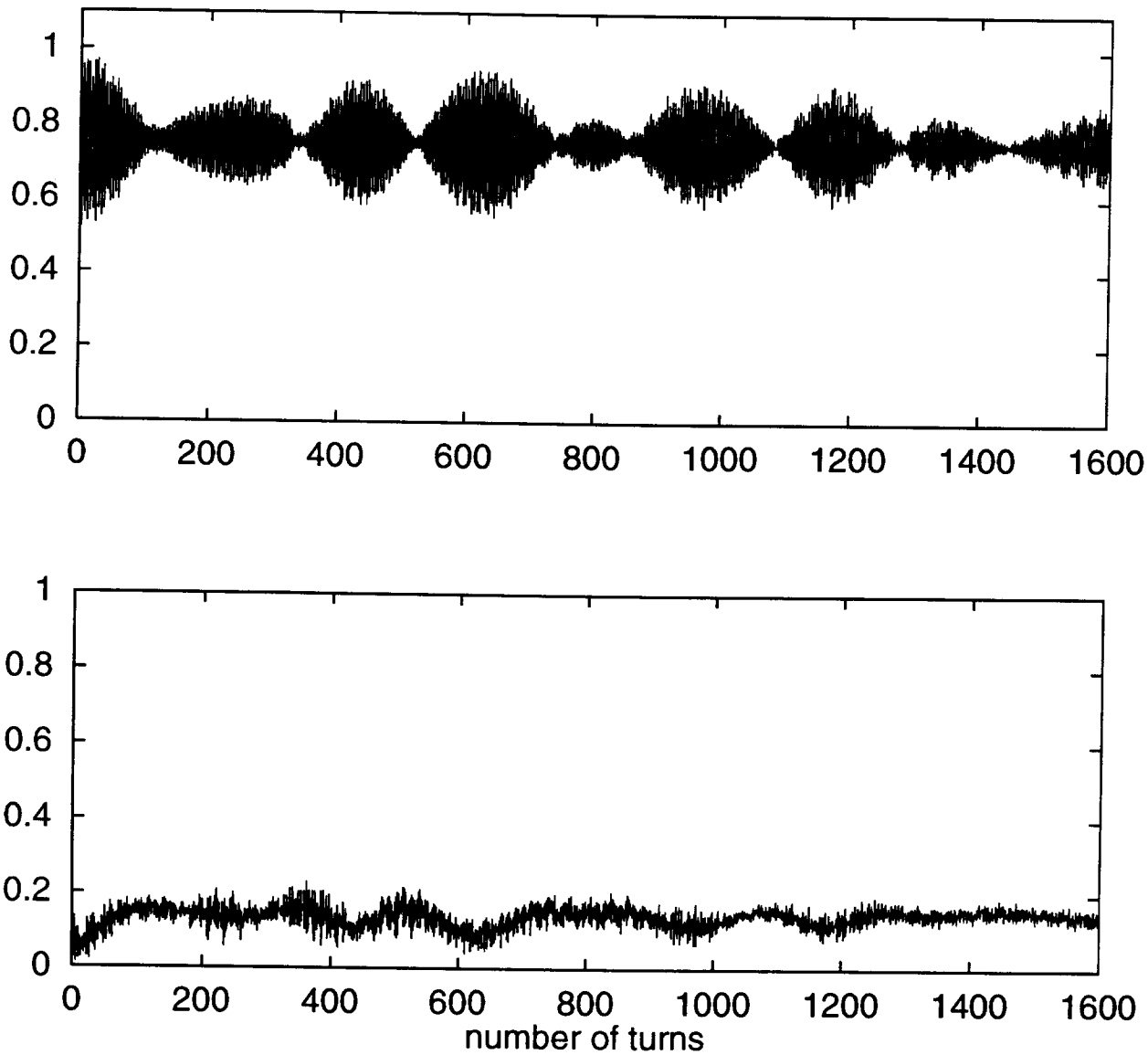

Figure 46: Flat HERA-p at E = 820 GeV with one snake near every IP (snake axis is ±22.5° from the beam direction). The view point is the East IP. Tracking of N = 64 particles for 1600 turns. Top: $< \vec{s} \cdot \vec{n}_0 >$. Bottom: $D\vec{s}$. Emittances: $\varepsilon_x = 4.0 \cdot 10^{-6}\, \pi\, m \cdot rad$, $\varepsilon_y = 4.0 \cdot 10^{-6}\, \pi\, m \cdot rad$, $\varepsilon_z = 1.5 \cdot 10^{-5}\, m \cdot rad$.

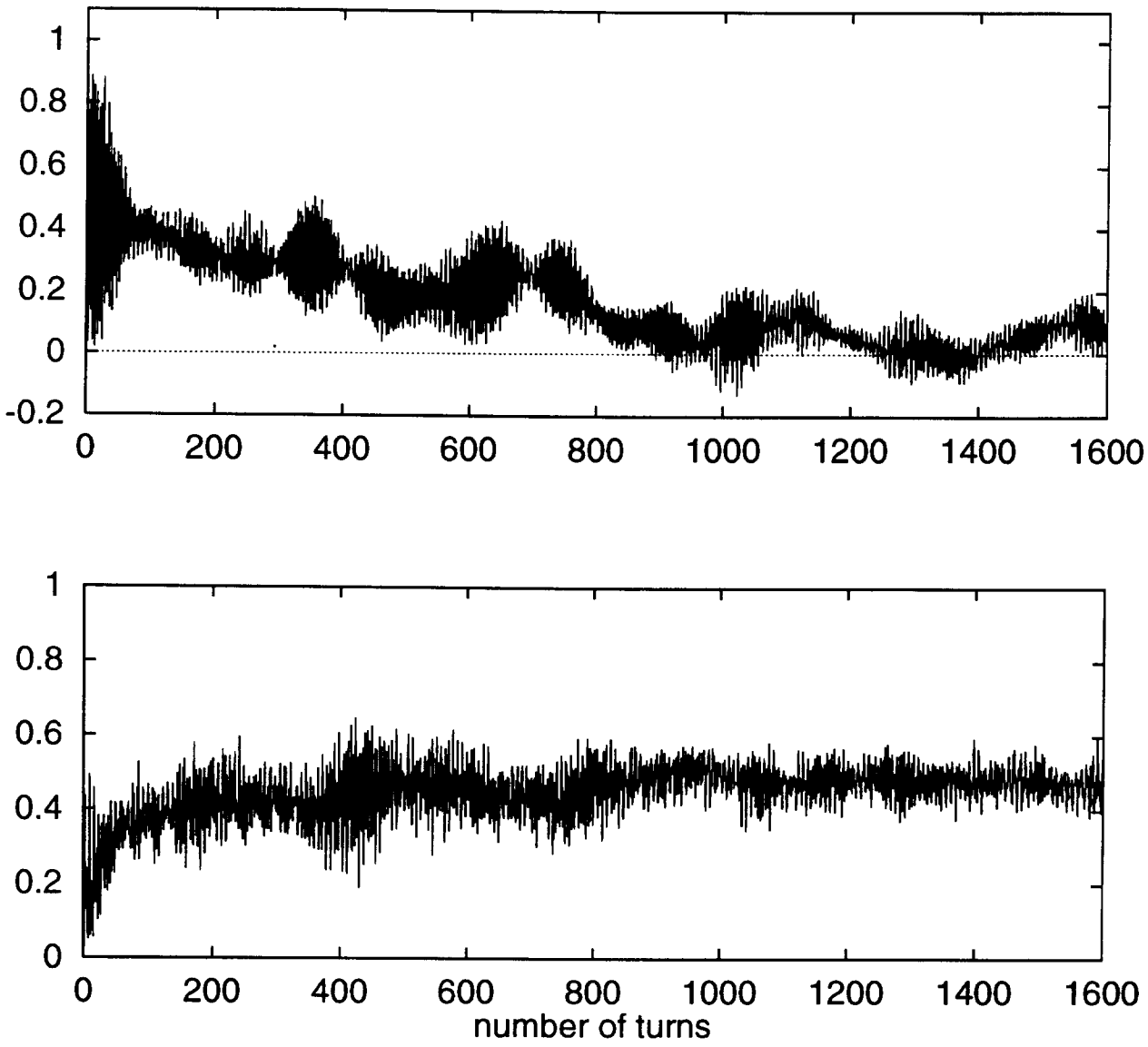

Figure 47: Flat HERA-p at E = 814.8 GeV with one snake near every IP (snake axis is $\pm 22.5°$ from the beam direction). The view point is the East IP. Tracking of N = 64 particles for 1600 turns. Top: $< \vec{s} \cdot \vec{n}_0 >$. Bottom: $D\vec{s}$. Emittances: $\varepsilon_x = 4.0 \cdot 10^{-6}\, \pi\, m \cdot rad$, $\varepsilon_y = 4.0 \cdot 10^{-6}\, \pi\, m \cdot rad$, $\varepsilon_z = 1.5 \cdot 10^{-5}\, m \cdot rad$.

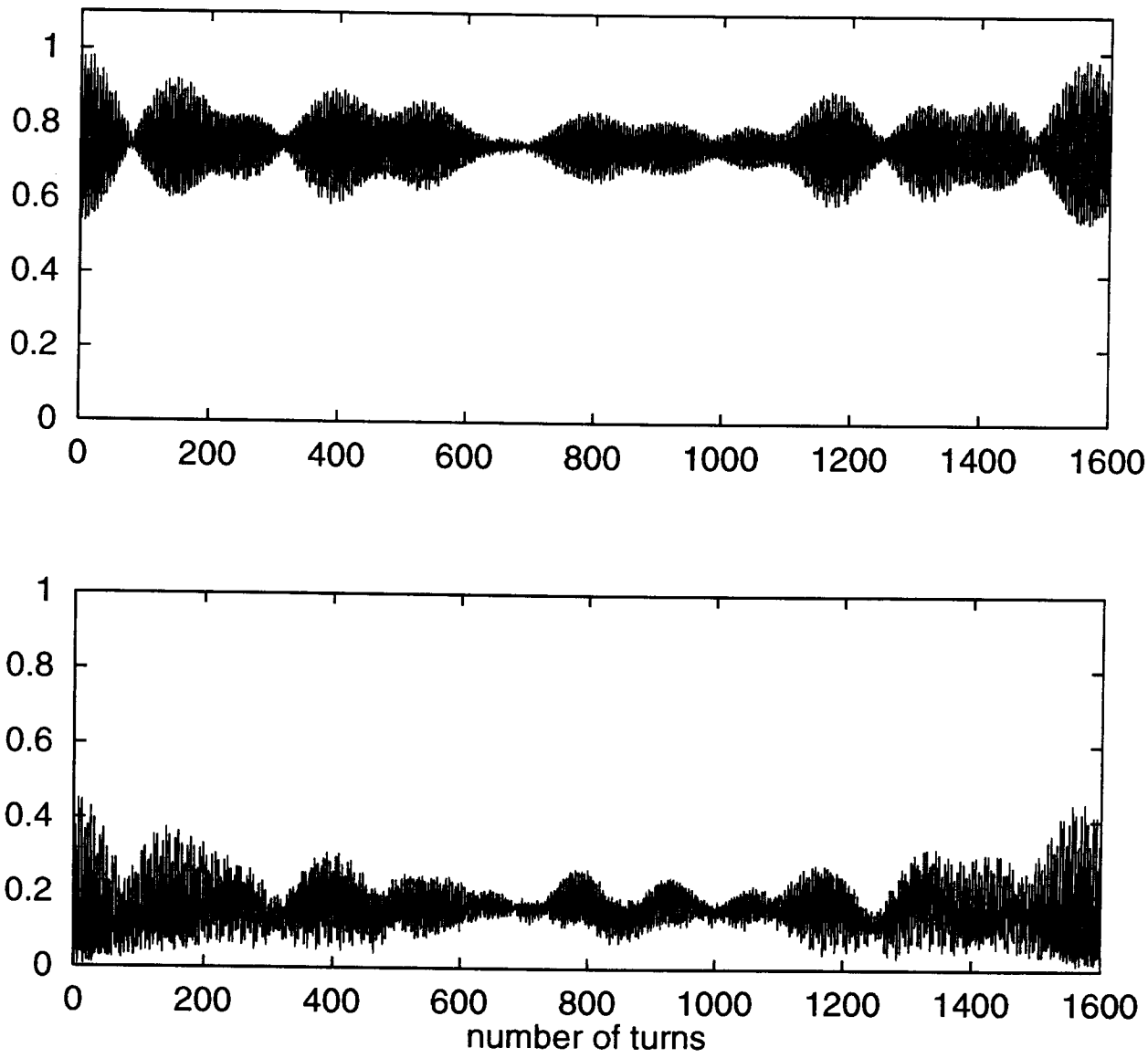

Figure 48: Flat HERA-p at E = 814.8 GeV with two snakes (longitudinal snake in the West and radial snake in the East). The view point is the East IP. Tracking of N = 64 particles for 1600 turns. Top: $< \vec{s} \cdot \vec{n}_0 >$. Bottom: $D\vec{s}$. Emittances: $\varepsilon_x = 4.0 \cdot 10^{-6}\, \pi\, m \cdot rad$, $\varepsilon_y = 4.0 \cdot 10^{-6}\, \pi\, m \cdot rad$, $\varepsilon_z = 1.5 \cdot 10^{-5}\, m \cdot rad$.

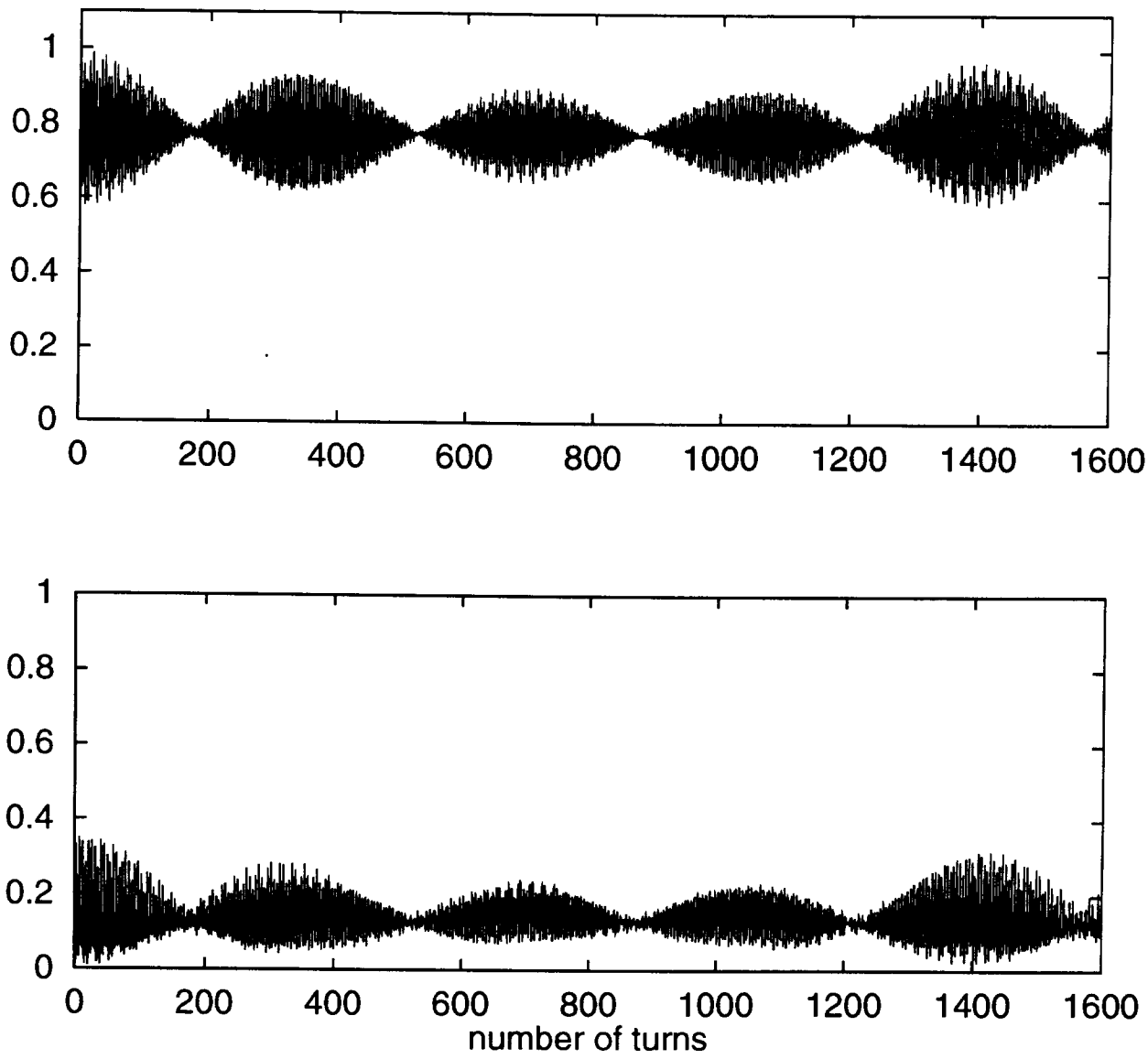

Figure 49: Nonflat HERA-p at E = 820 GeV (without vertical bends in the East) with 4 snakes (one longitudinal snake in the South, the West and the North and a radial snake in East). The view point is the East IP. Tracking of N = 64 particles for 1600 turns. Top: $< \vec{s} \cdot \vec{n}_0 >$. Bottom: $D\vec{s}$. Emittances: $\varepsilon_x = 4.0 \cdot 10^{-6}\, \pi\, m \cdot rad$, $\varepsilon_y = 4.0 \cdot 10^{-6}\, \pi\, m \cdot rad$, $\varepsilon_z = 1.5 \cdot 10^{-5}\, m \cdot rad$.

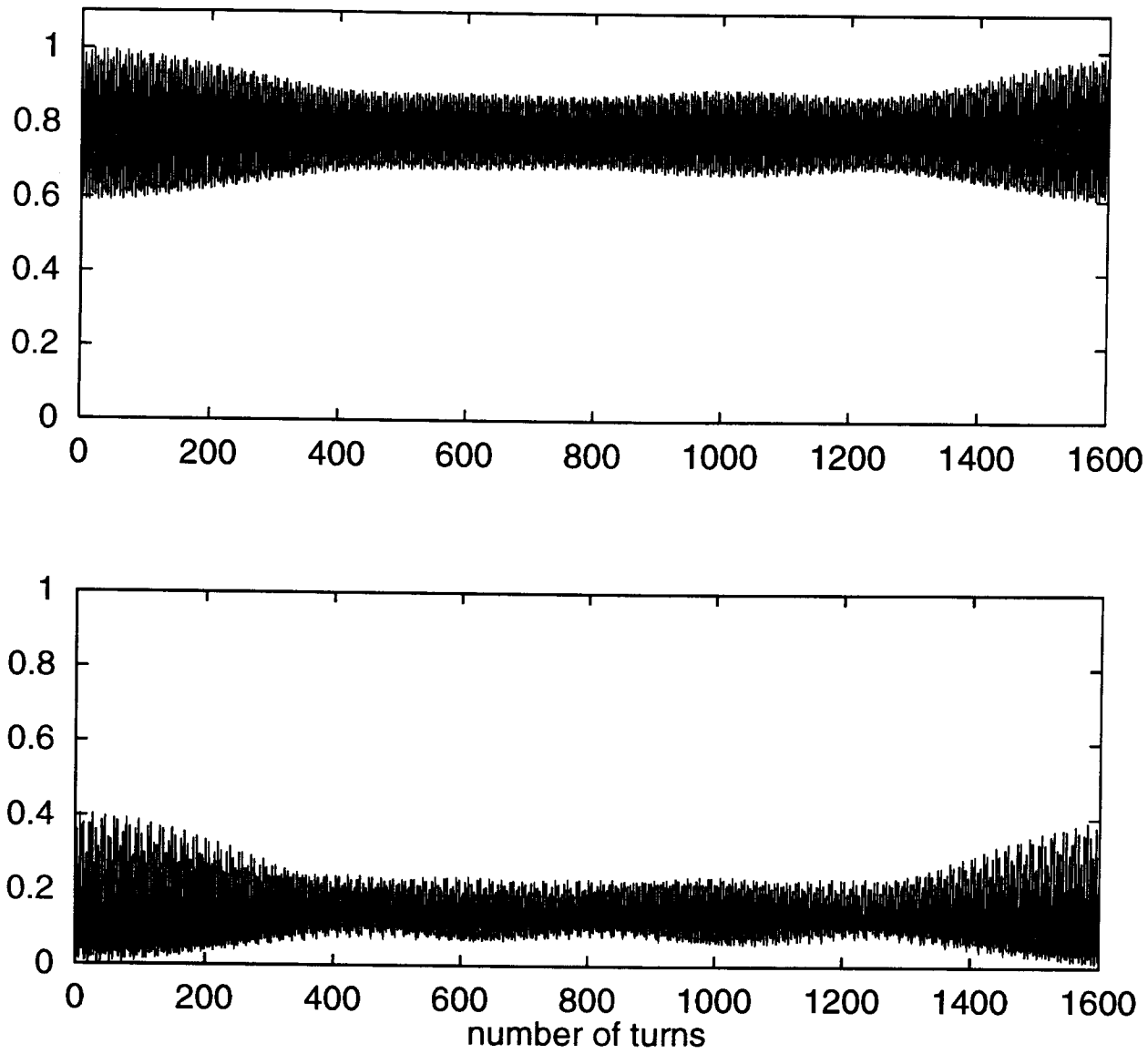

Figure 50: Flat HERA-p at E = 820 GeV with 4 snakes (one longitudinal snake in the South, the West and the North respectively and one radial snake in the East). The view point is the East IP. Tracking of N = 64 particles for 1600 turns. Top: $< \vec{s} \cdot \vec{n}_0 >$. Bottom: $D\vec{s}$. Emittances: $\varepsilon_x = 4.0 \cdot 10^{-6}\, \pi\, m \cdot rad$, $\varepsilon_y = 4.0 \cdot 10^{-6}\, \pi\, m \cdot rad$, $\varepsilon_z = 1.5 \cdot 10^{-5}\, m \cdot rad$.

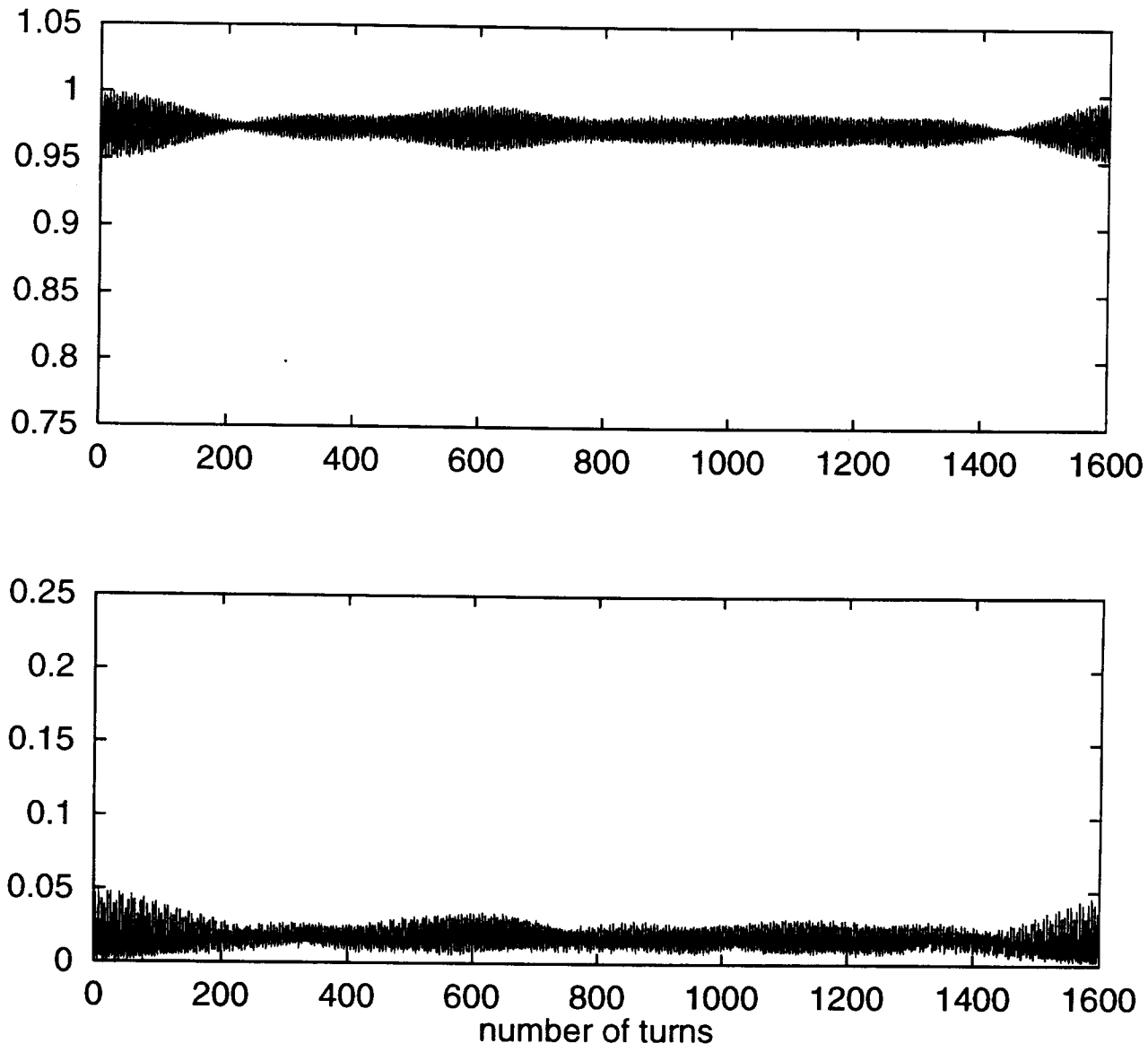

Figure 51: Flat HERA-p at E = 820 GeV with 4 snakes (one longitudinal snake in the West and one radial snake in the South, the North and the East respectively). The view point is the East IP. Tracking of N = 64 particles for 1600 turns. Top: $< \vec{s} \cdot \vec{n}_0 >$. Bottom: $D\vec{s}$. Emittances: $\varepsilon_x = 4.0 \cdot 10^{-6}\, \pi\, m \cdot rad$, $\varepsilon_y = 4.0 \cdot 10^{-6}\, \pi\, m \cdot rad$, $\varepsilon_z = 1.5 \cdot 10^{-5}\, m \cdot rad$.

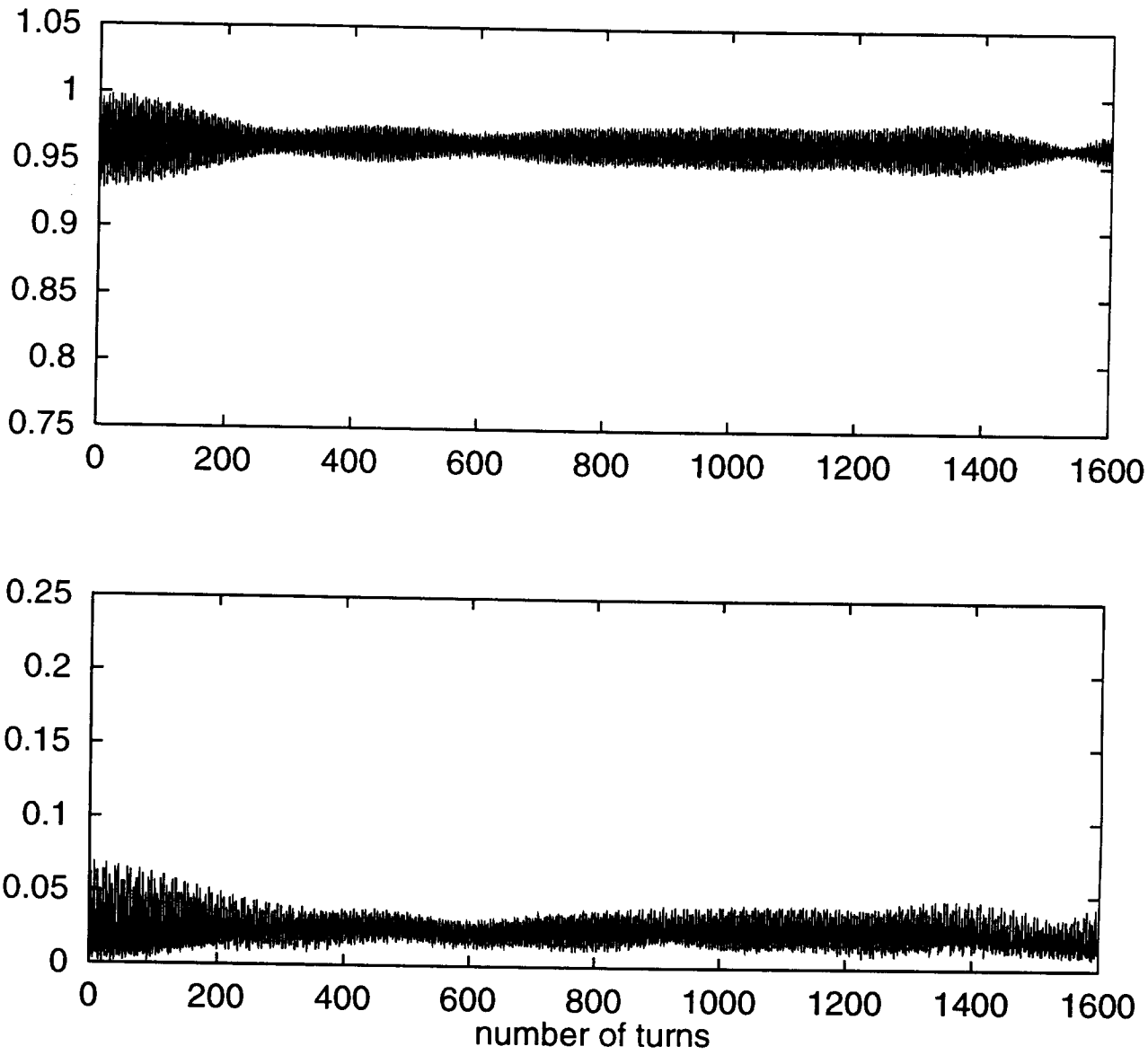

Figure 52: Nonflat HERA-p at E = 820 GeV with 4 snakes (one longitudinal snake in the West and one radial snake in the South, the North and the East respectively). The view point is the East IP. Tracking of N = 64 particles for 1600 turns. Top: $< \vec{s} \cdot \vec{n}_0 >$. Bottom: $D\vec{s}$. Emittances: $\varepsilon_x = 4.0 \cdot 10^{-6}\, \pi\, m \cdot rad$, $\varepsilon_y = 4.0 \cdot 10^{-6}\, \pi\, m \cdot rad$, $\varepsilon_z = 1.5 \cdot 10^{-5}\, m \cdot rad$.

4 Preliminary Conclusions

In this section we extract some preliminary conclusions from this study of the behaviour of proton spin motion at final energy in HERA-p without any misalignments.

1. Due to the fact that in the nonflat HERA-p the sections with vertical magnets have mirror symmetry, it is possible to apply siberian snakes without large changes in the layout.

2. Without considering how to obtain polarized protons at the final energy, we can state that the polarization may be conserved even with one snake in the ring (of course, in the framework of the considered model without misalignments).

Acknowledgements

We wish to thank G. Hoffstätter and E. Gianfelice-Wendt for their contributions to this study. We thank Yu.S. Derbenev and A.M. Kondratenko for interesting discussions.

References

[1] Ya.S. Derbenev and A.M. Kondratenko, Dokl.Akad.Nauk SSSR, **223**, 830 (1975) and later papers.

[2] See for example the papers by D.P. Barber and T. Roser in the proceedings of the Workshop on the Prospects of Spin Physics at HERA, Zeuthen, Germany, September 1995, DESY Report 95-200.

[3] V.Balandin and N.Golubeva, Siberian Snakes for Nonflat Rings, to be published.

[4] E.D. Courant and R.D. Ruth, The Acceleration of Polarized Protons in Circular Accelerators, Brookhaven Report, BNL 51270 (1990).

[5] V.Balandin and N.Golubeva, Taylor Map and Calculation of Equilibrium Polarization Direction for Proton Storage Rings, 1993 Particle Accelerator Conference, Washington USA (1993).

[6] Ya.S. Derbenev and A.M. Kondratenko, Sov.Phys.JETP., **37**, 968 (1973).

[7] V.Balandin and N.Golubeva, Proc. of the XV Int. Conf. on High Energy Particle Accelerators, Int. J. Mod. Phys. A, **2B**, 998 (1992).

[8] V.Balandin and N.Golubeva, Investigation of Spin Motion in the Booster Lattice, TRIUMF Report TRI-DN-93-K236 (1993).

[9] V.Balandin and N.Golubeva, Fast Betatron Tune Jumps and Partial Siberian Snakes for Preserving the Polarization in the Booster Lattice, TRIUMF Report TRI-DN-93-K240 (1993).

[10] V.Balandin, to be published.